Ambient mercury concentrations at industrially influenced sites on the Highveld

R Meyer

orcid.org 0000-0003-3434-46644

Dissertation submitted in fulfilment of the requirements for the degree *Master of Science in Environmental Sciences with Chemistry* at the North-West University

Supervisor:	Prof JP Beukes
Co-supervisor:	Prof PG van Zyl

Graduation May 2019

22774688

Acknowledgements

I would like to express my sincere gratitude and appreciation to the following people for their help and support during the last two years. They played a vital role in the completion of my dissertation and helped me to grow both academically and as a person.

- My mentors Prof. Paul Beukes and Prof. Pieter van Zyl for their guidance and patience,

- Dr. Andrew Venter for his assistance with MATLAB programming and data processing,

- My parents André and Retha Meyer; and wife, Hanet Meyer, for their support, love and motivation,

- The financial support of the National Research Foundation (NRF) towards this research is hereby acknowledged. Opinions expressed and conclusions made are those of the authors and are not necessarily to be attributed to the NRF,

- The authors gratefully acknowledge financial support from Sasol Technology R&D, Sasolburg. In addition Sasol Technology R&D, Sasolburg, as well as Eskom Holdings, Rosherville, are thanked for providing the atmospheric and meteorological data used in this dissertation,

- God Almighty for the strength and perseverance to complete this study.

Preface

Declaration by the candidate:

"I hereby declare that the dissertation submitted for the degree MSc: Atmospheric Chemistry, as stipulated by the North-West University (NWU), is my own original work and has not previously been submitted to any other institution of higher education. I further declare that all sources cited or quoted are indicated and acknowledged by means of a comprehensive list of references".

Rean Meyer

Table of Contents

ABSTRACT

Mercury (Hg) is a toxic atmospheric pollutant that has the ability to bio-accumulate in the aquatic food chain, leading to animal and human exposure. During this study, assessments of ambient Total Gaseous Mercury (TGM) concentrations at industrially influenced sites in the interior of South Africa were conducted. Continuous TGM and ancillary data, i.e. other pollutant species and meteorological parameters, were measured at the Eco-Park (EP), Elandsfontein (EL) and Marapong (MP) monitoring stations. Mean TGM concentrations during the monitoring period was 3.95 ± 2.97 ng.m^{-3} for EP, which is substantially higher than at other South African and most international first world urban sites. The mean TGM measured at EL (2.49 ± 2.06 ng.m^{-3}) was comparable to levels reported for urban South African and American cities, yet elevated above international background levels. Mean TGM levels at MP (1.61 ± 1.42 ng.m^{-3}) was comparatively lower than the other two monitoring sites considered, but fell within ranges reported at suburban South African and Northern Hemisphere background sites. TGM spikes, which were associated with pollution events and diurnal cycles, were frequently observed and contributed to the relatively high afore-mentioned standard deviations. Multiple linear regression (MLR) was applied on the data as a receptor model approach. The derived site-specific optimum MLR equations allowed for relatively accurate calculation of TGM concentrations when correlated with measured concentrations, with the exception of very high or low concentrations. Combining information derived from the MLR analyses, diurnal plots, pollution roses and polar plots enabled identification of the dominant TGM source(s) for each site. A nearby coal-fired power station was identified as the most significant source at EP, while household combustion also made a discernible contribution. The dominant source contributing to elevated levels measured at EL was high stack emissions from various coal-fired power plants distributed across the region. At MP, household combustion in the surrounding semi- and informal settlements dominated TGM contributions. At all the monitoring sites, anthropogenic sources were much stronger than natural re-emission processes. Possible chemical processes that are likely to be important for atmospheric Hg in the South African interior were identified by information derived from the analytical tools utilised.

List of Figures

List of Tables

Chapter 1 - Background, motivation and objectives

1.1. Background and motivation

Mercury (Hg) is a global threat to human and environmental health. The concern of this hazardous pollutant arises mainly from the human health effects caused by methylated mercury through the consumption of fresh water and marine fish (Lin and Pehkonen 1999). This dissertation focuses mainly on anthropogenic emissions of mercury, as well as its transport and transformation in the South African environment.

Hg was included in the United Nations Economic Commission for Europe Convention for Long Range Transboundary Air Pollution (UNECE-CLRTAP) heavy metals protocol, which was adopted in 1979 (Byrne, 2017). Mercury is also listed under the European Commission's Air Quality Framework Directive 96/62/EC (European Commission, 2016). The Clean Air Mercury Rule was introduced by The US Environmental Protection Agency (US-EPA) in March 2005, enforcing mercury emissions from new and existing coal-fired power plants to be capped. In 2013, the Minamata Treaty was signed by South Africa and 98 other countries to protect human health and the environment from anthropogenic emissions and releases of elemental Hg and relevant Hg compounds. Since South Africa is considered to be the 6th largest emitter of mercury globally, this will significantly influence the way South Africa adopts Hg control legislation, and it is expected that the Minamata Treaty will have far-reaching implications for South Africa (Venter et al., 2015).

There are many important gaps in the current knowledge and understanding of the wide spectrum of complex atmospheric Hg issues (Pirrone et al., 2010; Gworek et. al., 2017; Schroeder & Munthe, 1998). It is extremely important to obtain reliable data on the physical/chemical speciation of both natural and anthropogenic emissions, since the physical and chemical properties of the species emitted by a given source are a major determinant, along with the prevailing meteorology/climatology, of their atmospheric behaviour and fate.

The global Hg emissions estimate still has large associated uncertainties, giving a range of 1010-4070 tons (Lin et al., 2006). Thirty percent of the total uncertainty is associated with anthropogenic Hg emissions, while the uncertainties associated with emissions from oceans and terrestrial surfaces are 50% (Lindberg et al., 2007). Long-term, high resolution monitoring of Hg is important in order to reduce these associated Hg emissions uncertainties, as well as to provide important information relating to the oxidation mechanism of atmospheric Hg (Slemr et al., 2008, 2013). Although atmospheric Hg is monitored extensively in the Northern Hemisphere, few studies have been published for the Southern

Hemisphere (Slemr et al., 2013). Notwithstanding the recent scientific advances on Hg long-term trends, depletion events, seasonal cycles and flux rates based on measurements conducted at the Cape Point Global Atmosphere Watch (CPT-GAW) station, this sampling location is not representative of the South African interior. In is somewhat remote from any large point sources (e.g. coal-fired power plant, petrochemical operations, metallurgical smelters) located in parts of the Mpumalanga Highveld, Gauteng, North-West, and Free State provinces (Baker et al., 2002; Slemr et al., 2008; Brunke et al., 2010a, b). This implies that data and publications based on CPT-GAW data is not representative of the industrialised interior of South Africa, but rather being an estimate for southern hemisphere oceanic background conditions. Long-term speciated mercury measurements in industrial, urban and rural locations are lacking for the southern Hemisphere (Dabrowski et al., 2008; Masekoameng et al. 2010; Schroeder & Munthe, 1998). As far as the candidate could asses, the has been only one paper published in the peer reviewed public domain that specifically considered active measurements of atmospheric Hg in the South African interior, i.e. Belelie et al. (2018), who reported on three measurement stations on the Mpumalanga Highveld.

From the above-mentioned it is evident that there is a need for quantification of long-term Hg trends for the interior of South Africa. For the South African atmospheric science community, which include industry and environmental regulatory authorities, to meaningfully participate in future discussions related to ambient Hg standard levels, it is important to perform scientific research related to Hg. This dissertation serves to partially fulfil that goal.

1.2. Objectives

The general aim of this study was to enhance the understanding of atmospheric total gaseous mercury (TGM) levels in the South African interior. The specific objectives were:

- Since the candidate did not have access to an atmospheric Hg device, the first objective was to obtain data from at least three measurement sites operated by reputable operators. Since the datasets will be from different measurement operations, methods should be developed to convert the different datasets into a single useful format. Additionally, the datasets should be statistically processed to verify data quality.
- Make air quality related deductions based on the levels of TGM found at the various sites, as well as identify possible contributing sources.
- Apply a mathematical receptor model to calculate ambient TGM and compare this calculated dataset with actual measured results.
- Provide insight into chemical processes influencing TGM in the South African interior.

Chapter 2 - Literature study

2.1. Introduction on mercury

Mercury (Hg) is one of the most toxic trace elements emitted into the atmosphere due to its detrimental effects on the environment and human health (Gworek et. al., 2017). Emissions of this volatile element with its characteristic physical and chemical properties has a relatively long atmospheric lifetime (refer to Chapter 2.1.2) and can travel long distances in the atmosphere. Current Hg emission inventories also indicate increasing atmospheric concentrations (Pirrone et al. 2010). Its persistence in the environment also accounts for the bio-accumulation of methylated mercury in fish and animals we eat. These negative environmental impacts associated with Hg, as well as the shortage of information regarding its processes have led to a global increase in atmospheric Hg research (Lindberg et al. 2007).

2.1.1. General information on Hg

Hg occurs naturally in the environment, with more than 25 Hg-containing minerals known to occur in Earth's mantle (Schroeder & Munthe, 1998). The average crustal abundance of this element is ~0.5 ppm. Hg is generally found in geological formations as a sulphide ore (cinnabar - HgS), while it is also found as a trace element in other naturally occurring deposits, e.g. coal (Dabrowski, 2010). Although Hg is relatively inert, as indicated by its oxidation potential (E = -0.854 V for $Hg = Hg^{2+} + 2e^-$), it readily combines with noble metals (Au. Ag, Pt, Pd) to form amalgams (Schroeder & Munthe, 1998). This element has been directly mobilised by humans into aquatic and terrestrial ecosystems through mining, precious metal extraction, as well as through its use in certain products manufacturing (e.g., paint, electronic devices) and as a catalyst in the chlor-alkali industry (Driscoll et al., 2013). The commercial extraction of Hg entails the heating of cinnabar ore is heated in air from which Hg vapour is condensed:

$$\mathbf{HgS + O_2\ (600^{\circ}C) \rightarrow Hg + SO_2} \qquad \mathbf{[2.1]}$$

During the Industrial Revolution Hg was used increasingly in commerce, industry, mining, metallurgy, manufacturing, medicine and dentistry due to its useful properties. These unique and/or technologically important physical and chemical properties include high surface tension, high specific gravity (13.55 at 20°C), low electrical resistance, and a constant volume of expansion over the entire temperature range of its liquid state. The latter the reason for Hg commonly used in thermometers. The melting point of mercury is -39°C and it boils at 357°C at 1 atm, meaning it is the only metal that is a liquid at STP (Schroeder &

Munthe, 1998). If not enclosed at room temperature, Hg can evaporate and form colourless and odourless vapours UNEP Chemicals Branch, 2008).

In addition to the natural sources of Hg, the increased anthropogenic uses of Hg during the industrial age resulted in increased mobilisation of Hg in in the environment (UNEP Chemicals Branch, 2008). Deposition studies conducted by Lindberg et al. (2007) and Drevnick et al. (2011) from lake sediments, peat cores and ice cores indicate that atmospheric Hg deposition has increased globally by a factor of ~3 since preindustrial times. The mobilisation of Hg between the surface of the earth and the atmosphere is of specific interest to this study.

2.1.2. Hg speciation

The properties of Hg depend on its oxidation state and the species it is associated with in compounds. Therefore it is important to understand Hg speciation. Speciation of gaseous Hg species is very important to control mercury emissions into the atmosphere. Hg has seven stable isotopes with characteristic isotope patterns, as well as four unstable (radioactive) isotopes (Schroeder & Munthe, 1998). Although Hg can exist in three oxidation states, i.e. 0, +1 and +2, it exists predominantly in the elemental form (Hg^0) and in the divalent (Hg^{2+}) oxidised state (Kim & Zoh, 2012; Schroeder & Munthe, 1998) under atmospheric conditions. Its elemental form or gaseous elemental mercury (GEM/Hg^0), has an atmospheric residence time ranging between 6 to 18 months (Stephens et al. 2012; Gworek et. al., 2017), enabling long-range transport around the globe. In contrast, gaseous oxidised mercury (GOM/Hg^{2+}) that consists of reactive gaseous mercury (RGM) and particulate bound mercury (PBM) is more reactive, water-soluble and semi-volatile, which therefore has shorter atmospheric residencies (Stephens et al. 2012). Residence times of GOM species are estimated to range between hours and days (Gworek et. al., 2017). Thus, they are deposited relatively quickly from air with their impacts mainly on a local or regional scale. Although most (95-98%) tropospheric Hg emissions occur as GEM, Hg is also emitted as GOM (Lindberg et al., 2002). Total gaseous mercury (TGM) - the specie measured during this study - includes both elemental and oxidised species (TGM = GEM + GOM). The contribution of RGM (Hg^{2+}) is typically less than 5% of the TGM concentration in the atmosphere (Kim & Zoh, 2012).

The atmospheric transformation from GEM to GOM has been intensively researched during the last decade, and these processes are explained later in Section (2.4). Once GOM has been deposited, it is likely to undergo additional reactions, transforming it into methylmercury (MeHg). This process, as well as the toxicological and accumulation effects of MeHg will be elaborated on in Section 2.1.3. Various chemical reactions can transform deposited Hg to

GEM, which can be readily re-emitted (see Section 2.2.4), (UNEP Chemicals Branch, 2008). The characterisation of atmospheric chemistry of Hg thus controls the spread of Hg contamination from industrial and natural sources to distant ecosystems (refer to Fig. 2.1 in Section 2.2).

2.1.3. Hg toxicity

Driscoll et al., (2013) concluded that the key link between Hg emitted into the environment, and human and animal exposure is the net production of MeHg. Deposited Hg in soil and water is transformed into the highly toxic MeHg primarily through microbial processes. MeHg has the ability to bio-accumulate more than a million-fold in the aquatic food chain, resulting in elevated concentrations in organisms higher up in the food chain (UNEP Chemicals Branch, 2008) (Driscoll et al., 2013). MeHg enters the food chain, primarily through fish consuming bacteria or plankton. As these smaller organisms are consumed by larger entities, MeHg bio-accumulates resulting in increased levels with each step up the food chain, and ultimately human exposure (Clean Air Network, 1999). This bio-accumulation of MeHg is the main concern associated with mobilisation of Hg into the biosphere (Schroeder & Munthe, 1998). More than 90% of elevated human exposure to MeHg is due to food intake (Kim & Zoh, 2012), primarily from dietary consumption of estuarine and marine fish (Driscoll et al., 2013). Globally, fish provides >1.5 billion people with ±20% of their average intake of animal protein (FAO, 2011). Therefore, the widespread contamination of fish by MeHg is a global threat to human health, resulting in regulatory fish consumption guidelines and health advisories worldwide (Schroeder & Munthe, 1998).

MeHg concentrations in fish have been the topic on numerous studies. Driscoll et al., (2013) compiled a review of Hg concentrations in 36 fish species (34 300 samples), which amongst other findings showed the following:

- fish at the top of the marine food chain such as tuna and swordfish have the highest MeHg concentrations;
- mackerel and sardines from the Mediterranean Sea contain more MeHg compared to other harvesting areas;
- molluscs and crustaceans have relatively low MeHg concentrations (below 100 ng g^{-1}) (Sioen et al., 2007);
- within-species Hg concentration variability often exceeds the interspecies variability (FAO/WHO, 2011).

The understanding of the dose−response relationship between MeHg exposure and its toxic effects has also improved in recent times. Important information was obtained from

observations of the MeHg poisoning incident in Minamata, Japan. During this incident more than 2000 people consumed fish contaminated MeHg with the total Hg concentrations exceeding 10 $\mu g.g^{-1}$, which caused several neurological disorders collectively known as Minamata disease (Harada, 1968). Exposure levels 27 times higher than reference areas were observed in pregnant women in Minamata (Sakamoto et al., 2010). MeHg is able to penetrate the placenta (Schroeder & Munthe, 1998; Kim & Zoh, 2012), which is why developing foetuses are most at risk from this neurotoxin. At Minamata, exposed foetuses displayed severe symptoms similar to those showed by cerebral palsy patients i.e., microcephaly, blindness, severe mental and physical developmental retardation, which was even observed for infants born from mothers in that area who had mild or no indications of poisoning (Kim & Zoh, 2012). In addition, pre- or postnatal exposure to increased MeHg were found to cause long-term psychiatric symptoms, impairment of intelligence and mood, as well as behavioural dysfunction in adults (Yorifuji et al., 2011). This may be due to ability of MeHg to cross the blood-brain barrier, which normally protects the human brain from toxins in the blood stream (Schroeder & Munthe, 1998).

Studies on infants and young children exposed to MeHg during foetal development due to fish consumption during pregnancy, yields convincing evidence of neurological and associated developmental deficiencies. Driscoll et al., (2013) and the references therein presented comprehensive studies of neurobehavioral development in children in populations consuming large amounts of fish/seafood. The median maternal hair Hg concentration from these studies varied between 4.27 and 8.3 $\mu g.g^{-1}$. The relationship established between maternal hair Hg concentrations and child IQ suggested a loss of 0.18 IQ points (95% confidence interval, −0.378 to −0.009) per 1 $\mu g.g^{-1}$ increase of maternal hair Hg (Axelrad et al., 2007). These studies have resulted in a derived reference dose (RfD) suggested by the U.S. Environmental Protection Agency (EPA), which suggests a daily MeHg intake of 0.1 $\mu g.kg\ body\ weight^{-1}.d^{-1}$ to prevent appreciable risk of harmful effects during a lifetime (Rice et al., 2003). The magnitude of this public health problem is illustrated by between 3 and 15% of women in the U.S. (Mahaffey et al., 2009) and 27.7% of woman in Korea (Kim & Lee, 2010) at child bearing ages exceeding this RfD. The estimated lethal dose for ingested MeHg ranges from 1.4 to 4.2 g for an adult, depending on body weight (US EPA, 1992; Trüe, 2010).

Although studies on MeHg exposure is focused on human health, some researchers have shifted their attention to the impact of MeHg on the condition of fish and other wildlife. Lethal and sub-lethal effects on fish were only observed for exceptionally high MeHg concentrations, i.e. in the range of 5-10 $\mu g.g^{-1}$ (Wiener & Spry, 1996). It was also recently

shown that fish reproduction and embryonic development is compromised by MeHg uptake, while changes in biochemical processes, as well as damage to cells and tissue were observed. In addition to fish, alarmingly high MeHg concentrations are also found in fish-eating birds and mammals (Clean Air Network, 1999), which causes hormonal changes, impairment of motor skills and decline in reproduction (Bowerman et al., 2002; Yates, et al., 2005) in these species. This resulted in a wildlife criterion value of 3.0 $\mu g.g^{-1}$ MeHg to be established (Evers et al., 2004), which is equivalent to levels observed in animals in eastern North America (Evers et al., 2007). Insectivorous songbirds and bats have shown elevated levels of Hg, in particular species in wetland habitats associated with methylation processes (Evers et al., 2012). These observations should raise concern as it demonstrate that elevated Hg can affect the health of key wildlife species in diverse ecosystems. For example, Hg poisoning was attributed to be the major factor for the death of an endangered Florida panther species, which scientists believe was feeding on fish-eating raccoons (Clean Air Network, 1999).

These environmental impacts of elevated Hg contamination, as well as increased exposure by humans and wildlife to toxic MeHg have prompted policy makers to limit Hg emissions and control its transport (Driscoll et al., 2013). Integration of environmental Hg science with national and international policies is an important objective of global pollution control efforts (Driscoll et al., 2013; UNEP Chemicals Branch, 2008).

2.2. The Hg cycle

It is important to understand the emission sources, fate, and transport mechanisms of Hg species in the environmental. Long term Hg monitoring at stations in the Northern and Southern Hemispheres indicates global atmospheric Hg concentrations have decreased by roughly 20-38% since 1996 (Slemr et al., 2011). This reduction is unusually large compared to most atmospheric trace gasses and is in conflict with current emission inventories indicating relatively constant anthropogenic emissions over this period. Thus, a major shift in the biogeochemical cycle of mercury including soil and ocean reservoirs is suggested. These changes are highly dependent on Hg residence times in water, substrate and air (Slemr et al., 2011).

Figure 2.1 shows a schematic diagram of the atmospheric Hg cycle. Once Hg is released into the planetary boundary layer (PBL) within the troposphere, Hg is subjected to a variety of physical and chemical processes. The majority of Hg that enters the atmosphere is GEM/Hg^0, whereas Hg is generally deposited on the surface as GOM/Hg^{2+}, which then forms MeHg. The complexity of atmospheric Hg is evident in Figure 2.1. In this scheme, the specific pathway(s) and the fate experienced by a given Hg species depend on numerous

factors, which include its physical and chemical characteristics, as well as the prevailing meteorological conditions (Schroeder & Munthe, 1998). There are several primary and secondary sources of atmospheric Hg, while atmospheric Hg is also deposited/removed through various processes.

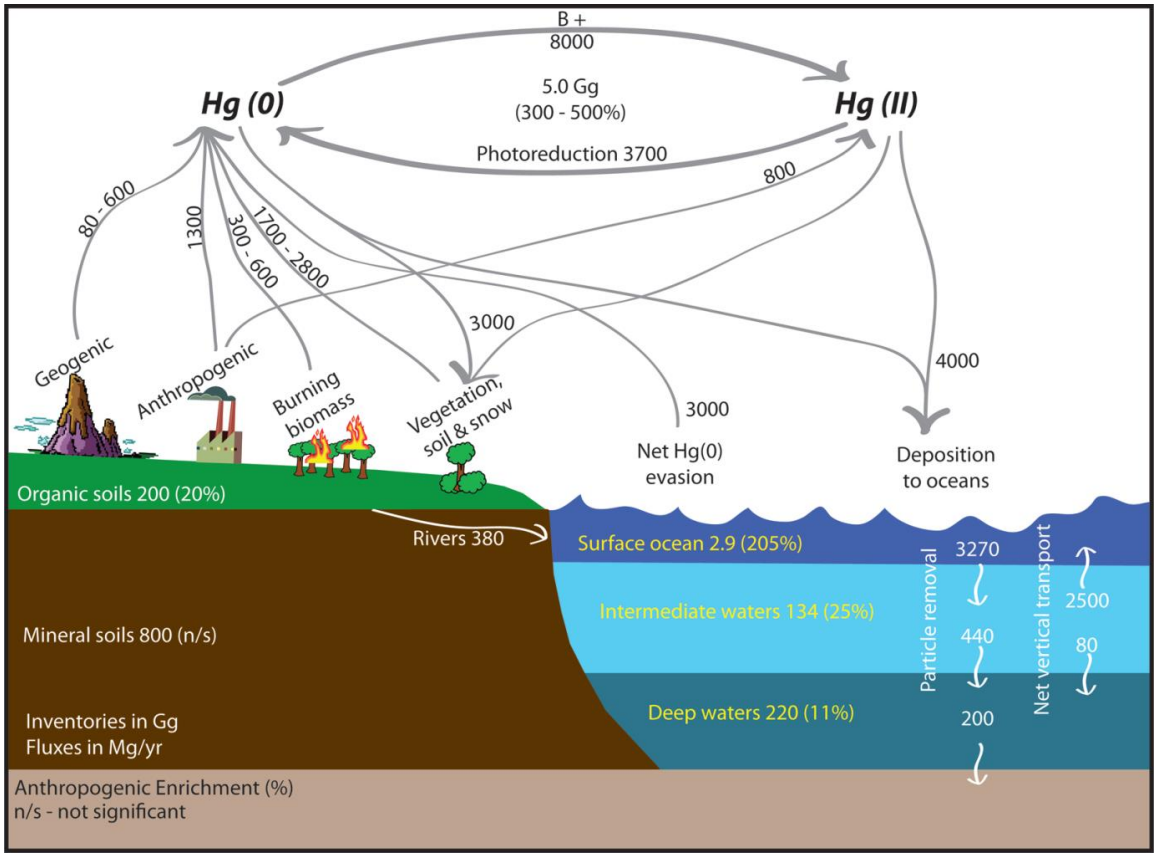

Figure 2.1: Current global atmospheric estimates for mercury emission and deposition at the Earth's surface. Hg(II) refers to GOM (RGM + PBM). The percentages in brackets are estimated increases in fluxes due to anthropogenic activities over the past 150 years. Fluxes are in t.yr^{-1} and reservoirs are given in Gigagram, i.e. 1 Gg = 1000 t (Driscoll et al., 2013).

Typical primary natural sources, include volcano and geothermal activity, wildfires, and weathering of rocks and soils. Anthropogenic primary sources include burning of fossil fuels, ore processing, and several other industrial processes e.g. the chlor-alkali industry. Furthermore, it is also found in numerous commercial and consumer products, which is released upon incineration (Driscoll et al., 2013). Deposited Hg can also be re-emitted (secondary source) in various ways from surface reservoirs (Driscoll et al., 2013; UNEP Chemicals Branch, 2008). Primary sources increase the global pool of Hg in surface reservoirs, while secondary sources redistribute Hg throughout ecosystems. The global quantification of these processes is very complex and several uncertainties exist, which is further complicated by complex Hg chemistry. In addition to local sources of Hg, the long range transport of Hg due to its relative persistent atmospheric lifetime can also contribute to increased Hg concentrations within a region. Furthermore, the long atmospheric lifetime of

Hg also results in relatively consistent background Hg concentrations (UNEP Chemicals Branch, 2008). Typical background atmospheric concentrations in the Northern Hemisphere range from 1.3 to 1.7 ng.m^{-3}, where somewhat lower Southern Hemisphere concentrations of 1.1 to 1.3 ng.m^{-3} are found. However, background Hg concentration in eastern Asia can be as high as 4 ng.m^{-3} (Sprovieri et al., 2010; Lindberg et al. 2007; Pirrone et al. 2008; Dommergue et al 2010).

2.2.1. Emissions

Driscoll et al., (2013) and the UNEP Chemicals Branch (2008) referenced recent global assessments and associated modelling studies, which has improved our understanding of Hg emissions from both primary and secondary sources, as well as their atmospheric transport and deposition. Long-term temporal emissions trends were also investigated by the UNEP Chemicals Branch (2008), indicating that global anthropogenic Hg emitted into the atmosphere in 1990 were estimated at about 1910 tonnes. In 1995, the estimated emissions increased to approximately 2050 tonnes, and by 2000 the emissions decreased to approximately 1930 tonnes. These decreases were attributed to the introduction of emission control technologies in Europe and North America. However, during this period emissions in Asia, South America, Africa and Oceania increased moderately due to economic growth. Thus, if emission controls were expanded worldwide, Hg emissions from anthropogenic sources could even drop further. (Schroeder & Munthe, 1998). The major contributors to global natural Hg emissions are indicated in Figure 2.2. Currently, the total global natural Hg emissions into the atmosphere are estimated to range from 6500 to 8200 t.y^{-1}. Oceanic Hg emissions are the main natural sources contributing 51% followed by biomass burning (13%) (Pirrone, 2010). Primary emissions from natural geogenic sources i.e. volcanoes and erosion, were estimated to be 500 t.y^{-1}. The apportionment of global anthropogenic emissions is indicated in Figure 2.3. Primary anthropogenic Hg sources emitted 1900−2900 t.y^{-1} (Driscoll et al., 2013). The Hg emissions from fuel combustion, waste incineration, and mining was estimated to be 2100 t.y^{-1}. Driscoll et al., (2013) compared the primary emission source factor, which increased by a factor of 2−15 (due to human activity), with the afore-mentioned factor of 3 for average increase in Hg deposition, and states that the Earth system is not in a steady-state, and that Hg in surface reservoirs will continue to increase even if future anthropogenic emissions remain constant.

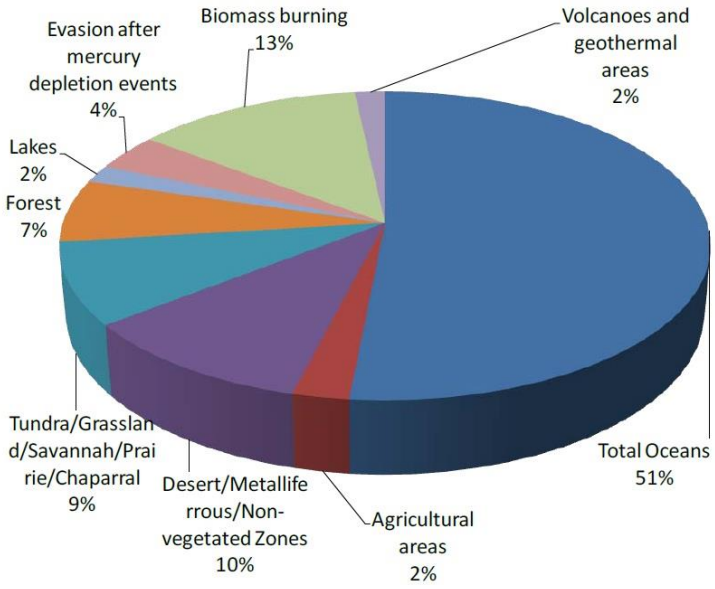

Figure 2.2: Global distribution percentages of natural mercury emissions (Pirrone, 2010).

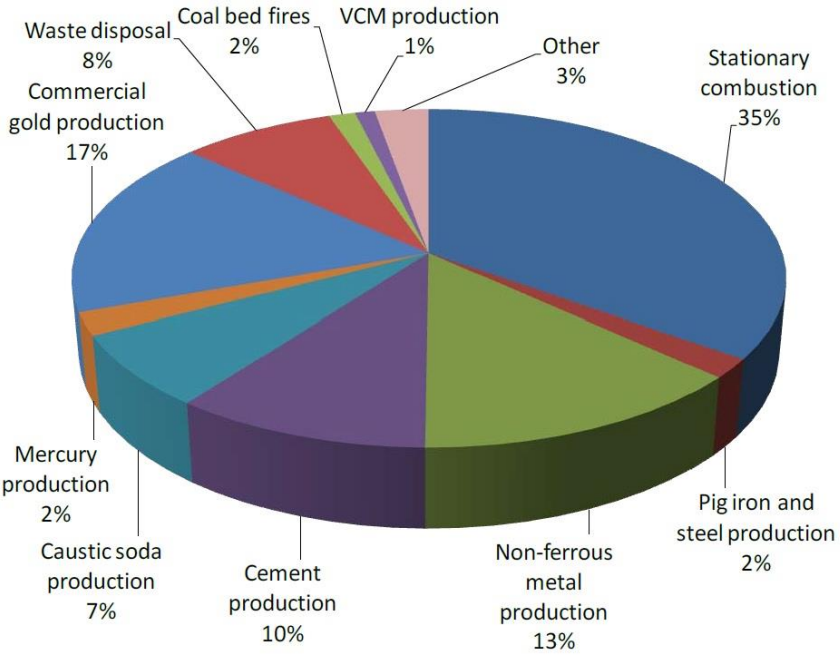

Figure 2.3: Global distribution percentages of anthropogenic mercury emissions (Pirrone, 2010)

The burning of fossil fuels, primarily coal, is the major source of emissions from human activities, accounting for 35% of the global anthropogenic Hg emissions. A recent modelling study over Europe suggests coal and lignite combustion for power generation are the largest Hg sources, contributing 60% to the total Hg. (Rafaj et al., 2014). Industrial gold production is responsible for approximately 17%, whereas various metal production activities contribute approximately 15%. Cement production contributes 10%, followed by numerous smaller, but not insignificant, anthropogenic emissions sources (Pirrone, 2010). Non-combustion processes emit mainly GEM. However, approximately 50% of Hg emissions associated with combustion processes is GOM (Streets et al. 2011), which includes RGM and PBM. This partitioning of emissions is of considerable importance, since quicker deposition of GOM result in a local deposition enhancement, rather than a global influence associated with GEM emissions (Driscoll et al., 2013). Schroeder & Munthe, 1998 also stated that PBM may originate from certain natural sources (e.g. volcanoes, soil erosion or biomass burning). For example, Timonen et al., (2013), and Murphy et al., (2006) reported PBM concentrations below 30 $pg.m^{-3}$ in the free troposphere (FT), whereas elevated PBM concentrations (30–45 $pg.m^{-3}$) were observed during biomass burning episodes.

2.2.2. Transport

Emitted Hg, especially GEM, can be thoroughly mixed vertically in the troposphere, which allows for global transport before being deposited. Thus, understanding the transport of atmospheric Hg is important. The atmosphere is the most important transport pathway of Hg emissions, while the redistribution of Hg in terrestrial, freshwater, and marine ecosystems (and the production of MeHg) occur through land and ocean processes (Driscoll et al., 2013). Hg transport in the atmosphere and its transfer to ecosystems depend primarily on its chemical and physical forms. As mentioned, due to the inert nature of GEM it can be transported over long distances on local, regional, and global scales before being oxidised and deposited. Kim & Zoh (2012), for instance, indicate high MeHg concentrations in fish in non-industrial areas, even as far as the Arctic. This is also attributed to accumulation of re-emitted Hg via air-soil and air-water interfaces, which will be discussed in Section 2.2.4.

As mentioned previously, GOM (RGM and PBM) are generally deposited locally or regionally due to their shorter atmospheric residence time (Driscoll et al., 2013). However, long range transport of GOM can occur, after vertical mixing of Hg and its oxidants (or oxidant precursors) to the free troposphere and subsequent oxidation of GEM. During long-range transport to downwind regions, the conversion to RGM can occur on relatively short timescales (several days) in the free troposphere, where photochemical conditions are expected to be more favourable for accumulation and transport of secondary RGM (Timonen

et al., 2013). Eventually the generated RGM will be entrained back to the boundary layer (Lyman and Gustin, 2009), followed by deposition and subsequent incorporation to the bio-system. A few Hg studies above the boundary layer cited by Timonen et al. (2013) demonstrated that the free troposphere is depleted in GEM and enriched in GOM.

Detailed information on transport and transformation of Hg in the free troposphere is limited due to a poor understanding of RGM sources, lacking long-term measurements at high altitudes (Timonen et al., 2013), and the uncertainty associated with exact oxidants of GEM (Holmes, 2012). Although more studies of Hg in the free troposphere are needed to better understand its atmospheric chemistry, Timonen et al. (2013) indicated that changes in RGM partitioning during transport contributes to high observed RGM concentrations during marine boundary layer mixing events. The eventual fate of all atmospheric Hg is being deposited on a variety of available interfaces.

2.2.3. Deposition

As expected, Hg deposition increased concurrently with the increase in global emissions, with sediments typically containing roughly three times more Hg at present compared to pre-industrial times (UNEP Chemicals Branch, 2008). Atmospheric conditions (e.g. wind direction, oxidant concentrations, temperature) are in many instances more important for governing deposition than proximity to Hg sources (Sprovieri et al., 2010; Holmes et al., 2010). Hg mostly removed from the atmosphere as GOM, which has dry deposition and wet scavenging rates approximately an order of magnitude higher compared to GEM (Lindberg et al., 2002; Kim & Zoh, 2012). Lindberg et al. (2007) also stated the slow removal of GEM from the atmosphere via wet and dry deposition, due to its very low water solubility. On the other hand, GOM species are removed rapidly because of their higher water solubility and reactivity with surfaces. Consequently, as mentioned previously, the atmospheric lifetime of Hg is directly correlated to the transformations between these two oxidation states. In other words, oxidation ($Hg^0 \rightarrow Hg^{2+}$) increases atmospheric deposition, and reduction ($Hg^{2+} \rightarrow Hg^0$) decreases atmospheric deposition (increasing atmospheric residence time). Thus, it is essential to understand the redox processes influencing the speciation of Hg in the atmosphere. In addition, an understanding of the sorption of gaseous Hg species to particulate matter (PM) is also important, because gas-to-particle conversion also affects Hg deposition (Lindberg et al., 2007).

Hg deposition is also greatly influenced by altitude with modelling studies conducted by Nair et al., (2013), suggesting that 60% of Hg deposited to the surface in rainwater originates from above the boundary layer (> 2km). Their model assumes that soluble Hg (i.e. GOM) concentrations are initially vertically uniform. Thus, the free troposphere could supply a

larger fraction of deposited Hg through wet deposition if GOM and PBM concentrations increase with altitude, as other studies suggested (Timonen et al., 2013; Holmes et al., 2010; Selin et al., 2007; Lyman and Jaffe, 2011). Although the model used idealised simulations, it accurately depicts wet scavenging by stratiform (low-level) and thunderstorm events (Nair et al., 2013). Stratiform clouds scavenge Hg from the lowest ±4 km of the atmosphere, while thunderstorms can scavenge up to ±10 km, yielding higher Hg concentrations.

After deposition, Hg is either adsorbed into sediments and water where it can be transformed to MeHg through microbial activity (as previously discussed in Section 2.1.3), or be reduced to dissolved gaseous mercury (DGM) in water (Holmes 2012; Tokos et al., 1998). DGM, a form of Hg^0, can be produced in surface waters by aqueous photo-reduction of RGM, which can be accelerated by various physical and chemical environmental conditions, including light intensity, water temperature, pH, and the concentration of dissolved organic matter (Amyot et al., 1997; Zhang et al., 2001; Kim & Zoh, 2012). Atmospheric deposition is the most important pathway for Hg to enter the terrestrial and marine environment. However, Hg deposited on land is retained mostly by soils and vegetation, representing a pool for further remobilisation (Kocman et al., 2013). The total global pre-industrial soil Hg burden for the top 15 cm of soil is estimated to be in the order of 10^6 t, with human activities enhancing this burden by approximately 15% (Selin, 2009). Hg in soil can be transported to aquatic systems via leaching, runoff and erosion processes (Kocman et al., 2013), causing further contamination and increases risk of methylation. Releases of Hg from undersea hydrothermal vents to open oceans also contributes to environmental Hg, which is estimated to be ±600 $t.y^{-1}$ globally (Kocman et al., 2013; Mason et al., 2012).

2.2.4. Re-emissions

A characteristic of Hg that sets it apart from other metals commonly found in the atmosphere, is its specific property to be continuously recycled between air and water phases (Schroeder & Munthe, 1998). Deposited Hg can be re-emitted (secondary source) in various ways from surface reservoirs (Driscoll et al., 2013; UNEP Chemicals Branch, 2008), which mainly entail deposited RGM being photo-reduced to elemental Hg and emitted from the surface (Lindberg et al., 2002). Re-emission of Hg into the atmosphere contribute to more uncertainty regarding natural emissions, since it is particularly difficult to distinguish between natural and anthropogenic emissions associated with re-emissions (Gworek et. al., 2017). Re-emissions from substrates and water also further enhances long distance transport via the grasshopper effect, allowing pollutants to travel further than expected in a series of deposition and re-emission ‘hops’ (UNEP Chemicals Branch, 2008). As a result of

this sort of transport, Hg may be accumulated in the Polar Regions, where conditions are less favourable for re-emission (Ebinghaus et al., 2002; Lindberg et al., 2002).

Several complex processes exists at the interface between the atmosphere and surface, which are mostly photolytic processes, although thermal and biological processes also play a role. For instance, DGM can be re-emitted from water to the atmosphere by volatilisation, which is the only process that removes GEM from aquatic systems, and possibly limit MeHg production and accumulation in fish (Kim & Zoh, 2012). Another example is the removal of the more reactive GOM species, where photolytic reduction of GOM in the surface layer of the ocean, results in the re-emission of GEM to the atmosphere (Pirrone et al., 2013). Approximately 75% of the total Hg in soils are concentrated in the organic-rich A horizon (top layer), resulting in huge pools that can be re-mobilised from air-soil interfaces. Volatilisation of Hg from soils and rocks has been shown to be a significant source of atmospheric Hg (Engle et al. 2005). Several experiments were performed by Engle et al. (2005) to investigate Hg emissions from soils, who indicated that O_3 interaction with substrates either increases the Hg^{2+} to Hg^0 conversion rate that is subsequently emitted, or promotes the volatilisation of existing Hg^0. Furthermore, they developed conservative calculation methods, from which they conclude that since O_3 concentrations have roughly doubled (from 10 to 20 ppb) in the last 100 years; it could have resulted in a 65–72% increase in Hg^0 emissions from terrestrial substrates, and are likely to continue to increase with time (Engle et al. 2005). In addition to chemical mechanisms, the emission of Hg from substrates are also influenced by many other factors, such as light intensity (radiation), soil gas concentration, precipitation, temperature and Hg concentration and speciation in the substrate (Gustin et al., 2000). Although the relative importance of each factor is not clearly understood, Hg concentration in the substrate is seen as an important parameter controlling Hg flux from naturally enriched areas.

Overall, numerous global models of Hg cycling suggest annual contribution of re-emissions from soils to be 1700–2800 $t.y^{-1}$ and oceans contributing 2000–2950 $t.y^{-1}$ (Kocman et al., 2013). Although anthropogenic and natural components of re-emissions cannot be distinguished from another, the relative proportions are likely to be similar to the original emissions. In addition, re-emission of Hg is increased by anthropogenic activities (Kocman et al., 2013). Biomass burning (wildfires) have the potential to volatilise deposited Hg in terrestrial surfaces. This must be considered an important global source, even when using conservative estimates (ranging from 300 to 600 $t.y^{-1}$), and perhaps the major source in the Southern Hemisphere (Lindberg et al. 2007). Measurements of total gaseous Hg at Cape

Point, suggested that biomass burning could be a substantial and neglected source of Hg in the southern Hemisphere (Brunke et al., 2001).

2.3. Chemistry

As mentioned previously, the largest fraction of airborne Hg is in the GEM form, which is relatively inert (UNEP Chemicals Branch, 2008). Atmospheric oxidation of GEM generates gas- and particle-phase GOM compounds, primarily inorganic Hg^{2+} species that deposit quickly as they are more reactive, more water-soluble, and less volatile (Schroeder & Munthe, 1998; Lin & Pehkonen, 1999; Holmes et al., 2009). Any process that reduces the atmospheric lifetime of Hg increases its potential accumulation in the biosphere, which is why an understanding of the oxidation processes of GEM to RGM or GOM is of utmost importance.

Until recently, most models assumed that gaseous hydroxyl radicals ($HO^{\bullet}$) and gaseous ozone (O_3) are the main global oxidants of Hg^0, which is probably attributed to the strong correlation between oxidation of Hg^0 and O_3 depletion. However, this correlation does not necessarily imply that O_3 is directly responsible for the oxidation of Hg^0, as O_3 also correlates negatively with other pollutants (Jia and Xu, 2014). Some thermodynamic considerations also argue against the importance of the O_3 oxidation mechanism of Hg^0 (Holmes et al., 2010; Calvert and Lindberg, 2005), while studies also imply that O_3 alone cannot explain the observed seasonal and diurnal variations of atmospheric Hg. Studies have also shown that the gas phase oxidation of Hg^0 by O_3 is also very slow under atmospheric conditions (Hynes et al., 2009; Dibble et al., 2012), while laboratory kinetic studies consistently indicate that O_3 exhibits a second order kinetic gas-phase mechanism for oxidation of Hg^0. Furthermore, due to the rapid thermal dissociation of HgOH, oxidation of Hg^0 by $HO^{\bullet}$ is much slower than previously reported and is insignificant under atmospheric conditions (Calvert and Lindberg, 2005). These inconsistencies resulted in intensive studies aimed at clarifying uncertainties associated with oxidation processes of Hg^0 under environmental conditions. These studies suggested that Hg^0 oxidation mechanisms may be mediated by complex/unstable intermediate species and by surfaces (Hynes et al., 2009; Subir et al., 2012) or by photochemical processes (Holmes et al., 2010).

A major development in recent work is the oxidation of Hg^0 by Br atoms and related radicals (Holmes et al., 2010 & Rafaj et al. 2014), which reveal that Br oxidation of Hg^0 is most-likely the dominant global sink for Hg^0 in the marine boundary layer (MBL). This model reproduces spring depletion and summer rebound observed at polar sites, as well as a better simulation of Hg^0 oxidation during subsidence events over Antarctica (Holmes et al., 2010). The morning RGM increase and midday peaks are also consistent with oxidation of

Hg^0 by Br atoms in models. Oxidation of Hg^0 by Cl are indicated to be minor (3–7%) in the model (Holmes, 2010). In Figure 2.4 the dynamic atmospheric factors and species governing atmospheric Hg chemistry are presented. These reactions are typically used in air quality models utilised to model dispersion of atmospheric Hg (Rafaj et al. 2014). The most recent developments related to the reactions of Hg with bromine are considered in this schematic diagram

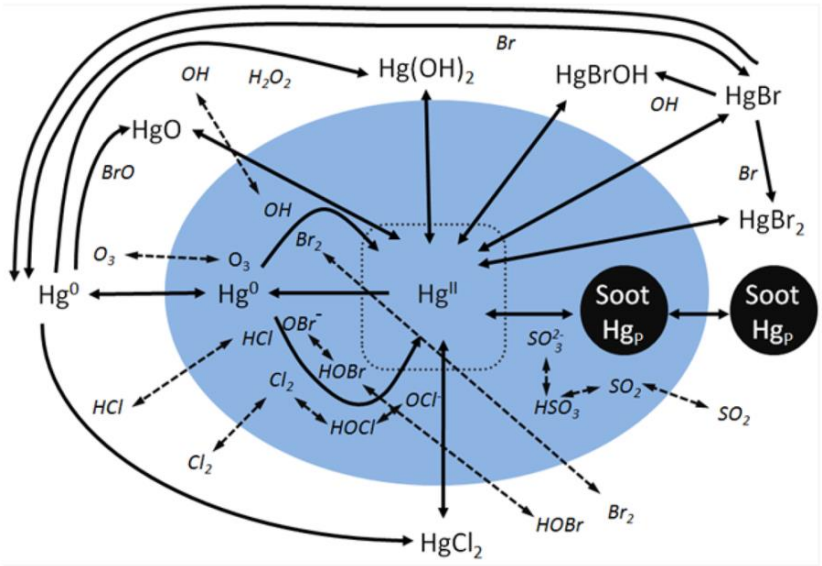

Figure 2.4: A chemical model for mercury, showing oxidation via several mechanisms. Gaseous and aqueous Hg phases are marked by white and blue, respectively. The line arrows show possible transformations of mercury, and the dashed arrows show additional species that react with mercury (Rafaj et al., 2014).

It is also evident from Figure 2.4 that the atmospheric cycling of Hg includes chemical oxidation/reduction in both gaseous and aqueous phases. Furthermore, while the kinetics of Br-initiated Hg^0 oxidation is better understood than by O_3, $HO^{\bullet}$, and $NO_3^{\bullet}$, the global distribution of Br radicals is highly uncertain (Timonen et al., 2013). Reactive halogens do exist at temperate and low latitudes, but their influence on Hg in the atmosphere outside Polar Regions has remained uncertain (Obrist et al., 2011). However, several known sources of reactive halogen species exist for the interior of South Africa exist, which include emissions from industry, fossil fuel burning, biomass burning (Afe, [s.a]) and pesticides (Andreae et al., 1996 & Manö & Andreae 1994).

Initial mechanisms for the reaction between Hg^0 and O_3 proposed that RGM is formed through rapid, *in-situ* oxidation of Hg^0 in the gaseous phase during Hg depletion events (Lindberg et al., 2002). The production of RGM is attributed to the same photochemical active halogen species involved in surface O_3 destruction, with a clear diurnal cycle, suggesting that the overall process is heterogeneous. Subsequent mechanisms relate to the

reaction between Hg^0 and halogen oxides or halogen atoms to produce HgO, $HgBr_2$, and $HgCl_2$. In this reaction mechanism, bromine ($Br^\bullet$) and chlorine ($Cl^\bullet$) radicals are produced from a heterogeneous photochemical mechanism involving sea-salt aerosols. Equation 2.2 shows the photochemical formation of these halogen radicals and halogen oxide radicals ($BrO^\bullet$, $ClO^\bullet$), which serves as the primary oxidants to produce RGM. (Lindberg et al., 2002):

$$\mathbf{Br_{aq}\ (Cl_{aq}) + \mathit{hv} \rightarrow Br^\bullet\ (Cl^\bullet) + O_3 \rightarrow BrO^\bullet\ (ClO^\bullet) + O_2} \qquad \mathbf{[2.2]}$$

$$\mathbf{BrO\ (ClO) + Hg^0 \rightarrow HgO + Br^\bullet\ (Cl^\bullet)} \qquad \mathbf{[2.3]}$$

$$\mathbf{Hg^0 + Br^\bullet\ (Cl^\bullet) \rightarrow HgBr\ (HgCl) + Br^\bullet\ (Cl^\bullet) \rightarrow HgBr_2\ (HgCl_2)} \qquad \mathbf{[2.4]}$$

This mechanism correspond to Hg^0 and O_3 concentrations during Hg plumes and associated O_3 depletion. Lindberg et al., (2002) suggested that the *in-situ* RGM formation is not likely caused by molecular Cl_2, Br_2 and BrCl, as these species are rapidly photolysed in sunlight (Dickerson et al., 1999). Considering the low concentrations of reaction species, Equation 2.3 would be the favourable pathway yielding HgO. However, recent studies indicate that the reaction between BrO (ClO) and Hg is most likely endothermic and not important at tropospheric temperatures. In fact, Tossell (2003) shows that HgO is almost certainly not a stable molecule.

Recent more widely accepted mechanisms utilise similar oxidants in revised combinations. These mechanisms involve the recombination reaction between Hg and $Br^\bullet$ (Equation 2.5), instead of the unstable HgO molecule. Studies show the reaction between Hg and $Br^\bullet$ is surprisingly fast, which is why reaction (2.5) is the prime candidate to initiate the oxidation of Hg (Goodsite et al., 2004). M is a third chemical species and $Y^\bullet$ presents Br, OH, Cl, HO_2, NO_2, BrO, IO, I or O_2. The rate at which HgBr decomposes (Equation -2.5) is also identified as the crucial factor in the conversion of Hg^0 to Hg^{2+}. Furthermore, there is competition between further addition of Br and Y to form $HgBr_2$ or HgBrY (Equation 2.6), and thermal decomposition of HgBr (Equation -2.5). Equation 2.6 is however predicted to be very fast at atmospheric pressures.

$$\mathbf{Hg^0 + Br^\bullet\ (+ M) \rightarrow HgBr} \qquad \mathbf{[2.5]}$$

$$\mathbf{HgBr\ (+ M) \rightarrow Hg + Br^\bullet} \qquad \mathbf{[-2.5]}$$

$$\mathbf{HgBr + Y^\bullet\ (+ M) \rightarrow HgBrY} \qquad \mathbf{[2.6]}$$

In Table 2.1 the rate coefficients of the most relevant reactions of Hg in the atmosphere are presented, which includes relevant oxidation mechanisms and take into account the main reactions occurring in the gaseous, aqueous and particulate phases.

	Reaction:	**Rate or equilibrium[1] Coefficients[2]**
1	$Hg^0 + O_3 \rightarrow HgO + O_2$	3.0×10^{-20}
2	$HgO_{(g)} \leftrightarrow HgO_{(aq)}$	K_{eq}[1]
3	$HgO_{(aq)} \rightarrow Hg^0_{(g)}$	1.12×10^{-5}
4	$Hg^0 + Cl$ [+ Br + M] $\rightarrow HgClBr$[3]	$2.2 \times 10^{-32} \times \exp(680\times (1/T - 1/298)) \times [M]$[4]
5	$HgClY_{(g)} \leftrightarrow HgClY_{(aq)}$[5]	K_{eq}[1]
6	$HgClY_{(aq)} \leftrightarrow Hg^0_{(g)}$	1.12×10^{-5}
7	$Hg^0 + Br + M \rightarrow HgBr$	$1.46 \times 10^{-32} \times (T/298)^{-1.86} \times [M]$
8	$HgBr + M \rightarrow Hg^0 + Br + M$	$4.0 \times 10^9 \times \exp(-7292/T)$
9	$HgBr_{(g)} \leftrightarrow HgBr_{(aq)}$	K_{eq}[1]
10	$HgBr + Y \rightarrow HgBrY$	$2.5 \times 10^{-10} \times (T/298)^{-0.57}$
11	$HgBr + Br \rightarrow Hg^0 + Br_2$	3.9×10^{-11}
12	$HgBrY_{(g)} \leftrightarrow HgBrY_{(aq)}$	K_{eq}[1]
13	$HgBrY_{(aq)} \rightarrow Hg^0_{(g)}$	1.12×10^{-5}
14	$HgBr + X \rightarrow HgBrX$[6]	1×10^{-10}
15	$HgBrX_{(g)} \leftrightarrow HgBrX_{(aq)}$	K_{eq}[1]
16	$HgBrX_{(aq)} \rightarrow Hg^0_{(g)}$	1.12×10^{-5}
Notes:		
[1]	Equilibrium coefficient is parameterised by $K_{eq} = (SA-PM)/10^{((-4250/T)+10)}$, where SA = the specific aerosol surface area, and PM = the particulate mass.	
[2]	Rate coefficients are given in either $cm^3\ molec^{-1}\ s^{-1}$ or s^{-1}.	
[3]	Assumes $Hg^0 + Cl \rightarrow HgCl$ is rate limiting, followed quickly by $HgCl + Br \rightarrow HgClBr$	
[4]	[M] is the number density of air in molecules cm-3	
[5]	Y = $Br^{\bullet}$, $HO^{\bullet}$.	
[6]	X = HO_2, NO_2, BrO, IO, I.	

Table 2.1: Summary of atmospheric mercury reactions. Rate or equilibrium coefficients and parameterisations can be found in Coburn et al., (2015), and the references therein.

O_3 also plays an important role in Hg oxidation precursors. The formation of most of the Hg oxidants (e.g. Br, OH, Cl, HO_2 and BrO) in the atmosphere is mediated by O_3. In addition, the reaction with Br has been recognised as the primary pathway for ozone depletion, which is accompanied by RGM production (Lindberg et al., 2002; Parella et. al., 2012). During this "bromine explosion" mechanism, gas-phase Br reacts with O_3 – producing O_2 and BrO (Equation 2.2), followed by heterogeneous surface reactions resulting in the release of additional reactive Br, which drives HgBr formation (Equation 2.5), increasing TGM

deposition through scavenging by reactive radicals (Equation 2.6). The importance of relative humidity (RH) for free radical formation should also be emphasised.

Studies have shown that a mechanism based on the initial recombination of Hg with Br (Equation 2.5), followed by addition of a second radical (Equation 2.6) in competition with thermal dissociation of HgBr (Equation -2.5), is able to account for the observed rate of Hg^0 removal in Arctic depletion events and on a global scale (Goodsite et al. 2004). Nevertheless, oxidation of Hg in the atmosphere is very sensitive to temperature and Br concentration, because of the instability of HgBr (Goodsite et al. 2012). The influence of reactive halogens on atmospheric Hg outside cold polar regions (and especially in the southern Hemisphere) remains uncertain (Obrist et al., 2011). However, Obrist et al. (2011) indicated near-complete (up to 90%) conversion of Hg^0 to Hg^{2+} by Br and BrO in the warm Dead Sea atmosphere in their modelling study. It was concluded that the reaction kinetics are highly temperature dependent, specifically the thermal back-dissociation of HgBr (Equation -2.5), which is a crucial rate limiting reaction more than two orders of magnitude faster under mid-summer Dead Sea conditions compared with cold Arctic temperatures (Obrist et al., 2011). Martínez-Coronado et al. (2016) also stated that RGM appears to be more dependent on factors involved in photolysis processes (temperature) than the availability of primary contaminants or RGM transport processes from other areas. Generally photolysis reactions are also more active when irradiation is more intense (Martínez-Coronado et al., 2016). In addition, the southern hemisphere has slightly faster oxidation than the northern hemisphere due to the oceanic source of bromo-carbons and high temperatures experienced.

2.4. Influence of atmospheric properties on Hg chemistry

Timonen et al. (2013) identified three main types of air mass regimes influencing the oxidation mechanisms converting GEM to RGM:

Type 1. Dry upper tropospheric air with high O_3 and RGM concentrations, which is likely to be associated with $Br^{\bullet}$ chemistry. In the upper troposphere-lower stratosphere region $Br^{\bullet}$ is expected to be abundant and cold temperatures favour the stability of $HgBr^{\bullet}$ (Goodsite et al., 2004, 2012; Holmes et al., 2010; Dibble et al., 2012; Parrella et al., 2012).

Type 2. Aged anthropogenic emissions with elevated Hg concentrations occurring simultaneously with increased in RGM levels and tracer species of anthropogenic pollution plumes. This suggests that the oxidant responsible for RGM production might also be associated with anthropogenic pollution, which supports the previously mentioned mechanisms (Section 2.3). O_3, HO, and NO_3/NO_2 radicals may all play a role in Hg^0

oxidation, while halogen chemistry could also contribute during these events. Oxidation via heterogeneous chemistry involving aerosol particles can also occur (Subir et al., 2012).

Type 3. Clean air with background Hg and a potential contribution from natural oceanic emissions. These events exhibit a clear anti-correlation between RGM and O_3, indicating that O_3 is not likely the primary oxidant. Also, as these events are only seen in clean air masses, it seems unlikely that the oxidant would have an anthropogenic origin (e.g., $NO_3^{\bullet}$). Timonen et al. (2013) suggested that reactive halogens are the most likely oxidants during these events, although O_3/$HO^{\bullet}$ cannot be entirely ruled out. During type 3 events, Hg^0 oxidation by halogens results in very high RGM that can subsequently undergo long-range transport in the upper troposphere (Timonen et al., 2013).

This approach of classifying different air type regimes associated with different oxidation mechanisms governing conversion of GEM to RGM, can also be useful in this study as the different location of each of the measurement sites contribute to variable chemical mechanisms that may be site specific.

2.5. Sources of primary oxidants (halogens)

Andreae et al., (1996) quantified methyl halide (CH_3Br, CH_3Cl, & CH_3I.) emissions from savannah fires in southern Africa, and found that these species were significantly enhanced in smoke plumes (smouldering phase). It was deducted that savannah fires make a significant - if not the largest (Lobert et al., 1999) - contribution to the atmospheric budget of CH_3Cl and CH_3Br. The halogen concentrations in savannah fuels are considerably higher than those in most forest fuels. The generally high chloride content in savannah vegetation contributed to very high levels of chloride occurring in aerosols and precipitation during biomass burning events in southern Africa (Andreae et al., 1996). Using emission ratio estimates, it was calculated that the global annual CH_3Cl contribution of savannah fires alone amounts to approximately 420 000 $t.yr^{-1}$, which is almost a third of the total pyrogenic CH_3Cl emission of 1100 000-1500 000 $t.yr^{-1}$. Furthermore, savannah fires also make a modest contribution (± 7 000 $t.yr^{-1}$) to the global emissions of CH_3Br (± 100 000 $t.yr^{-1}$) (Andreae et al., 1996). Similarly, Blake et al., (1996) estimated that ~25% and ~20% of global CH_3Cl and CH_3Br emissions, respectively can be derived from biomass burning.

In addition to biomass burning, smouldering combustion associated with household combustion, coal-fired power plants and coal dumps can also contribute to halogen emissions. Also, garbage burning, which is a poorly characterised emission source that can be significant in urban-rural areas of developing and developed nations, were found to be a main global source of toxic chlorinated compounds (Akagi et al., 2011). The halogen

emission factors depend both on the proportion of flaming to smouldering combustion and on the halogen content of the fuel (Andreae et al. 2001). Roughly 90% of the halogen content of the fuel burned is released into the atmosphere, mostly as halide species, and a significant fraction (3-38%) is emitted in methylated form (Andreae et al., 1996; Fabian et al., 1999). Global emissions of methyl bromide from combustion processes and biomass burning is comparable to the amount produced by ocean emission and pesticide use, although the overall uncertainty is considered to be large (Manö & Andreae, 1994; Fabian et al., 1999).

The distribution of Hg and halogens in coal is an important factor in determining the amount of Hg emitted into the atmosphere by coal combustion (Kolker et al., 2012). Generally, low rank coals (widely used in SA) have lower Hg and halogen content than bituminous coals. However, greater amounts of these coals should be used achieve an equivalent energy output (Kolker & Quick, 2015). Interestingly, halogen species in coal can also assist in reducing Hg emissions into the atmosphere from modern coal-fired power plants fitted with either Air-Pollution Control Devices (APCDs), or scrubbers to primarily remove SO_2, NO_x and dust. Hg in coal exists mainly as Hg^0, which is unreactive and insoluble, making it unable to be captured by APCDs or scrubbers (Kolker et al., 2012; UNEP Chemicals Branch, 2008). However, halogens can convert Hg^0 to GOM at coal combustion temperatures, which can either be directly removed by scrubbers, or it can combine with halogens to form Hg-halogen complexes that are much more readily captured by APCDs. Cl is the most abundant halogen in coal, and it has the largest influence on Hg oxidation and capture before emission into the atmosphere. Br is much less abundant in most coals than Cl (approx. 2%), but these heavier Br halogens are proportionally a more effective Hg oxidising agent than Cl (Manö & Andreae, 1994; Kolker et al., 2012). The type of coal burned is a consequence of geological processes, i.e. halogen concentrations and [Br]/[Cl] ratios, which governs the actual proportion of Hg that conventional APCDs and scrubbers capture.

For most conditions the oxidation of Hg^0 by Br atoms requires less than 2 ppt BrO (Holmes et al., 2010). It is thus evident that the amount of bromo-carbon, bromine and associated $Br^{\bullet}$ source gases is sufficient for these atmospheric oxidation processes to occur, especially considering further Br enrichments through ventilation of marine boundary layer air containing Br from debrominated sea-salt aerosol (Yang et al., 2005; Parella et. al., 2012) or heterogeneous reactivation of Br on aerosols (von Glasow et al., 2004; Yang et al., 2010).

2.6. Global Hg and relevance in South Africa

In 2006, a global anthropogenic Hg inventory ranked South Africa as the second largest Hg emitter worldwide, producing 256.7 $t.y^{-1}$, trailing only China that emitted 604.7 $t.y^{-1}$ (Pacyna

et al., 2006) at that time. This prompted local scientists to initiate the South African Mercury Assessment (SAMA), which assisted in informing and guiding subsequent Hg research in South Africa. This resulted in a revised publication of Hg emissions from South Africa, rating South Africa as the 6th largest emitter on the global list of major Hg polluters, contributing 19.5 $t.y^{-1}$ during 2004 (Dabrowski et al., 2008). The study of Dabrowski et al., 2008 was also critically revised by Leaner et al. (2008), giving a more realistic estimate of about 40 $t.y^{-1}$ during 2004. Additional studies estimated the total Hg released into the South African environment amounts to 62 tonnes in 2006 of which 50 tonnes were estimated to be released into the atmosphere, with the remaining 12 tonnes constituting general waste from production processes (Masekoameng et al. 2010; Scott & Mdluli 2012). Brunke et al. (2012) estimated total elemental Hg emissions of South Africa in 2007 and 2008. Considering current uncertainties regarding Hg and the fact that emission of GEM represents 50-78% of total Hg emissions, the estimate of 14.8 t (GEM).y^{-1} (Brunke et al., 2012) is in agreement with Leaner et al. (2008) for 2004 and slightly lower than the one calculated by Masekoameng et al. (2010) for 2006.

The estimated contribution of all major Hg polluting countries is depicted in Figure 2.5 below. According to Pirrone (2010) and references therein, China is the leading Hg polluter worldwide, contributing 609.1 $t.y^{-1}$ to the annual total global anthropogenic Hg emissions of 2319.7 $t.y^{-1}$, followed by India (240.9 $t.y^{-1}$), North-America (152.8 $t.y^{-1}$), Europe (145.2 $t.y^{-1}$), Russia (69.8 $t.y^{-1}$), South America (49.7 $t.y^{-1}$), South Africa (40.2 $t.y^{-1}$) and Australia (16.6 $t.y^{-1}$). Reference years for these estimates varied between 2003 and 2005, while emissions since then may have changed and, most-likely, probably increased. Interestingly, when Hg emissions are calculated per capita, approximately 0.24 g per person per year is emitted in South Africa, which is considerably higher than other leading industrialised nations such as Canada (0.15 g/pp.), China (0.13 g/pp.), Russia (0.16 g/pp.) and the USA (0.2 g/pp.) (Dabrowski, 2010). This suggests that, although the total emissions in South Africa are lower than previously expected, it appears that South Africa emit high Hg levels per capita, which suggests that the potential for human and environment exposure is relatively high.

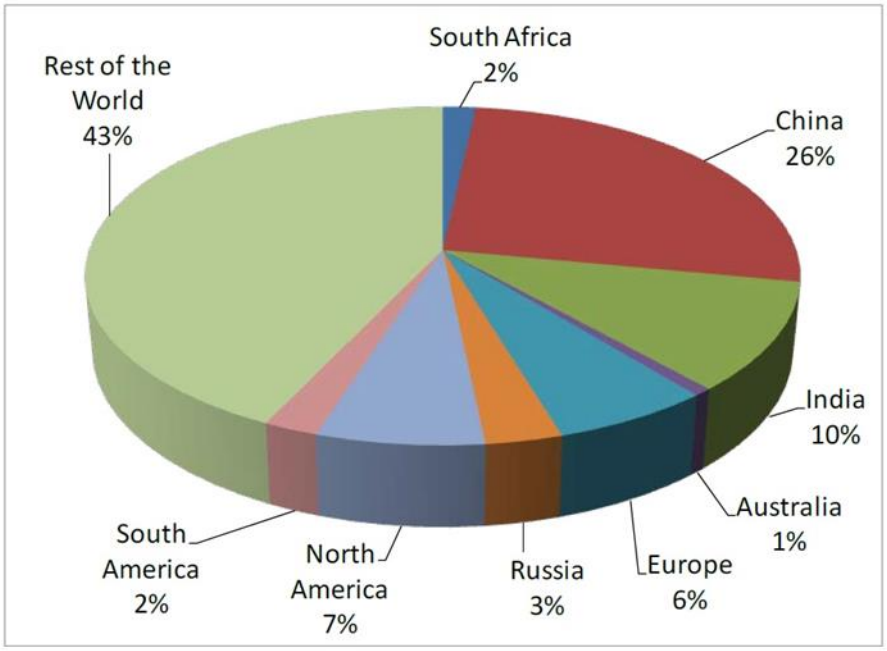

Figure 2.5: Source distribution percentages of global anthropogenic mercury emissions (Pirrone, 2010).

In 2013, the Minamata Treaty was signed by South Africa and 98 other countries to address impacts on human health and the environment associated with anthropogenic Hg emissions. Since South Africa is globally considered to be one of largest Hg emitters, mainly due to its reliance on fossil fuels, the Minamata treaty will have far-reaching implications for South Africa (Scott & Mdluli 2012). Typical anthropogenic sources of Hg in South Africa includes coal-fired power plants, gasification of coal to fuel and liquids, crude oil refining, production of ferrous and non-ferrous metals, biomass burning and household combustion (Masekoameng et al. 2010). Gold production does not contribute significantly to Hg emissions in South Africa (Masekoameng et al. 2010; Brunke et al. 2012). The major fraction of South African emissions is derived from coal-fired power generation, which contributes approximately 80% of the total emissions in South Africa (Masekoameng et al. 2010; Pirrone et al. 2010; Brunke et al. 2012)). Roughly 93% of South Africa's electricity is produced from coal burning (Kolker & Quick, 2015); while coal is also used in certain low-income households for heating and cooking (Masekoameng et al. 2010).

Low grade bituminous coal is generally used South African combustion power plants, which have a relatively low Hg concentration. Typical Hg concentrations in Highveld coals range from 0.04 to 0.27 ppm, with a mean of 0.15±0.05 ppm. Coal samples collected from the Witbank area had almost double the Hg content, with a mean of 0.3 ppm Hg (Wagner and Hlatshwayo, 2005; Bergh et al., 2011; Kolker & Quick, 2015). However, the quantities of coal burned annually is increasing e.g. in 2007 125 million tonnes of coal was consumed

compared to the 112.3 million tonnes burned 2004 (Dabrowski et al. 2008). This significant increase in coal usage accounts for large amounts of accumulated Hg. In addition, South Africa has an ever increasing energy demand, which implies that an increase in electricity supply will result in even more Hg emissions. It is, therefore, essential that continued monitoring and assessment Hg emissions and ambient concentrations in the South Africa takes place win order to assess atmospheric Hg trends (Dabrowski 2010). It has been It has been calculated that between 17 and 23 tons of Hg was emitted from coal-fired power stations in 2015 (Garnham & Langerman, 2016).

Most control devices currently employed by power utilities in South Africa are electrostatic precipitators (ESPs), fabric filters (FFPs), desulphurisation/flue-gas conditioning (FGCs), or a combination of thereof (Leaner, et al. 2008) - resulting in co-beneficial reduction of Hg emissions (Garnham & Langerman, 2016). The operation of ACPDs required by current standards to control air quality reduces Hg emissions by approximately 35% (Rafaj et al., 2014). Power stations with FFPs as emission control technology produce significantly lower Hg per GWh produced than stations with ESPs. A detailed description regarding the emission control devices of South African power stations is stipulated in a study by Garnham & Langerman (2016). More detailed sampling and analysis of Hg bearing coals are needed for South Africa to estimate the overall effectiveness of the capture mechanism discussed here (Kolker & Quick, 2015).

Atmospheric Hg in South Africa is relatively poorly understood, with very little existing data and published in peer-reviewed literature. Hg studies is mainly limited to Hg measurements conducted at the Cape Point Global Atmosphere Watch (CPT-GAW) station for which long-term Hg trends, depletion events, seasonal cycles and flux rates were reported (Baker et al., 2002; Slemr et al., 2008; Brunke et al., 2010a; Brunke et al., 2010b; Venter et al., 2015). However, since CPT-GAW is a southern hemispherical background station impacted by maritime air masses, Hg measurement at CPT-GAW is not representative of emissions within the interior of South Africa where the major point sources are located. Trüe et al. (2012) did conduct some Hg emission measurement in Pretoria and Witbank, where monitoring was performed for short weekly sampling periods with Hg sorbent tubes (Trüe, 2010; Trüe et al., 2012). The weekly exposure times results in averaged observations which, although accurate, does not give detailed information on e.g. pollution events and diurnal cycles. In addition, Hg levels was also determined in lichens by Trüe et al. (2012), which is indicative of late to long-term accumulation of atmospheric Hg. Recently, Belelie et al. (2018) reported high resolution Hg observations over the South African Highveld (refer to Section 4.2 for contextualisation), which gives good insight for the interior of South Africa.

However, they concluded that additional studies at locations in immediate proximity to large point sources (e.g. coal-fired power plants) is important as coal combustion is considered as the predominant TGM source in South Africa.

The significance of this study is that high resolution Hg data was collected in the interior of South Africa, in close proximity to point sources, over reasonable sampling periods, which enabled evaluation of pollution and depletion events on different temporal scales, which include diurnal patterns. This will enable us to compare results with current mass balance information and modelling results, which will, to a certain extent, shed some light on current uncertainties associated with ambient Hg in the interior of South Africa.

Chapter 3 - Experimental

3.1. Site descriptions

Figure 3.1 below shows a map of Southern Africa, which indicate the locations of the three measurement sites considered in this study, i.e. Eco-Park (EP), Elandsfontein, (EL) and Marapong (MP), within a regional perspective. This map also shows the extent of the three declared priority areas (South Africa, 2005; South Africa, 2007; South Africa, 2010). These priority areas were declared due to current and/or foreseen poor air quality (Scott & Mdluli, 2012). Eco-Park (EP) was situated in the Vaal Triangle Air Shed Priority Area (pink in Figure 3.1); Elandsfontein (EL) in the Mpumalanga Highveld Priority Area (green in Figure 3.1); and Marapong (MP) situated in the Waterberg Priority Area (blue in Figure 3.1).

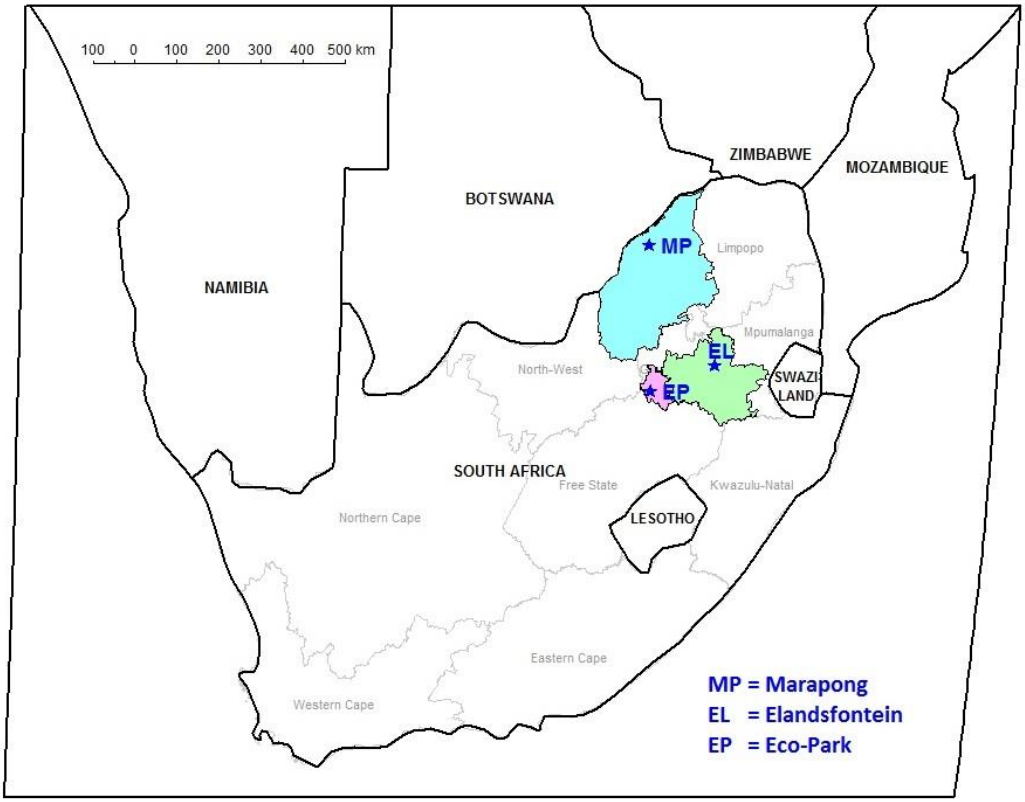

Figure 3.1: A map of southern Africa indicating the location of the measurement sites considered in this study within a regional perspective. Additionally, the extent of the three declared air quality priority areas of South Africa in indicated.

Figure 3.2 presents a southern Africa map, with a zoomed in window over the priority areas. Numerous coal-fired power plants, petrochemical operations, pyro-metallurgical smelters and other industries are distributed across the region, as well as the Johannesburg-Pretoria megacity (indicated as the grey area in the zoomed-in part of Figure 3.2). In Figure 3.2 there is also a small window surrounding each measurement station. These windows indicate the

boundaries of the Google Earth photos, shown in Figures 3.3 to 3.5. In the subsequent sections, each of the measurement sites will be discussed individually, indicating potential emission sources and briefly considering meteorological conditions.

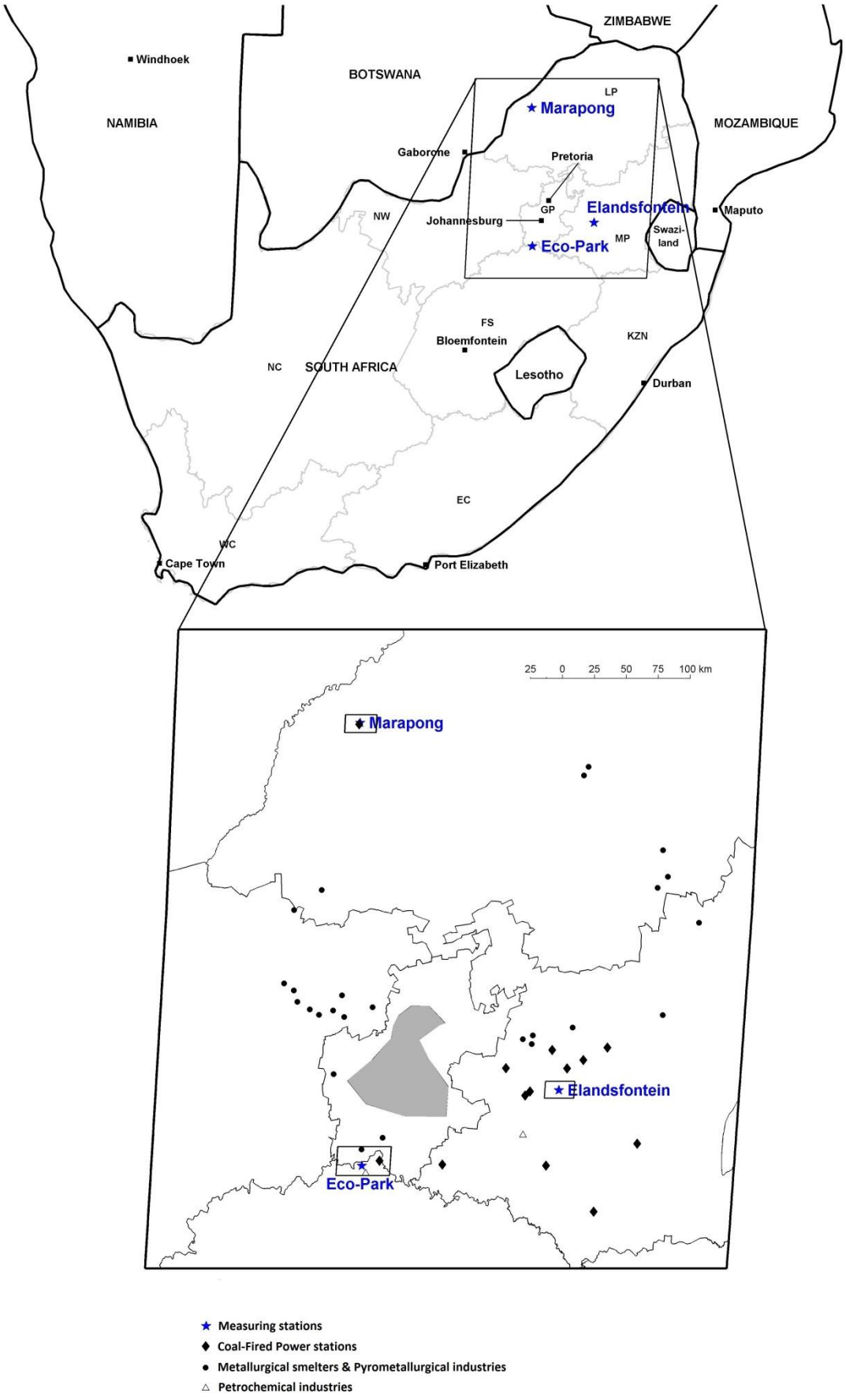

Figure 3.2: Map indicating large point sources and the locations of the measurement sites. The black windows surrounding the measurement stations indicate the boundaries of Google Earth photos, shown in Figures 3.3 to 3.5.

3.1.1. Eco-Park, Sasolburg, Vaal Triangle Air Shed priority area

The Eco-Park (EP) station that was operated by Sasol, is situated in the Bongani Mabaso Eco-Park nature reserve (Lat: -26.777540; Long: 27.837310) in Sasolburg – a large industrial town in the far north of the Free State province of South Africa. It is situated at a relatively high altitude (approximately 1500 m above sea level), with a fairly dry climate and large seasonal temperature variation. According to Meteoblue climate diagrams (meteoblue, n.d.), using hourly data derived from their global NEMS weather model, Sasolburg experiences hot summers, with average midday temperatures of 29°C and 34°C for hot days; and very cold winters, with average minimum temperatures of 2°C and -4°C for cold days. This area experiences annual rainfall of approximately 648 mm, where summer months get up to 107 mm rainfall and dry winter months almost no precipitation. The census of 2011 indicated the total population of the Sasolburg-Zamdela area to be 113 038 people, with a rather high population density of 1 400 people/km^2.

The EP monitoring station is in close proximity to several industrial operations, as well as Lethabo, a large coal-fired power station. Lethabo was rated the highest mercury-emitting coal power station in 2015, contributing roughly 19% of the total emitted by all the stations (Garnham & Langerman, 2016). Furthermore, various informal settlements are situated in the surrounding area, e.g. Zamdela, which has a population of 90 000 residents. Sasolburg, with the neighbouring towns Vereeniging and Vanderbijlpark, forms the Vaal Triangle, a major industrial region of South Africa. The Vaal Triangle, together with the southern portion of the Gauteng province form the Vaal Triangle Air Shed Priority Area (South Africa, 2005).

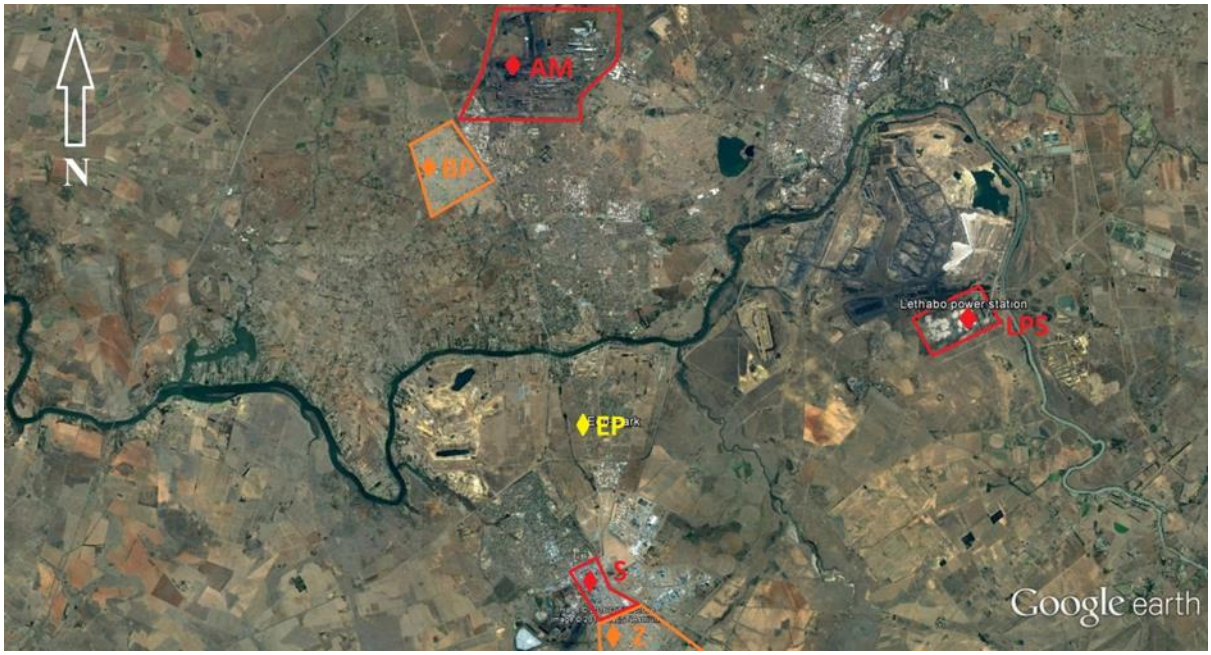

Figure 3.3: Google Earth image indicating position of EP within a local context. Possilbe anthropogenic pollution sources are also indicated, i.e. semi- and informal settlements in orange and large point sources in red. EP = Sasol Eco-Park monitoring station; S = Sasol chemical and petrochemical operations; LPS = Lethabo coal-fired power station; AM = ArcelorMittal pyro-metallurgical smelter; BP = Bophelong informal settlement; Z = Zamdela informal settlement (only partly shown).

Figure 3.3 presents a Google Earth image of the area around the EP monitoring station. It is evident from Figure 3.3 that there are several possible pollution sources surrounding the EP station. The station can be influenced from the north by ArcelorMittal pyro-metallurgical smelter (13 km) and the Bophelong informal settlement (11 km) that occurs in/near Vanderbijlpark. Point sources to the ENE direction of EP worth noting is the Lethabo coal-fired power station (14.5 km). Southern influences include numerous chemical-/petrochemical operations (5.5 km) (combined referred to as Sasol, but actually various operation such as Natref, Omnia, Karbochem, etc.), as well as the Zamdela informal settlement (9 km). Other possible emission sources in the area include several smaller pyro-metallurgical smelters, large brick kilns, coal mining with associated smouldering coal dumps, smaller industries and a large and ageing vehicle fleet.

3.1.2. Elandsfontein, Mpumalanga Highveld Priority Area

The Elandsfontein (EL) atmospheric monitoring station (Lat -26.245487; Long 29.417382) that was operated by Eskom, is located in Mpumalanga, surrounded by farming communities and small farming towns, e.g. Kriel and Bethal in the immediate vicinity. According to Meteoblue climate diagrams (meteoblue, n.d.), the region experiences hot summers, with average midday temperatures of 28°C and 33°C for hot days; and very cold winters, with average minimum temperatures of 2°C and -4°C for cold days. This area experiences annual

rainfall of approximately 616 mm, where summer months get up to 122mm rainfall and winter months almost nothing.

Figure 3.4: Position of the Elandsfontein monitoring station within a local context. Dorsfontein and Middelkraal collieries can be seen to the NW and NE direction of EL.

As indicated earlier, the EL atmospheric monitoring station is located in the Mpumalanga Highveld Priority Area (South Africa, 2007). Figure 3.4 presents a Google Earth image of the immediate area surrounding EL. As is evident from this figure, there are not large point sources very close to the site, although some open pit coal mining takes place nearby. Several large anthropogenic point sources (refer back to Figure 3.2) could impact EL. Coal-fired power plants within in a 100 km radius from the EL monitoring site include the following (arranged from nearest to furthest): Kriel- (15 km, W); Komati- (18 km, NNE); Matla- (28 km, W); Hendrina- (29.5 km, NE); Duvha- (32 km, NNW); Kendal- (48 km, NW); Tutuka- (60 km, S); Camden- (79 km, SE) and Majuba power stations (100 km, S). Additionally, Sasol's large petrochemical operations in Secunda is situated 42 km southwest of EL, while numerous metallurgical operations occur in/near the cities of Witbank and Middelburg, located 45 km and 66 km approximately north of EL, respectively. Numerous smouldering coal dumps are distributed across the Mpumalanga Highveld, which also affects air quality.

3.1.3. Marapong, Waterberg Priority Area

The Marapong (MP) atmospheric monitoring station (Lat -23.656023, Long 27.627999) was operated by Eskom, is situated inside an informal settlement in Marapong, one of the subsections of the town Lephalale. Lephalale (previously known as Ellisras), is a coal mining town in the Limpopo province of South Africa, situated west of the Mokolo river, a

tributary to the Limpopo river. The station is at an altitude of 820 m above sea level and experiences summer rainfall with dry winters. According to Meteoblue data (meteoblue, n.d.), the annual rainfall in this area amounts to approximately 237 mm, which is far less than the other monitoring sites. Summer months get up to 49 mm and winter months almost no rainfall. Temperatures here are also higher when compared to the other sites. The mean daily temperatures for summer months are 33°C, and 38°C for hot days, with mean minimum temperatures in winter of 6°C, and 1°C for cold days.

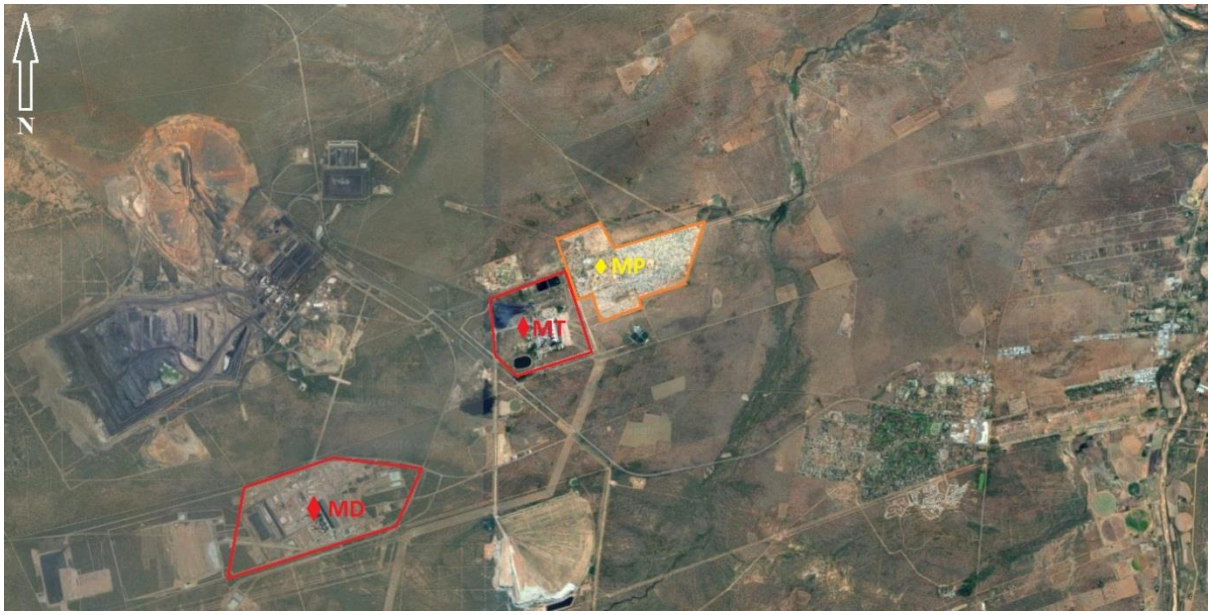

Figure 3.5: Position of the MP monitoring station within a local context, relative to Matimba (MT) & Medupi (MD) coal-fired power stations. MP = Marapong (situated in an informal settlement).

From a local context, the MP station is situated in the Waterberg Priority Area, which was declared a national air quality priority area in October 2010 (South Africa, 2010). As is evident from Figure 3.2, the Matimba (2 km, SW) and Medupi (8.2 km, SW) coal-fired power plants are the only large point sources near the measurement station. At the time when measurements were conducted the Medupi power station was still under construction. The Matimba station was rated the 2nd highest mercury-emitting coal power station in 2015, contributing roughly 18% of the total emitted by all the stations combined (Garnham & Langerman, 2016). However, one expects the influence of household combustion, originating from the semi- and informal settlement surrounding the monitoring station, to have a significant influence on pollutant concentrations.

3.2. Measurement methods

Continuous Hg measurements were conducted at all three sites with an automated, dual channel, single amalgamation, cold vapour atomic fluorescence analyser (Tekran Model

2537A or B analyser, Tekran Inc., Toronto, Canada). The instrument utilises two gold cartridges. While one is adsorbing mercury during a sampling period, the other is being thermally desorbed using argon as a carrier gas. Mercury is detected using cold-vapour atomic fluorescence spectroscopy (CVAFS). Operation and calibration of the instruments followed established and standardised procedures of the Global Mercury Observation System (GMOS) project. These Tekran analysers has a TGM detection limit of ± 0.05 ng.m^{-3}, and are capable of measuring even low background Hg concentrations (Ebinghaus et al., 1999).

In addition to TGM, several trace gases and/or meteorological parameters were also measured. Unfortunately, not all these species/parameters were measured at each site. These parameters included: SO_2, NO, NO_2, O_3, WS, WD, RH%, Rain, H_2S, PM_{10}, $PM_{2.5}$, and temperature. The analysers for the afore-mentioned species were the API SO_2 Analyser (utilising EQSA-0495-100 equivalent method), the API NO/NO_2/NO_x Analyser (RFNA 1194-099 equivalent method), and the API Ozone Analyser (EQOA-0992-087 equivalent method). Meteorological parameters (temperature, relatively humidity (RH), as well as wind speed and direction were measured with RM Young analysers.

3.3. Data cleaning and quality assurance

Most of the data processing (e.g. data cleaning, visualisation graphs, and statistical analysis) was performed using the statistical programming software MATLAB. In order for the Multiple Linear Regression (MLR) analysis technique (explained in Section 3.4) to be utilised, a dataset with complete data rows were required, i.e. where every parameter has a valid entry for each time entry. The initial datasets supplied by the site operators had moderate amounts of missing data points for some parameters. Rows that contained any data gaps were automatically removed by a fit-for-purpose MATLAB script. The remaining data was then visualised and further data cleaning done via inspection and manual removal (input required for MATLAB script) of discontinuous/unusable data, e.g. no change in concentration(s) over prolonged periods, or spikes due to instrument failure/errors/power outages.

3.4. Data analysis

Various multivariate statistical data analyses methods have previously been used in atmospheric receptor modelling, e.g. principal component analysis (PCA) (e.g. Venter et al., 2017) and positive matrix factorisation (PMF) (e.g. Jaars et al., 2018). In the current study, multiple linear regression (MLR) was used as a receptor model approach. A similar approach have been applied by many previous researchers (e.g. Du Preez et al., 2015;

Jaars et al., 2016). The main advantage of analysing data using a multiple regression model is that insight into possible chemical processes and/or contributing sources can be obtained. Normal linear regression is denoted by a constant (c), an independent variable (x) and a dependent variable (y). Multiple linear regression (MLR) is characterised by more than one independent variable (x). MLR models the relationship between the dependent variable (y) and independent variables (x) by fitting a linear equation to the observed data; denoted by Equation 3.1 below:

$$y = c_0 + c_1x_1 + c_2x_2 + c_3x_3 + \ldots\ldots\ldots\ldots\ldots c_zx_z \quad [3.1]$$

In this study, MLR was used to determine an equation for the dependent variable, i.e. TGM, expressed in terms of the independent variables, i.e. all other available species concentrations and/or meteorological parameters. This was achieved by utilising a fit-for-purpose MATLAB program, which calculates the optimum combination of independent variables, and returns a derived equation to predict TGM concentrations. Calculated values were compared to measured values by means of root mean square error (RMSE) calculations. RMSE values were calculated as indicated in Equation 3.2 below:

$$\%\ \boldsymbol{RMSE\ Diff.} = \frac{D_x - D_{x+1}}{D_1 - D_z} \times 100 \quad [3.2]$$

Where $\boldsymbol{D_x}$ represents the RMSE between calculated and actual TGM concentrations for $\boldsymbol{x}$ number of variables, $\boldsymbol{D_z}$ is the RMSE for all possible independent variables, subtracted from $\boldsymbol{D_1}$, the RMSE for a single independent variable.

Wind direction was one of the meteorological parameters that was measured at all the sites, therefore, it should be included as an independent parameters in MLR analysis. However, since wind direction is a circular variable (0 to 360 degrees, with 0 and 360 degrees indicating the same wind direction). Consequently, sine and cosine of wind direction were included as independent variables, similar to the approach by Jammalamadaka & Lund (2006). Furthermore, wind direction was used in data interpretation by plotting pollution roses and polar plots. A pollution rose (a variant of the wind rose) is useful for considering pollutant concentrations as a function of wind direction, or more specifically the percentage time the concentration is in a particular range. Pollution roses can also be used to show which wind directions dominate the overall concentrations. The polar plot function plots a bivariate polar plot of concentrations, i.e. shown to vary by wind speed and wind direction. Such a plot is shown as a continuous surface and is useful since it gives a graphical impression of potential sources at a location.

Chapter 4 - Results and discussions

4.1. Data preparation for multiple linear regression analysis

Multiple linear regression analysis was used as a receptor model in this study. As mentioned earlier (Section 3.4), the MLR analysis technique requires each data row to be complete, i.e. every parameter has a valid entry for each time stamp. Due to analyser maintenance, faulty readings, data cleaning and various other reasons, there will however be data gaps for certain parameters. This resulted in the entire data row being omitted from the MLR analysis, which reduces the available data significantly. As indicated in Section 3.2, datasets from three sites were considered in this study, i.e. Eco-Park (EP), Elandsfontein (EL) and Marapong (MP). After the MLR data preparation procedure was applied on the EP dataset it contained data for the period 2013/04/01 to 2013/06/30, which consisted of 12 401 continuous high resolution measurements for all species. For EL the remaining dataset ranged from 2010/01/01 to 2015/04/30, with 2 316 data rows remaining. However, radiation, particulate matter (PM) with diameter less than 10 µm (PM_{10}), PM with diameter less than 2.5 µm ($PM_{2.5}$) and relative humidity (RH) had to be totally removed from the dataset in order to retain the afore-mentioned data. If these species were retained, too little data would have remained. The MP dataset was reduced to 8 681 data rows covering the period 2010/02/04 to 2013/08/06. RH also had to be removed from this dataset, in order to retain enough data.

Although all three datasets were significantly reduced in size in preparation for MLR analysis, the remaining data quantity for each site was deemed satisfactory to utilise in MLR analysis, but insufficient to determine seasonal patterns and/or long-term trends.

4.2. Contextualisation

In order to contextualise the total gaseous mercury (TGM) concentrations obtained at EP, EL and MP, concentrations measured there were compared against mercury concentrations measured elsewhere, as presented in Table 4.1. Only a limited number of sites were referenced in this comparison. A more detailed list of mercury studies conducted can be found in Gworek et al. (2017). Caution should be exercised when comparing Hg results from different time-periods, sites and obtained using different instruments (as indicated in Table 4.1). However, the objective here was not to compare the Hg results quantitatively with one another, but merely to contextualise the levels measured at the sites considered.

	Site	Period	Mean (±SD) (ng/m^3)	Species	Reference
South Africa	Eco-Park	2013	3.95 ± 2.97	TGM	This study
	Elandsfontein	2010-2015	2.49 ± 2.06	TGM	This study
	Marapong	2010-2013	1.61 ± 1.42	TGM	This study
	Cape Point (average)	2007-2011	0.92 ± 0.27	GEM	Slemr et al., 2013;
	Cape Point (inland air masses)	2007-2011	1.09 ± 0.15	GEM	Venter, et al., 2015
	Hatfield, Pretoria	2009-2010	2.6 ± 0.6	TGM	Trüe et al., 2012
	Brummeria, Pretoria	2009-2010	1.8 ± 0.4	TGM	Trüe et al., 2012
	Pretoria West	2009-2010	2.0 ± 0.4	TGM	Trüe et al., 2012
	Witbank	2009-2010	1.70	TGM	Trüe et al., 2012
	Balfour	2009	1.99 ± 0.94	TGM	Belelie et al., 2018
	Middelburg	2009	1.04 ± 0.62	TGM	Belelie et al., 2018
	Standerton	2009	1.25 ± 1.38	TGM	Belelie et al., 2018
International measurements	Guiyang, China	2009	7.40 ± 4.80 & 6.20 ± 5.10	TGM	Liu et al., 2011
	Guangzhou, China	2010-2011	4.60 ± 1.36	TGM	Chen et al., 2013
	Northern Hemisphere	2014	1.50 - 1.70	TGM	Sprovieri et al., 2010
	Puertollano (Spain)	2010-2012	1.81	GEM	Martínez et al. 2016
	Canadian Atm. Network	1995–2005	1.58	TGM	Temme et al., 2007
	Houston, USA	2011-2012	1.62 ± 0.56	TGM	Lan et al., 2014
	Detroit, USA	2004	2.50	GEM	Liu et al., 2010
	Birmingham, Alabama, USA	2005–2008	2.12	GEM	Nair et al., 2012
	Pensacola, Florida, USA	2005–2008	1.35	GEM	Nair et al., 2012
	Atlanta, Georgia, USA	2005–2008	1.35	GEM	Nair et al., 2012
	Seoul, Korea	2005-2006	3.22 ± 2.10	TGM	Kim et al., 2009
	Mace Head, Ireland (Europe)	1998–2004	1.72	TGM	Kock et al., 2005
	Zingst, Germany (Europe)	1998–2004	1.66	TGM	Kock et al., 2005

Table 4.1: Comparison of measurement stations in this study with other recorded Hg concentrations from various sites over different periods.

Background TGM levels in the northern hemisphere (NH) are generally a factor of about 1.5 higher than those in the southern hemisphere (SH) due to higher emissions and lag in inter-hemispheric transport (NH/SH gradient). Thus, concentrations above these baseline levels are of specific interest when making comparisons. A general observation from Table 4.1 is that Hg concentrations in densely populated and highly industrialised cities are obviously significantly higher, which indicates fuel burning for power generation and household combustion must be a profoundly influential factor for the observed differences in concentrations. As is evident from the comparison presented in Table 4.1, the mean TGM measured at EP (i.e. 3.95 ng.m^{-3}) is significantly higher than other concentrations cited for South Africa and most international urban sites, with the exception being the densely populated cities in China and Korea. The majority of TGM observations for EP fell within the range of 2.66 ng.m^{-3} (10th percentile) and 6.11 ng.m^{-3} (90th percentile), which indicates relatively consistent elevated TGM concentrations. Although the possible reasons for this relatively high TGM levels will be explored in greater detail later, it can already be stated that EP is situated in close proximity to numerous possible anthropogenic Hg sources, i.e. a large coal-fired power station (Lethabo), petrochemical and/or chemical- and pyro-metallurgical operations, etc. (also see Section 3.1.1). It is also well known that the ambient atmosphere of the Vaal Triangle (the area wherein EP is situated) is comparatively polluted, therefore this area (with a section of the southern Gauteng province) have been declared as an air pollution priority area, i.e. Vaal Triangle Air Shed Priority Area (South Africa, 2005; Leaner et al., 2008).

Furthermore, a prominent feature of TGM at EP was the frequent occurrence of well-defined TGM spikes ranging from ±10.00 to 67.02 ng.m^{-3}. The amplitude of the afore-mentioned spikes were higher than spikes documented for Houston, where a maximum of 43.54 ng.m^{-3} was observed (Lan et al., 2014). As a consequence of these TGM spikes, the standard deviation calculated for EP was 2.97 ng.m^{-3}, which is comparatively higher than measurements from most other urban sites, such as Houston (0.56 ng.m^{-3}, Lan et al., 2014), and Reno, USA (0.4 - 0.8 ng.m^{-3}; Stamenkovic et al., 2007), and considerably lower than the city of Guiyang, China (4.8 - 5.1; Liu et al., 2011). Further consideration of the 14 month Houston dataset (Lan et al., 2014) revealed 81 spikes above 2.68 ng.m^{-3}. 34 of these were higher than 4.46 ng.m^{-3} and on 12 occasions peaks of TGM levels higher than 8.93 ng.m^{-3} were observed. Six peaks higher than 26.78 ng.m^{-3} were reported (Lan et al., 2014). When compared to the 3 month dataset of EP, 61 spikes above 4.50 ng.m^{-3} were noticed, 38 of which were above 9.00 ng.m^{-3}, and 5 peaks exceeded 25.00 ng.m^{-3}. In fact diurnal patterns for EP exceed 2.68 ng.m^{-3}. These extremely frequent and large spikes documented in this study certainly explain the high standard deviation values obtained from EP.

The mean TGM measured at EL (2.49 ng.m^{-3}; Table 4.1) was comparable to Hg levels reported for Hatfield in Pretoria, Detroit (USA) and Birmingham (Alabama, USA). However, it was substantially lower than the mean reported for EP. The majority of TGM observations fell within the range of 1.04 ng.m^{-3} (10th percentile) and 5.14 ng.m^{-3} (90th percentile). Frequent occurrences of TGM spikes were also observed at EL, with the maximum TGM spike having a concentration of 21.06 ng.m^{-3}, which relates to approximately 30% of the maximum peak concentration observed at EP, and to 48% of the maximum peak concentration observed at Houston (Lan et al., 2014). EL is located on the Mpumalanga Highveld, where numerous coal-fired power stations occur, as well as a large petrochemical operation and several semi- and informal settlements. This area, together with the eastern portion of the Gauteng Province have also been declared as a priority area, i.e. Highveld Priority Area (South Africa, 2007; Leaner et al., 2008). However, in contrast to EP, EL is not located in the immediate proximity of these sources. For instance the nearest coal-fired power station (Kriel) is approximately 15 km from the site.

TGM observations from MP, which is located in a semi- and informal settlement, approximately 2 km from a large coal-fired power station (Matimba), was significantly lower if compared to the other two measurements sites considered in this study. The mean for MP (1.61 ng.m^{-3}) was comparable with that reported for Houston (urban) and observations in the Northern Hemisphere background, as well as ambient levels reported for suburban sites in the interior of South Africa, i.e. Witbank (1.70 ng.m^{-3}) and Brummeria (1.80 ± 0.40 ng.m^{-3}). Again, as with the other sites, frequent well-developed spikes were evident in the data. Maximum spike concentrations at MP ranged from ±4.00 to 18.54 ng.m^{-3}, which is lower than documented for Houston (43.54 ng.m^{-3}).

It is also deemed necessary to compare TGM levels reported for the sites considered in this study to levels at the Cape Point Global Atmospheric Watch station (CPT-GAW). To the best of the candidate's knowledge, gaseous elementary mercury (GEM) data reported for the CPT-GAW station represent the only long-term (exceeding a decade) Hg time series reported for South Africa. The CPT-GAW station is operated as a remote monitoring site in the mid-latitudes of the Southern Hemisphere as one of the World Meteorological Organisation's (WMO) GAW baseline stations. As previously indicated, the CPT-GAW station is not representative of the interior of southern Africa, as it is influenced predominantly by southern hemisphere background maritime air masses (Brunke et al., 1995). Therefore, GEM levels from this site represent true oceanic southern hemisphere background concentrations. Additionally, Venter et al. (2015) isolated air masses that had passed over the South African interior (i.e. the Karoo and Kalahari biomes where

anthropogenic pollution is limited) before being sampled at CPT-GAW, i.e. “Cape Point (inland air masses)” in Table 4.1. Such air masses are likely to be representative of GEM levels over the clean continental background of South Africa. From this comparison, it can be deduced that the levels at all three sites were elevated above the concentrations expected for the clean continental regional background.

In addition to the afore-mentioned comparisons of the mean/median values of the different measurements sites considered in this study, the 5th, 25th, 75th and 95th percentiles are indicated in Appendix A, for referencing purposes.

4.3. Site specific discussion

4.3.1. Eco-Park, Sasolburg, Vaal Triangle

In an effort to determine relationships between atmospheric TGM concentrations and other atmospheric parameters measured at EP, and also to establish whether TGM levels could be calculated/estimated from these parameters, MLR analysis was conducted. This was done by applying a linear equation (Equation 3.1) and minimising the RMSE difference between the calculated and actual TGM concentrations with the least number of independent variables. In Figure 4.1 RMSE difference between the calculated and measured TGM values, as a function of independent variables included in the optimum MLR solution, is presented.

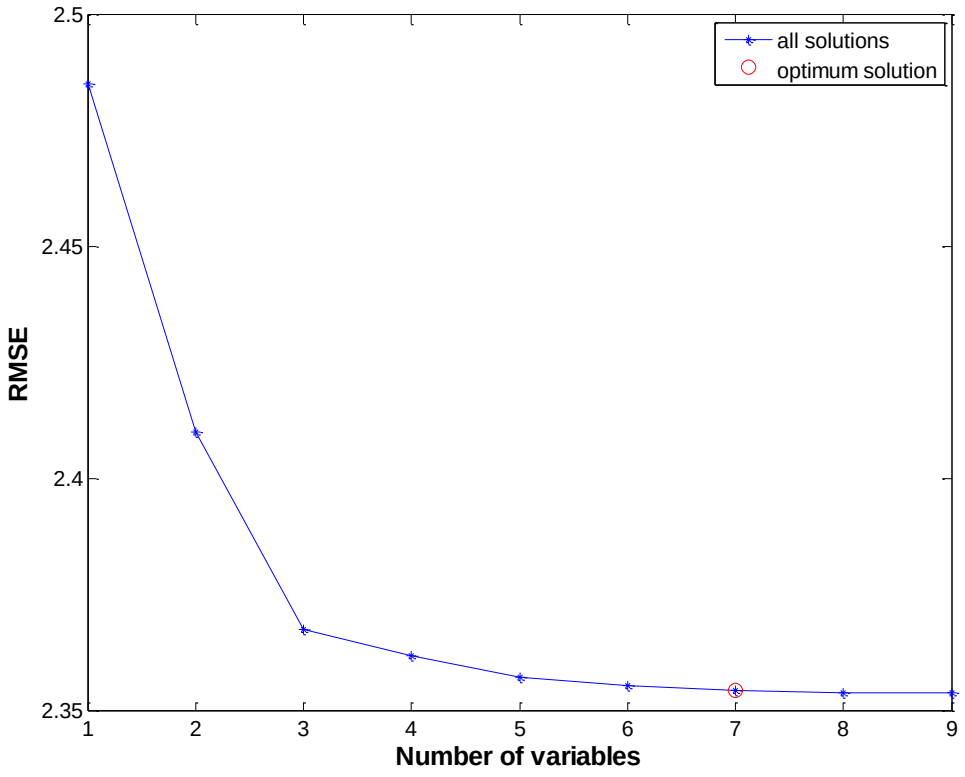

Figure 4.1: The root mean square error (RMSE) difference between the calculated and actual TGM values, in order to determine the combination of independent variables to include in the optimum MLR equation to calculate the dependant variable, i.e. TGM concentration.

From Figure 4.1, it is evident that the optimum MLR equation containing only one independent variable, i.e. SO_2 (Table 4.2), had a RMSE of 2.48. However, the RMSE could be lowered to 2.41 if a MLR equation containing the optimum combination of two independent variables, i.e. SO_2 and NO (Table 4.2), were calculated. Additional independent variables were included until the relative improvement in RMSE difference, i.e. (RMSE for equation with x independent variables - RMSE for equation with x+1 independent variables)/(RMSE for equation with 1 independent variable - RMSE for equation with all possible independent variables), was less than 2% (refer to Equation 3.2 in Section 3.3). This was attained when the number of independent variables included in the optimum MLR solution was seven, which had an RMSE of 2.35. Table 4.2 indicates the identity of the independent parameters determined for each of the optimum MLR solutions.

Quantity	Independent variables						
1	SO_2						
2	SO_2	NO					
3	SO_2	NO	RH				
4	SO_2	NO	RH	WS			
5	SO_2	NO	RH	WS	NO_2		
6	SO_2	NO	RH	WS	NO_2	WD_{sin}	
7	SO_2	NO	RH	WS	NO_2	WD_{sin}	O_3

Table 4.2: The identity of independent variables included the optimum MLR equations to calculate TGM at Eco-Park.

By applying the above-mentioned procedure the overall optimum MLR equation was determined, as presented in Equation 4.1. The experimental *vs*. calculated TGM for EP are indicated in Figure 4.2. From this comparison, is obvious that Equation 4.1 can be used to calculate TGM for EP relatively accurately. Especially TGM peaks are calculated well with Equation 4.1, although the base line TGM seem to be less accurate. The frequent occurrence of well-defined TGM spikes mentioned earlier (Section 4.2) can be witnessed in Figure 4.2.

$$TGM = 2.575 + (1.1539E^{-1} \times SO_2) + (2.2199E^{-2} \times NO) + (9.5174E^{-3} \times RH) - (5.7119E^{-2} \times WS) - (2.1687E^{-2} \times NO_2) + (1.6392E^{-1} \times WD_{sin}) - (1.7185E^{-2} \times O_3) \quad [4.1]$$

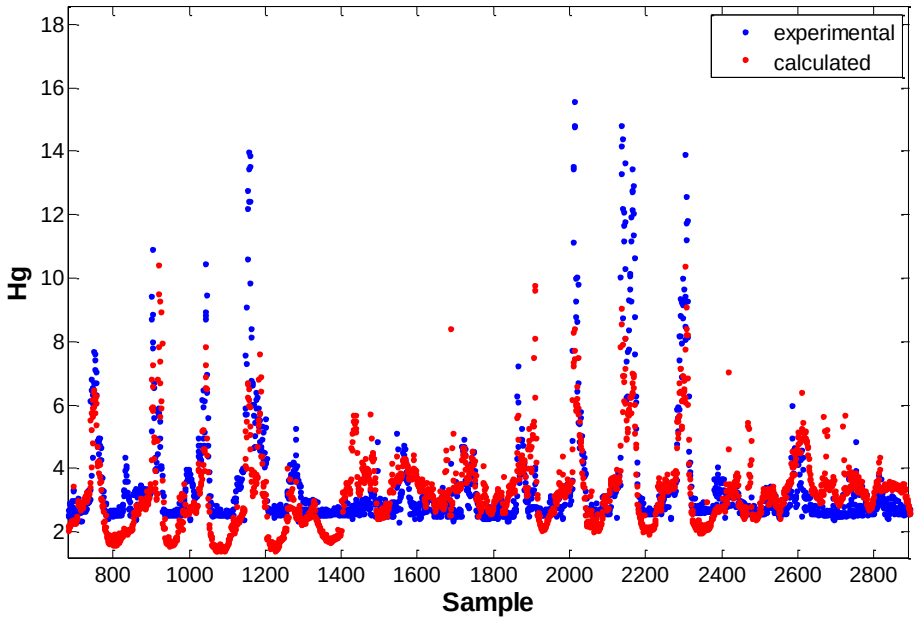

Figure 4.2: Measured (blue) vs calculated (red) TGM values for EP. This sample consists of ±2400 measurements.

Although the optimised MLR equation (Equation 4.1) cannot be used to explicitly derive the origin and/or reaction mechanistic information about TGM measured EP, it can provide some valuable insight. For instance, Table 4.2 indicated that SO_2 was the independent parameter that reduced the RMSE difference between the calculated and actual TGMs most. Combined SO_2 and NO reduced the RMSE difference even further. Both these independent parameters also had positive constants associated with them in Equation 4.1, which indicate that higher SO_2 and NO were statistically associated with higher TGM concentrations. Both the afore-mentioned species are emitted as primary pollutants originating from combustion sources. Furthermore, the relative importance of NO to reduce the RMSE difference (Figure 4.1 and Table 4.2), compared to NO_2 prove that higher TGM concentrations were associated with fresh plumes wherein NO have not yet oxidised significantly to NO_2. In fact, NO_2 was associated with a negative constant in Equation 4.1, implying that higher NO_2 statistically resulted in lower TGM concentrations. Similarly, O_3 was also associated with a negative constant, which supported the notion that aged (more oxidised) plumes resulted in lower TGM concentrations. Aged air masses typically have higher O_3 concentrations. Additionally, the negative constant associated with wind speed (WS) indicates that higher TGM concentrations were mostly associated with lower wind speeds. Combined all these facts indicate that nearby combustion sources contribute most significantly to higher TGM at EP. Wind direction, as represented by WD_{sin} in Equation 4.1 also played a statistically meaningful role, which would not have been the case if more distant sources were dominant. The significance of RH in Equation 4.1 will be discussed later. Obviously the above-

mentioned deductions made from the optimum MLR equation cannot unambiguously prove which Hg source(s) are most important at EP. Therefore, a pollution rose (Figure 4.3) and polar (Figure 4.4) plot were drawn for EP, since such plots combined concentration data with spatial and meteorological aspects.

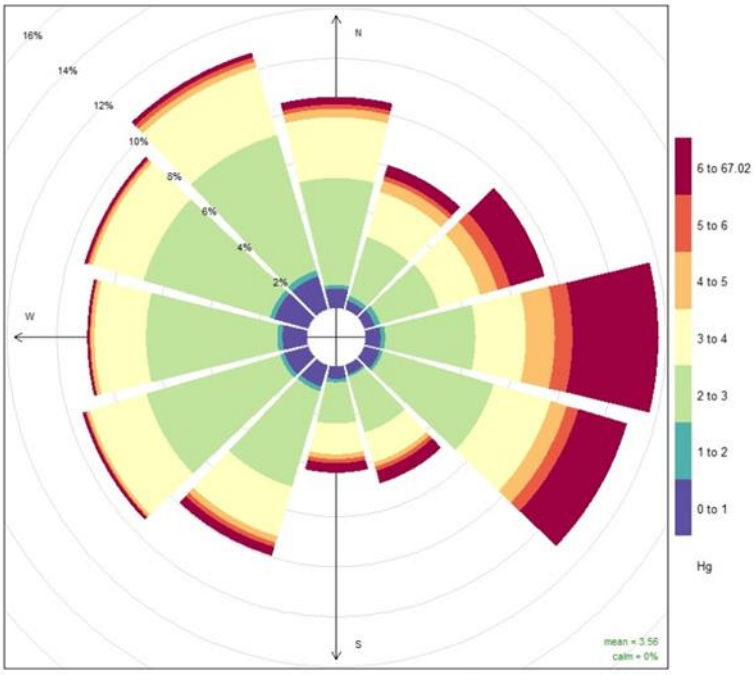

Figure 4.3: TGM pollution rose for Eco-Park over the measurement period.

The pollution rose (Figure 4.3) indicates that three relatively well distinguishable spatial sectors, with associated TGM concentration ranges, can be identified. The lowest TGM concentrations most frequently occurred if winds came from the sector between NNW and SW. In this sector there is significant formal residential developments, but very few large industries or semi- and informal settlements (Figure 3.3). Slightly higher TGM concentrations were more regularly observed for the sectors between NNW and NE, as well as between SW to SE. The ArcelorMittal Vanderbijlpark operation and Bophelong informal settlement is located in the sector between NNW and NE, while numerous chemical/petrochemical operations (e.g. Sasol, Natref, Omnia, Karbochem), as well as large semi- and informal settlements are present in the SW to SE direction. The highest TGM concentrations were most frequently measured if wind arrived from the directional sector between NE to SE, where the Lethabo coal-fired power station is situated.

The polar plot presented in Figure 4.4 clearly indicates that the Lethabo coal-fired power station is not the only source of TGM measured at EP, but it is certainly the largest point source. This interpretation is in accordance with the previous deductions made for the MLR analysis and the pollution rose.

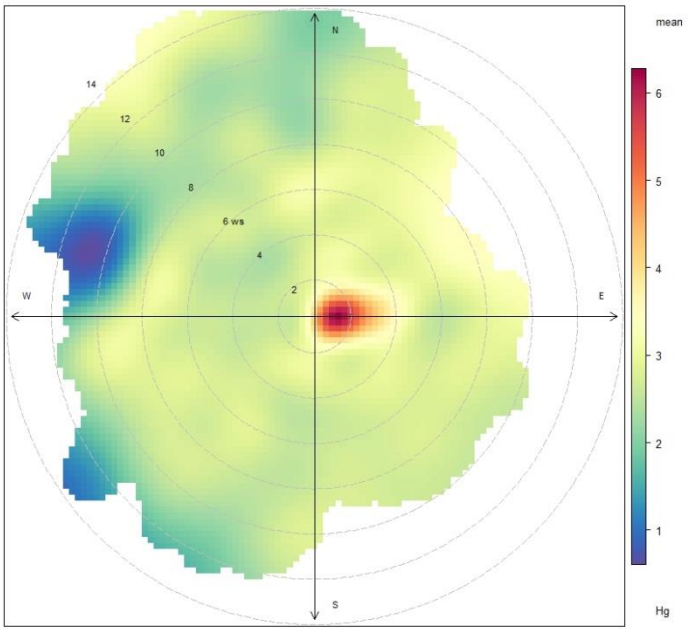

Figure 4.4: The polar plot for Eco-Park monitoring station for TGM concentrations.

In order to further investigate temporal effects, diurnal patterns were considered. Figure 4.5 presents the average diurnal patterns of April (the hottest month in the dataset) and June (the coldest month in the dataset) separately. Both these diurnal patterns indicate a single TGM peak that is observed after sunrise. Thereafter, TGM concentrations decrease significantly and remain low, until it starts building up again after midnight. The most prominent feature of these diurnal patterns that need to be explained is the peak of TGM after sunrise. If household combustion and/or traffic were the dominant TGM source(s), bimodal peaks (i.e. one in the morning and one in the afternoon) would have been observed. Korhoren et al. (2014) observed that the planetary boundary layer starts to grow on the Mpumalanga Highveld at approximately 08:00. Gierens et al. (2018) indicated that the breakup of the low-level inversion layer(s), which often occur at depths of less than 200 meters at a regional background site in the North-West Province, start after sunrise. Although the vertical structure of the PBL at EP could be different to the afore-mentioned sites, similar temporal trends can be expected. Therefore, the most likely dominant source of TGM at EP is downward mixing of high stack emissions, following the break-up of low-level inversion layer(s) after sunrise. This effect is stronger in the colder months (Gierens et al., 2018), hence the TGM peak in June being more pronounced.

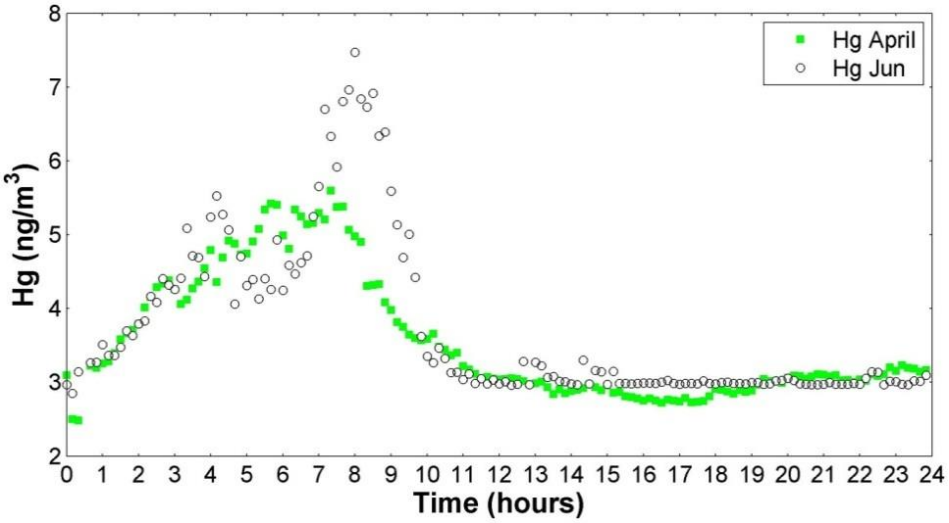

Figure 4.5: Average diurnal patterns for TGM measured during April (the hottest month in the dataset) and June (the coldest month in the dataset) at EP.

Sunrise in June is later if compared to April, which resulted in the April peak occurring earlier than the June peak, as indicated in Figure 4.5. The effect of the PBL evolution is further evident from the TGM levels that decrease and reach a plateau at approximately 15:00-16:00, which is when the PBL usually reaches a maximum depth (Gierens et al., 2018). Another feature observed in Figure 4.5 that needs to be explained is the build-up of TGM after midnight. In order to do this, a case study that indicate the time series concentrations of TGM, NO, NO_2 and SO_2 measured on the 7th June 2013, is presented in Figure 4.6. From this it is evident that NO concentrations increase during the evening, especially after midnight, which also coincided with increase TGM. The timing of this accumulation suggests that it must be due to low-level sources (below the inversion layer(s)). The most significant source during this period is household combustion for space heating. Thereafter NO peaks again after sunrise in conjunction with the most significant TGM peak, which is due to the downward mixing of high stack emission, as explained earlier. Lastly, NO peak late afternoon/early evening, which coincide with the peak traffic and early evening household combustion periods. However, no increase in TGM was observed during that time in this case study. NO_2 concentrations build-up in the evening similar to NO and TGM, and again peak due to late afternoon/early evening traffic and household combustion. SO_2 concentration also build-up with NO and TGM in the evening, but peak sharply due to the breakdown of the inversion layer(s) in the morning after sunrise with TGM. However, it does not peak significantly during the later afternoon/early evening traffic and household combustion periods.

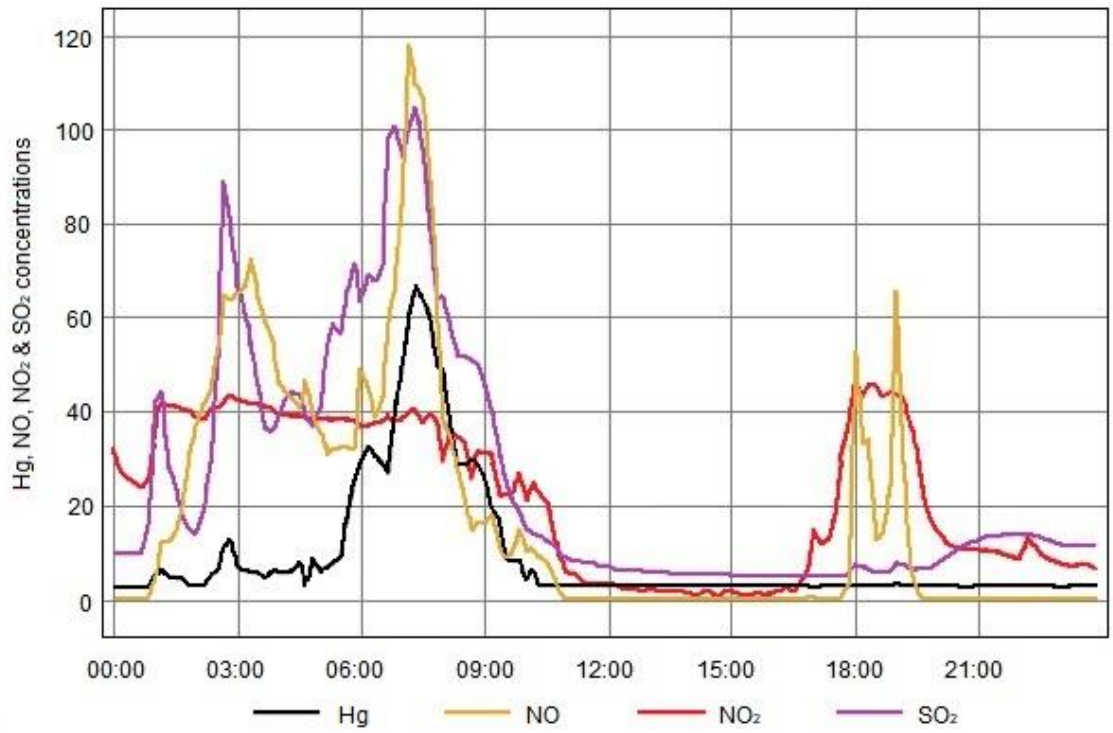

Figure 4.6: Time series of TGM, NO, NO_2 and SO_2 for 7 June 2013, which had a temperature of 3.8°C at 7:00 am local time.

All the afore-mentioned indicate that household combustion for space heating is the most likely cause of TGM accumulation during the evening. This pattern of overnight atmospheric Hg accumulation, followed by rapid depletion after sunrise under the influence of a low nocturnal boundary layer is quite common in urban areas where strong local emissions occur (Feng et al., 2004; Liu et al., 2007; Song et al., 2009). In addition to the PBL evolution and temporal source effects, atmospheric TGM chemistry may also influence observed diurnal cycles. Figure 4.7 present average TGM, O_3 and RH diurnal patterns for the entire measurement period.

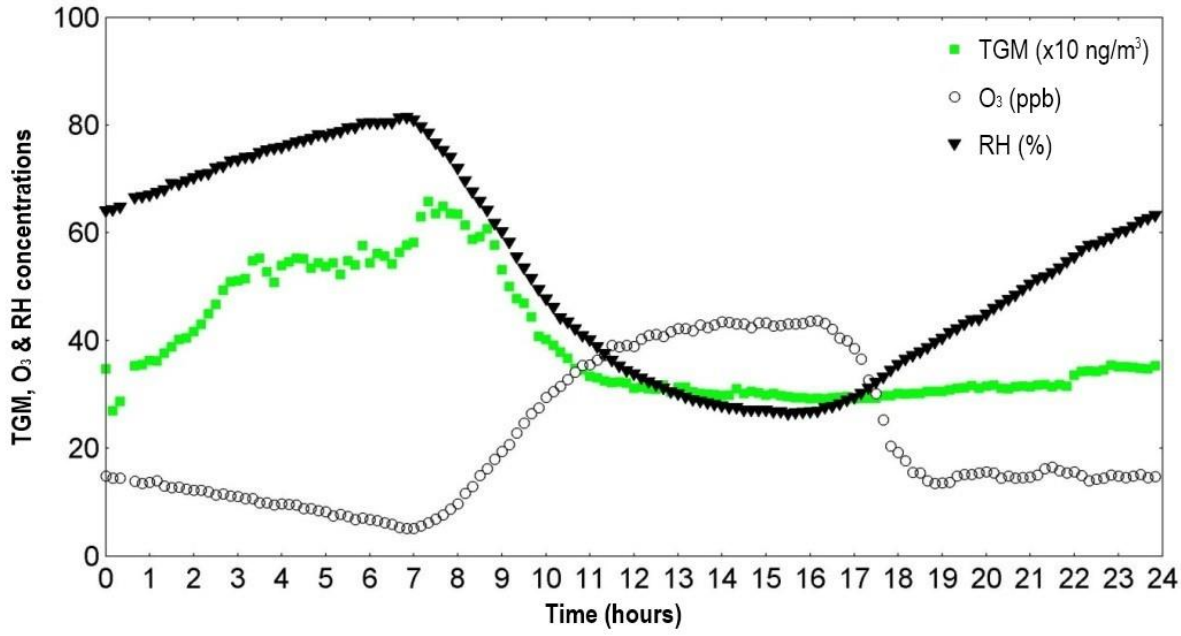

Figure 4.7: Diurnal variations for Hg at Eco-Park (green markers). Ozone and relative humidity is also shown, emphasising O_3 and RH influence on Hg conversion.

As can be seen a clear diurnal trend is recognisable, with RH exhibiting a minimum around 15:00-16:00, while O_3 peak during this time. Both these species can influence TGM concentrations, therefore the basic factors influencing their concentrations/levels are briefly considered. O_3 photochemical formation does not occur as TGM accumulation takes place overnight and RH increases as the temperature drops overnight, as colder air doesn't require as much moisture to become saturated as warmer air.

Following increased O_3 levels after sunrise, the photolysis of O_3 (to form molecular O) and subsequent reaction of the molecular O with water vapour (Connell, 2005) yields the very reactive hydroxyl radical ($HO^{\bullet}$). It is well-known that O_3, as well as radical species such as this, can contribute to the oxidation of GEM to form gaseous oxidised mercury (GOM) (Gworek et. al., 2017) that results in enhanced dry and wet deposition of atmospheric Hg (Marsik et al., 2007). Therefore, the reduction in TGM after sunrise can at least partially be attributed to atmospheric chemistry, in addition to the previously mentioned PBL evolution and temporal source patterns. The relationship between of water vapour (with RH as a proxy therefore) and O_3 is clearly illustrated by the anti-correlation between RH and O_3 that is commonly observed (Jia & Xu, 2014).

As previously indicated the TGM peak observed in Figure 4.7 just after sunrise could be due to downward mixing of high stack emissions, following the break-up of low-level inversion layer(s). Another possible chemical explanation could be Hg re-emissions from substrate- and water surfaces, which contributes to elevated TGM observations during this time (Gustin

et al., 2002). It is known that Hg deposited on land is retained mostly by soils and vegetation, representing a pool for further remobilisation (Kocman et al., 2013). Following sunrise the deposited GOM is photo-reduced back to GEM and mobilised from the surface (Lindberg et al., 2002). Experimental observations showed light-enhanced emissions of Hg from several natural samples in a gas exchange chamber, as a function of time at constant temperature. For all samples, an initial pulse of GEM released with the first light was observed. Thereafter, the emissions gradually decreased, yet remained higher than in the dark (Gustin et al., 2002). GEM emission from substrates are influenced by many factors. One factor that has been shown to have a significant impact on Hg flux is soil moisture, with soils that are wet, but not saturated, having higher GEM emissions than dry soils (Gustin et al., 2008). However, in Figure 4.5 the early morning GEM peak in April was less prominent that the June early morning peak. Since soil moisture in April can be assumed to be higher than in June, it seems as if the PBL effect (i.e. downward mixing of high stack emissions after sunrise) is dominant over the natural re-emissions.

It is also important to look into the mechanism of overnight deposition of Hg, wherein many species play a role (e.g. NO_2, the nitrate radical ($NO_3^{\bullet}$), halogens – according to Coburn et al., 2015) to establish whether the pool for further Hg remobilisation could differ between season. However, if the time-period between 20:00 and 03:00 in Figure 4.5 is considered, it seems as if there are little differences between GEM night-time concentrations in April (representing the hottest month in the dataset) and June (the coldest month in the dataset).

4.3.2. Elandsfontein, Mpumalanga Highveld

Similar to EP, MLR analysis was conducted in an effort to determine relationships between atmospheric TGM concentrations and other atmospheric parameters measured at EL, and also to establish whether TGM levels could be calculated from these parameters. Figure 4.8 presents the RMSE difference between the calculated and measured TGM values, as a function of independent variables included in the optimum MLR solution.

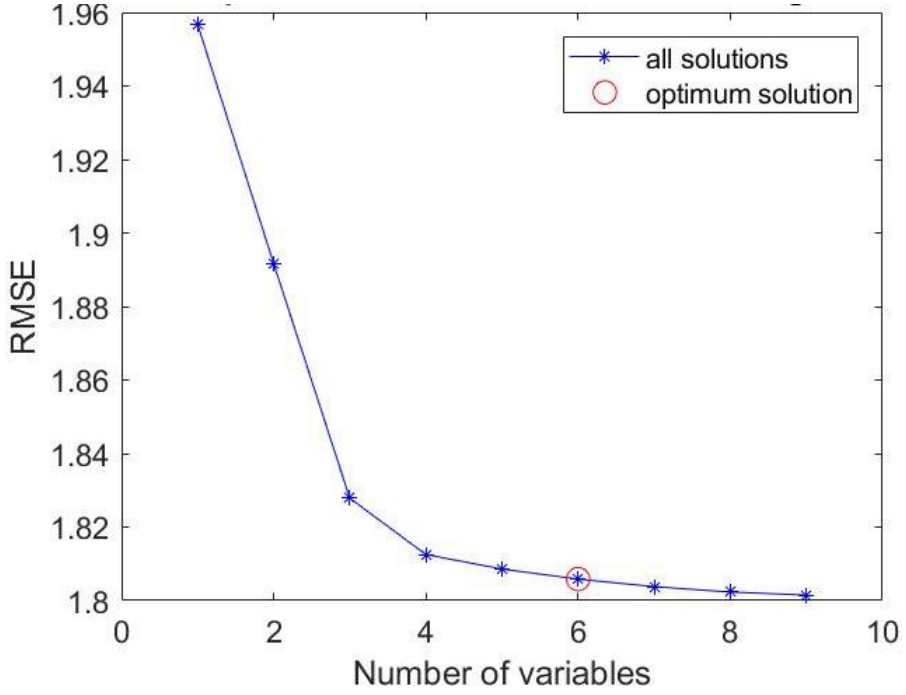

Figure 4.8: The root mean square error (RMSE) difference between the calculated and actual TGM values, in order to determine the combination of independent variables to include in the optimum MLR equation to calculate the dependant variable, i.e. TGM concentration.

Figure 4.8 indicates that the optimum MLR equation containing only one independent variable, i.e. SO_2 (Table 4.3), had a RMSE of 1.96. However, the RMSE could be lowered to 1.89 if a MLR equation containing the optimum combination of two independent variables, i.e. SO_2 and WD_{cos} (Table 4.3), were calculated. Additional independent variables were included until the relative improvement in RMSE (Equation 3.2) was less than 2%. This was attained when the number of independent variables included in the optimum MLR solution was six, which had an RMSE of 1.81. The inclusion of more independent variables in the MLR solution did not significantly reduce the RMSE. Table 4.3 indicates the identity of the independent parameters determined for each of the optimum MLR solutions.

Quantity	Independent variables					
1	SO_2					
2	SO_2	WD_{cos}				
3	SO_2	WD_{cos}	O_3			
4	SO_2	WD_{cos}	O_3	H_2S		
5	SO_2	WD_{cos}	O_3	H_2S	WS	
6	SO_2	WD_{cos}	O_3	H_2S	WS	NO

Table 4.3: The identity of independent variables included the optimum MLR equations to calculate TGM at Elandsfontein.

The overall optimum MLR equation to predict the dependent variable (TGM) was determined, as presented in Equation 4.2. Figure 4.9 presents a comparison between calculated (red markers, using Equation 4.2) and measured TGM values (blue markers). As is evident from this comparison, Equation 4.2 were able to recreate the TGM measurements at EL relatively well, with the exception of baseline levels and outliers.

$$TGM = 0.92122 + (5.1022\ E^{-2} \times SO_2) + (1.2014E^{-2} \times NO) + (2.6783\ E^{-2} \times O_3) - (2.9979\ E^{-2} \times H_2S) + (5.3499E^{-2} \times WS) + (8.3961\ E^{-1} \times WD_{cos}) \quad [4.2]$$

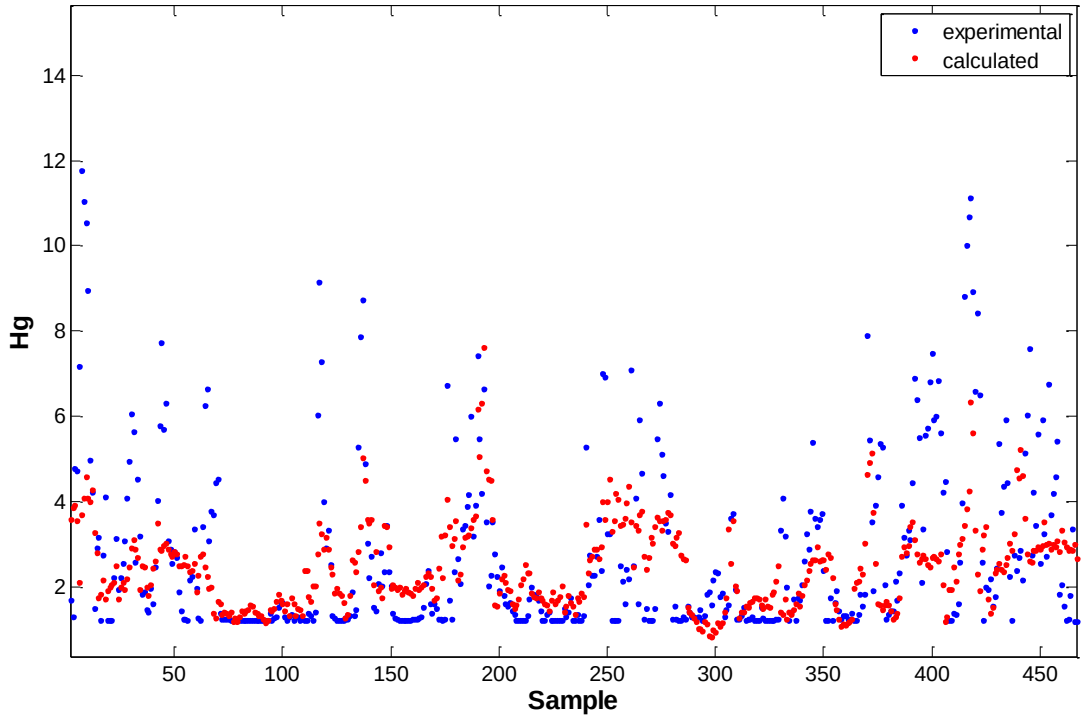

Figure 4.9: Measured (blue) vs calculated (red) TGM values for EL. This sample consists of ±475 measurements.

Considering the above-mentioned, the optimised MLR equation (Equation 4.2) can provide some valuable insight, but it cannot be used to explicitly derive the origin and/or reaction mechanistic information about TGM at EL. From Table 4.3 it is clear that SO_2 (primary emission species) was found to be the independent parameter that reduced the RMSE difference between the calculated and actual TGMs most. The positive constant associated with SO_2 indicates increased Hg pollution is statistically associated with anthropogenic combustion emissions such as coal-fired power plants, petrochemical, pyro-metallurgical and household combustion. Additionally, the positive value associated with NO (another primary emission species) also point towards contributions associated with fresh pollution plumes, which can be attributed to the closer coal-fired power stations, i.e. Kriel (15 km, W) and Komati (18 km, NNE).

Furthermore, the positive constants associated with O_3 is attributed to the contribution of more aged plumes to elevated TGM levels. Compared to EP and its associated sources, EL is further removed from possible sources (Figure 3.2 and 3.4, Section 3.1). For instance, the distances between EL and the coal-fired power stations on the Mpumalanga Highveld range from 28 km to 100 km. Therefore, species that are co-emitted with TGM have more time to oxidise, hence the positive association in Equation 4.2 with secondary formed pollutants such as O_3. Interestingly, when comparing these results to that of EP (Section 4.3.1) there are some significant differences, which can be attributed to the different surroundings of the monitoring stations. At EL we found primary- (SO_2 and NO), as well as secondary pollutants (O_3) having a positive influence on TGM variations, thus revealing that TGM levels are linked to both fresh and aged plumes. This is in contrast to EP where primary emission species correlated positively to increased TGM concentrations. Internationally it has also been found that either primary-, or secondary pollutants, or a combination of these, correlate to increased TGM (Martínez-Coronado et al. 2016).

The negative constant in Equation 4.2 associated with H_2S indicates that lower TGM concentrations are associated with air masses that have passed over the petrochemical operation near Secunda (42 km in SW direction of EL). This indicates that petrochemical processes does not seem to contribute significantly to the TGM measurements observed in the area. This observation will be investigated further in the pollution rose diagram for the EL. Furthermore, the positive value associated with wind speed suggests that higher TGM concentrations are more frequently associated with higher wind speeds, which can be attributed to faster travelling plumes from emission sources further from EL – this correlated with the earlier deduction that aged air masses also contribute to elevated TGM.

The influence of wind direction was again identified as an important factor for EL, i.e. it together with SO_2 was identified as the optimum combination of two independent variables (Table 4.3). Data availability was insufficient to enable a polar plot to be drawn. However, the pollution rose for the entire sampling period of EP data is presented in Figure 4.10.

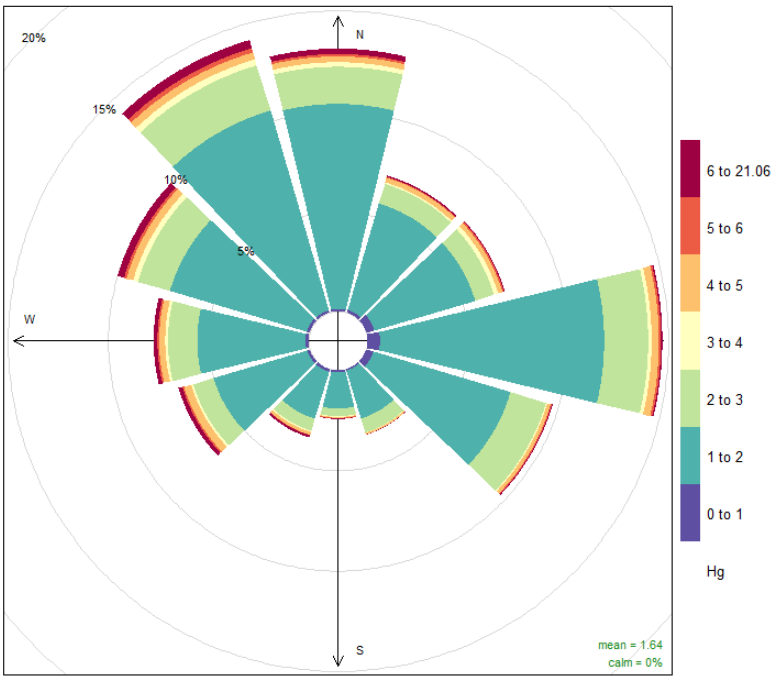

Figure 4.10: Hg pollution rose for Elandsfontein over the observed period.

The pollution rose presented in Figure 4.10 indicates higher TGM concentrations from SW to NNE, which correlate both with the occurrence of the closest and with the location of most coal-fired power stations, i.e. Kriel (15 km, W); Komati (18 km, NNE); Matla- (28 km, W); Hendrina- (29.5 km, NE); Duvha- (32 km, NNW); Kendal- (48 km, NW). Combustion processes (e.g. small industries and household combustion) and metallurgical operations in close proximity to the cities of Witbank and Middelburg; located approximately 45 km north of EL, may also contribute to higher concentrations observed from this direction. However, such contributions cannot be isolated from other emission sources such as power stations, with a pollution rose. From the pollution rose its seems that coal-fired stations further from EL, i.e. Tutuka- (60 km, S); Camden- (79 km, SE) and Majuba- (100 km, S) seems to have less of an impact on TGM levels.

Investigating the relationships between TGM and other species can provide important information concerning TGM sources. Figure 4.11 presents a case study TGM plume observed at EL, which is considered in context of NO, NO_2, SO_2, O_3 and H_2S levels. From this figure it is evident that TGM peaked at exactly the same time as NO, NO_2 and SO_2. The identity of the species confirm this plume to be from a coal-fired power station (Chiloane et al., 2017) and not from the petrochemical operation (since H_2S did not peak coincidentally with TGM). Additionally, the fact that the plume was measured after the breakdown of the lower level inversion layer(s) (Korhoren et al., 2014; Gierens et al., 2018) reinforces the notion of high stack origin. Also, lower O_3 concentrations in a coal-fired power plant plume can be expected, due to titration of O_3 (Laban et al., 2018). This case study (Figure 4.11)

also proved why primary- (SO_2 and NO), as well as secondary pollutants (NO_2) were positively associated with increased TGM concentrations in Equation 4.2.

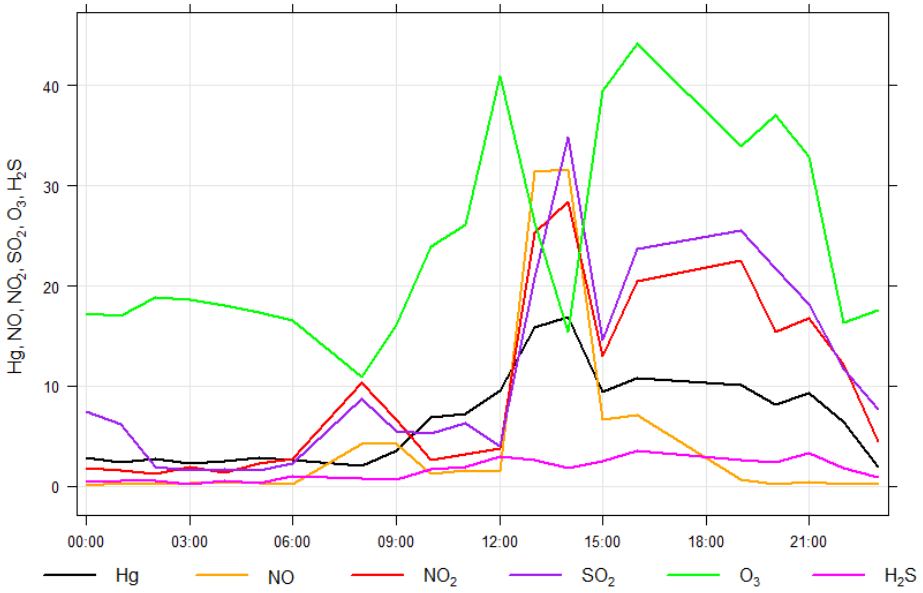

Figure 4.11: A case study time series of TGM, NO, NO_2, SO_2, O_3 and H_2S (peaking on 16.87 ng.m^{-3}). This peak occurred on midday 4 March 2010, with a temperature of 22.09°C at 14:00 pm (local time).

The pattern of overnight Hg accumulation, under the influence of a low nocturnal boundary layer in association with low-level emissions sources as observed at EP, was not observed at EL. This clearly indicate that low-level emission sources, such as household combustion for space heating, was not an important source at EL. It also supported the idea of high stack emission dominating TGM contributions at EL. Obviously all the re-emission and deposition processes (Marsik et al., 2007; Kocman et al., 2013; Lindberg et al., 2002) previously discussed in relation to TGM levels at EP, will also be relevant to measurements at EL, but it was clear that high stack emissions were dominant.

4.3.3. Marapong, Waterberg

In Figure 4.12, the RMSE differences between the calculated and measured TGM values, as a function of independent variables included in the optimum MLR solutions, are presented. The optimum MLR equation containing only one independent variable, which was determined as wind direction, had an RMSE of ± 1.40, and the RMSE was lowered to ± 1.39 if the optimum MLR equation containing two independent variables, i.e. wind direction and O_3.

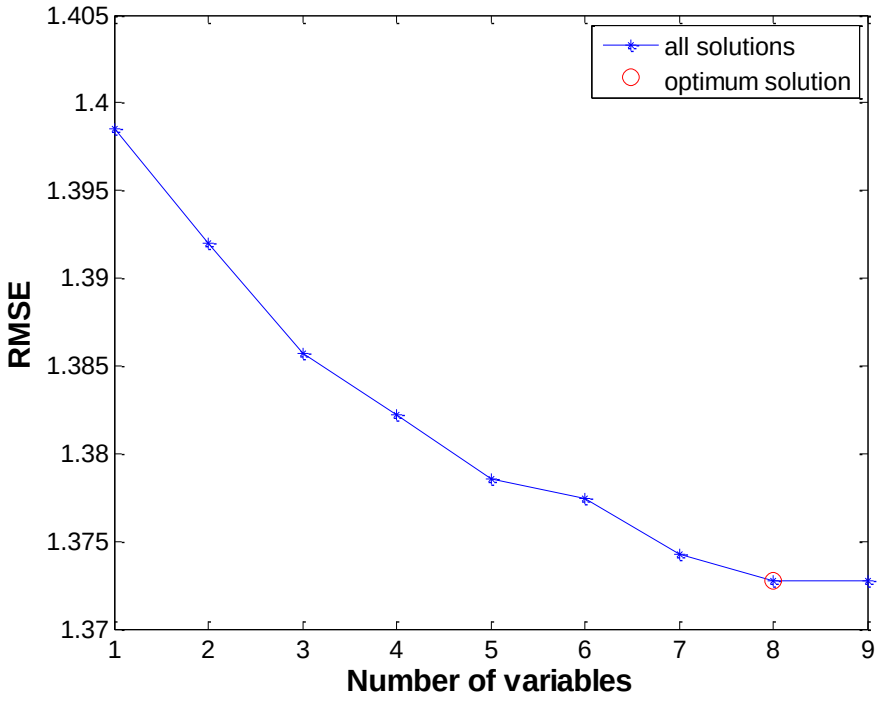

Figure 4.12: The root mean square error (RMSE) difference between the calculated and actual TGM values, in order to determine the combination of independent variables to include in the optimum MLR equation to calculate the dependant variable, i.e. TGM concentration.

Similar to the MLR calculations conducted for EP and EL, the RMSE difference was optimised utilising Equation 3.2, until the relative improvement in RMSE difference was less than 2%. This was attained when the number of independent variables included in the optimum MLR solution was eight, which had an RMSE of 1.37. Table 4.4 indicates the identity of the independent parameters included in each of the optimum MLR solutions.

Quantity	Independent variables							
1	WD_{cos}							
2	WD_{cos}	O_3						
3	WD_{cos}	O_3	NO_2					
4	WD_{cos}	O_3	NO_2	T				
5	WD_{cos}	O_3	NO_2	T	WS			
6	WD_{cos}	O_3	NO_2	T	WS	PM_{10}		
7	WD_{cos}	O_3	NO_2	T	WS	PM_{10}	$PM_{2.5}$	
8	WD_{cos}	O_3	NO_2	T	WS	PM_{10}	$PM_{2.5}$	NO

Table 4.4: The identity of independent variables included the optimum MLR equations to calculate TGM at Marapong.

From Table 4.4 it is evident that wind direction was found to be the most important independent parameter to lower the RMSE difference between actual and calculated TGM. Wind direction and O_3 were included in the optimum MLR equation containing two

independent parameters. It was found that the overall optimum MLR solution contained 8 independent variables, as presented in Equation 4.3 below:

$$TGM = 1.7137 - (3.3362E^{-1} \times WD_{cos}) - (1.1097E^{-2} \times O_3) - (1.5464E^{-2} \times NO_2) + (1.8074E^{-2} \times T) - (1.1721E^{-1} \times WS) + (2.0639E^{-3} \times PM_{10}) - (2.2973E^{-3} \times PM_{2.5}) - (4.6925E^{-3} \times NO) \quad [4.3]$$

Figure 4.13 presents a comparison of calculated (using Equation 4.3, red markers) and actual measured TGM levels at EL (blue markers). Although slight differences are observed, the MLR equation calculated TGM concentrations relatively well, with the exception of very high and low levels.

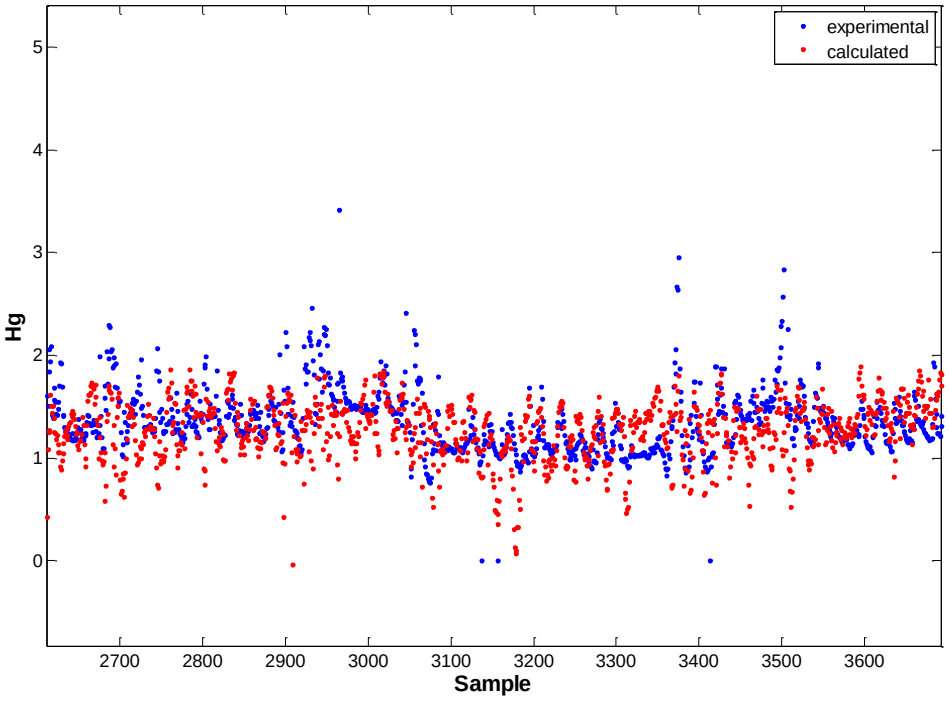

Figure 4.13: Measured (blue) vs calculated (red) TGM values for MP. This sample consists of ±1100 measurements.

As previously stated, MLR equations cannot be used to explicitly derive the origin and/or reaction mechanistic information about TGM at a specific site. However, it can provide valuable insight. From Equation 4.3 it is immediately apparent that elevated TGM measurements are likely to be predominately from local/nearby sources. There are several reasons for this deduction. The negative constant in Equation 4.3 associated with O_3 and NO_2, indicates that lower TGM levels are statistically associated with aged (oxidised) air masses. Because of their size the larger (PM_{10}) particles deposit locally, therefore the positive constant associated with it in Equation 4.3 implies local sources, i.e. Matimba power station and/or household combustion in the Marapong informal settlement. The negative constant associated with smaller particles ($PM_{2.5}$), which has a longer lifetime, supports the

afore-mentioned argument. In addition, the negative constant associated with wind speed also proves that local stagnant conditions will results in higher TGM concentrations. This points to household combustion in the Marapong informal settlement possibly being a more significant source than the high stack emissions from the nearby Matimba power station, since downward mixing of high stack emissions will be promoted by turbulent conditions (i.e. implying higher wind speeds). According to an environmental scoping report for the Lephalale area, the stack height of each of the Matimba power stations two stacks are 250 m and the exit velocity is 24.84 $m.s^{-1}$ (Scorgie et al., 2006). Therefore, even if the Matimba coal-fired power station is only approximately 2 km away from MP, one would argue that downward mixing to ground level within such a short distance would be the exception, rather than the rule.

Since WD_{cos} was the independent variable that reduced the RMSE difference between calculate and actual TGM levels most (Figure 4.12 and Table 4.4), wind direction played an important role in TGM variations at this site. In contrast to EL, enough data was available to enable plotting of a polar plot for MP, which combine wind direction, wind speed and TGM concentrations, to yield a spatial perspective of contributing sources.

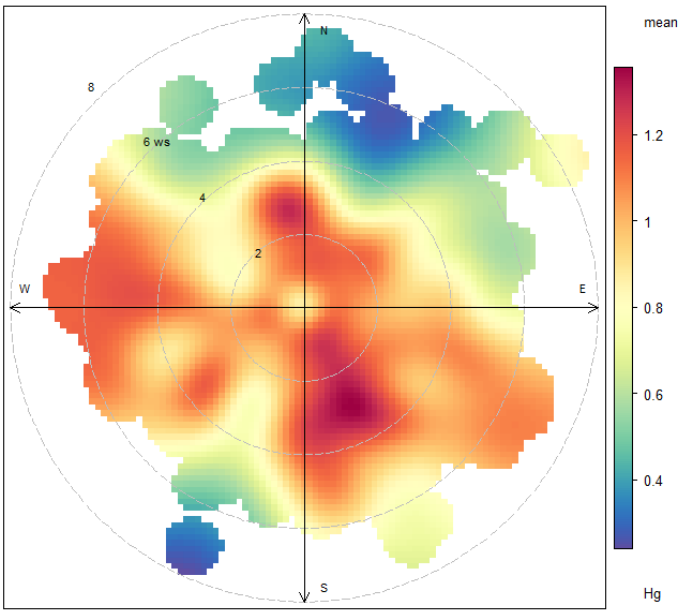

Figure 4.14: The polar plot function applied to the Marapong monitoring station for TGM concentrations.

The polar plot (Figure 4.14) clearly shows that the primary TGM pollution source occurred in all directions and in the vicinity of the measurement site. The likely source therefore seems to be household combustion, which confirms the earlier postulation. If Matimba power station was the dominant source, it would have been indicated clearly in the polar plot.

Furthermore, considering relationships between TGM and other species could provide additional source insights. Figure 4.15 presents a case study period, depicting a typical TGM plume. As is evident from this case study, the TGM peak did not coincide with a SO_2 peak, again casting doubt that the Matimaba power station is the likely source. In contrast, household combustion for space heating is commonly associated with elevated NO, NO_2 and PM_{10}.

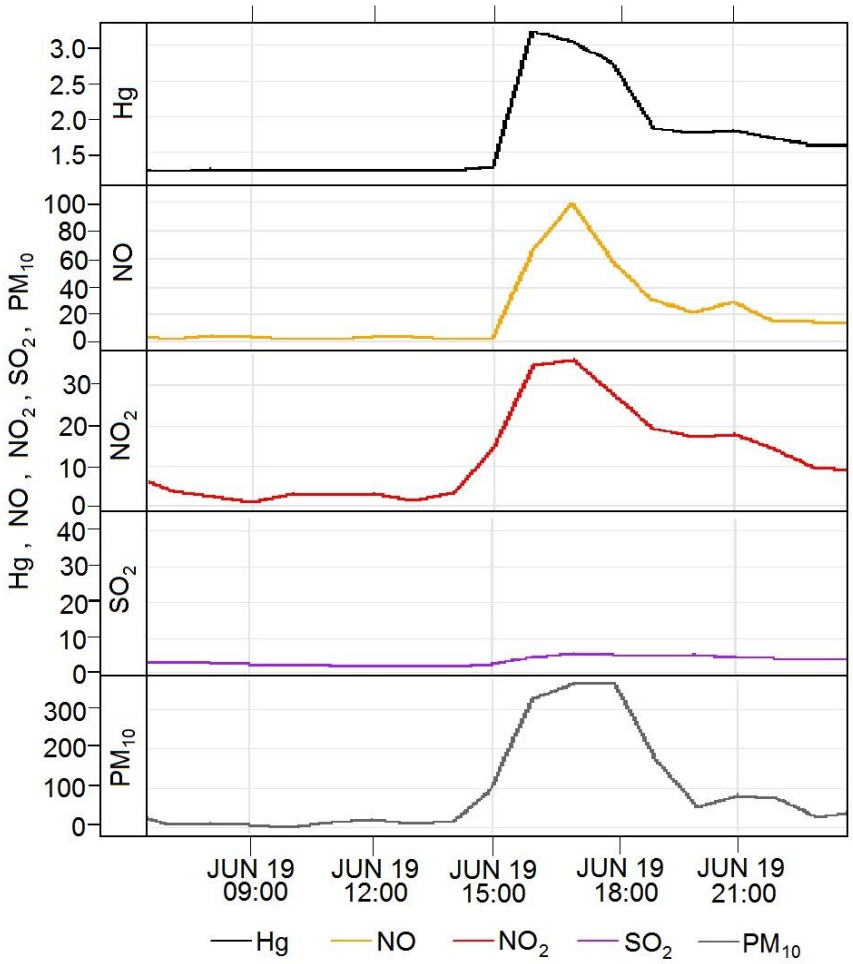

Figure 4.15: A case study time series plot of TGM, NO, NO_2, SO_2 and PM 10 on 19 June 2010 in Marapong. Parameters are not grouped due to large scaling differences between them.

Although MP is located very close to a large point source, it seems to have had no noticeable effect on the TGM variations, or were completely masked by the effects of daily household combustion practices. The deposition and photochemical re-emission processes (Marsik et al., 2007; Kocman et al., 2013; Lindberg et al., 2002) previously discussed will also be relevant to measurements at MP, but it was clear that household combustion was certainly the most significant source. Similarly, Belelie et al. (2018) observed a diurnal pattern dominated by the effects of local coal combustion over the South African Highveld. Thus, similar patterns may exist in in similar environmental settings locally and

internationally (e.g. India and China) where residents of low income settlements rely on fossil fuels for their daily needs.

4.4. Conclusions

Mean TGM concentrations during the monitoring period was 3.95 ± 2.97 ng.m^{-3} for Eco-Park (EP), which is relatively higher compared to other South African and most first world international urban sites. The mean TGM measured at EL (2.49 ± 2.06 ng.m^{-3}) was substantially lower than the mean reported for EP. However, it is comparable to Hg levels reported for urban South African and American cities, yet elevated above international background levels. Mean TGM levels at MP (1.61 ± 1.42 ng.m^{-3}) was significantly lower if compared to the other two monitoring sites considered. It is comparable with that reported some international urban sites, as well as ambient levels reported for suburban sites in the interior of South Africa.

By considering information derived from the MLR analyses, diurnal plots, pollution roses and polar plot, the most prominent TGM source(s) could be identified. A nearby coal-fired power station was identified as the most important point source at EP. High stack emissions from coal-fired power plants were the dominant source contributing to elevated levels measured at EL. Results from MP indicated that domestic combustion in the surrounding semi- and informal settlement dominated TGM contributions. The derived site-specific optimum MRL equations allowed calculation of TGM concentrations which correlated relatively accurately to the measured TGM concentrations, with the exception of very high or low concentrations.

Chapter 5 – Main conclusions, project evaluation and future perspectives

5.1. Summary of main conclusions

Total gaseous mercury, (TGM) was measured at three sites, i.e. Eco-Park (EP), Elandsfontein (EL) and Marapong (MP). The mean TGM at EP (3.95 ± 2.97 ng.m^{-3}) was substantially higher than what had been reported for other South African sites and comparable to polluted sites internationally. TGM means at EL (2.49 ± 2.06 ng.m^{-3}) and MP (1.61 ± 1.42 ng.m^{-3}) was lower than at EP, but still elevated above what had been reported for other South African sites, and comparable to levels reported for large urban areas internationally. Prominent features at the three sites considered in this study were the frequent occurrence of large TGM peaks associated with pollution plumes and relatively large diurnal variations. The afore-mentioned resulted in generally higher standard deviations, when compared to measurements at other local and international sites.

Multiple linear regression (MLR) was applied as a receptor model in order to gain information regarding the important factors influencing TGM levels at each site and possible important atmospheric chemistry processes. Site-specific optimum MLR equations were determined, indicating that dominant sources and/or factors influencing TGM levels were different at all the sites considered. Therefore, it is impossible to use one MLR equation to calculate/predict TGM for the entire South African interior. With the site-specific MLR equations (Equations 4.1 to 4.3) it was possible to calculate atmospheric TGM concentrations relatively accurately, with the exception of very high and low levels.

In addition to MLR analyses, diurnal patterns, pollution roses and polar plots were generated and analysed, which were considered in context of likely planetary boundary layer (PBL) levels and other meteorological information. Combined all of the afore-mentioned gave insights into the most prominent sources influencing the studied sites. At EP the dominant source was found to be the nearby coal-fired power station, with household combustion making a discernible contribution. However, the baseline TGM levels were also elevated, indicating that this area is relatively polluted. Fresh and aged plumes from high stack emissions (mainly from coal-fired power stations) were found to be the most significant source at EL. Household combustion from the surrounding Marapong semi- and informal settlement was identified as the dominant source at MP, which almost totally masked the possible contribution from the nearby coal-fired power station. Combined these results proved that coal-fired power generation is likely to be one of, if not the most important source of TGM in the South African interior, with household combustion being an important local

source. Therefore, in order to reduce TGM levels in the South African interior, emission from coal-fired power generation needs more attention, or alternative cleaner power generation technologies must be implemented over time. Additionally, the social issues pertaining to the use of low-grade coals in semi- and informal settlements needs to be addressed.

From the MLR analyses conducted it was evident that TGM levels were anti-correlated to O_3 concentrations and correlated to relative humidity (RH) levels. Both these species are involved in the formation of the hydroxyl radical ($^{\bullet}OH$), which together with O_3 are the most prominent oxidants during day-time. The nitrate radical is the main oxidant at night-time. None of the radical species were measured during this study, nor in any previous studies in South Africa. Therefore, it is currently impossible to indicate the relatively importance of the different oxidants in the formation of gaseous oxidised mercury (GOM), wherein halogens might also play a role. GOM is water soluble and more reactive, which facilitates the formation of methylated Hg (MeHg). MeHg is toxic and bio-accumulates. From the diurnal patterns of all sites considered during this study it was evident that GOM formation and subsequent deposition takes place on a daily basis in the South African interior.

5.2. Project evaluation

In order to evaluate the project, the specific objectives stated in Chapter 1 (Section 1.2) were repeated here again, where-after the outcomes associated with each were considered.

Objective 1: "Since the candidate did not have access to an atmospheric Hg device, the first objective was to obtain data from at least three measurement sites operated by reputable operators. Since the datasets will be from different measurement operations, methods should be developed to convert the different datasets into a single useful format. Additionally, the datasets should be statistically processed to verify data quality."

Data from sites measuring TGM and ancillary parameters were obtained from Sasol and Eskom. Both these companies have previously supplied data to the department of environmental affairs (DEA) to assess air quality in priority areas. In addition, most of the measurement sites operated by these companies are accredited. Considering the afore-mentioned, the datasets obtained were likely to be the best available at the time when this study was initiated (2015). Processing of the datasets were performed using the statistical programming software MATLAB. Complete data rows (each parameter has a valid entry for each time-stamp) of TGM and all ancillary parameters were required for MLR analyses. Therefore, the raw data was cleaned before being used, which resulted in substantially smaller datasets remaining for further consideration. The quality of the remaining data was

good and enabled subsequent data analyses relating to the identification of contributing sources and important atmospheric processes.

Objective 2: "Make air quality related deductions based on the levels of TGM found at the various sites, as well as identify possible contributing sources."

The relatively small datasets that remained after data cleaning and quality assurance prevented TGM seasonal cycles to be identified. Nevertheless, the mean and/or median TGM levels of the three measurement sites could be contextualised with other local and international measurements. Utilising information obtained from MLR analyses, diurnal plots, pollution roses and polar plots, the most significant sources contributing to observed TGM levels at the three sites could also be identified.

Objective 3: "Apply a mathematical receptor model to calculate ambient TGM and compare this calculated dataset with actual measured results,"

MLR analysis, which is one of the statistical multivariate methods (e.g. principal component analysis, positive matrix factorisation) commonly applied in atmospheric receptor modelling, was considered in this study. This led to site-specific optimum MLR equations being deduced. Calculated (with the optimum MLR equations) and measured TGM observations correlated well, with the exception of very high and low measured values.

Objective 4: "Provide insight into chemical processes influencing TGM in the South African interior."

From the identity of the independent parameters included in the optimal MLR equations and diurnal patterns, it was possible to identify processes that are likely to be important on a regional scale in the South African interior for atmospheric mercury. For instance, the importance of O_3 and RH, and likely importance of radicals, in the oxidation of gaseous elemental mercury (GEM) to GOM was indicated by the results. This is particularly important in improving the current understanding of the formation and impacts of MeHg.

5.3. Future perspectives

During this study the candidate identified various aspects that require future attention, in order to address some of the remaining questions associated with atmospheric mercury in the South African interior. These are subsequently discussed.

Long-term TGM datasets for the South African interior are limited. Data from only three sites operated by reputable operators could be obtained. After data cleaning and quality

assurance, as well as preparation for MLR analysis, the datasets were substantially smaller. The data quantity was sufficient to draw valid conclusions, however, seasonal patterns could not be identified. This again indicates the need for comprehensive (many instruments employed at one site), long-term (multiple years), high quality (very high data availability after data cleaning) atmospheric datasets for South Africa, which include measurement of TGM and/or speciated mercury. Measurements of radical species and halogens associated with atmospheric Hg also needs to be established in South Africa. Such measurements will assist in understanding atmospheric Hg processes in South Africa better. This will also lead to help verify if atmospheric models, which are mostly from internationally sources, incorporate all relevant chemical processes to enable accurate modelling of atmospheric Hg in South Africa.

Since this study was initiated, several more sites where TGM and/or speciated mercury are measured, have been established. Most of these sites are operated by industries, or are located in priority areas and/or areas which high population density. This rationale is understandable, since human health is likely to remain the most important driver of atmospheric measurements. However, measurements at regional background sites are also required, in order to quantify natural concentrations (e.g. re-emissions from substrate that contain trace levels of mercury). Knowledge of such levels will enable meaningful discussions regarding possible future atmospheric Hg legislation in South Africa.

The importance of deposited mercury (both wet and dry) through the formation of GOM became evident, since it is the link to understand the formation and impacts of MeHg better. As far as the candidate could assess, only one study (Brunke et al., 2016) at the Cape Point Global Atmospheric Watch (CPT-GAW) station have quantified wet deposition of Hg in South Africa. As indicated in Section 4.2, the afore-mentioned station is not representative of the South African interior. Therefore, deposition of atmospheric Hg needs substantially more research attention in South Africa.

Bibliography

Afe, O. (s.a.). Tropospheric Halogen Chemistry - A Short presentation. University of Bremen. http://www.iup.uni-bremen.de/doas/seminar/seminar_afe_halogens.pdf. Date of access: 25 Nov. 2016. [PowerPoint presentation].

Akagi, S.K., Yokelson, R.J., Wiedinmyer, C., Alvarado, M.J., Reid, J.S., Karl, T., Crounse, J.D. & Wennberg, P.O. 2011. Emission factors for open and domestic biomass burning for use in atmospheric models. *Atmospheric Chemistry and Physics*. 11:4039–4072.

Amyot, M., Mierle, G., Lean D. & McQueen D.J. 1997. Effects of solar radiation on the formation of dissolved gaseous mercury in temperature lakes. *Geochim Cosmochim Acta*. 61(5):975-987.

Andreae, M.O., Atlas, E., Harris, G.W., Helas, G., de Kock, A., Koppmann, R., Maenhaut, W., Mano, S., Pollock, W.H., Rudolph, J.H., Scharffe, D., Schebeske, G. & Welling, M. 1996. Methyl halide emissions from savanna fires in southern Africa. *Journal of Geophysical Research*. 101(D19):23,603-23,613.

Andreae, M.O. & Merlet, P. 2001. Emission of trace gases and aerosols from biomass burning. *Global Biogeochemical Cycles*. 15(4):955-966.

Ariya, P.A., Khalizov, A. & Gidas, A. 2002. Reactions of gaseous mercury with atomic and molecular halogens: kinetics, product studies, and atmospheric implications. *Journal of Physical Chemistry*. 106:7310-7320.

Axelrad, D.A., Bellinger, D.C., Ryan, L. M. & Woodruff, T.J. 2007. Dose-response relationship of prenatal mercury exposure and IQ: An integrative analysis of epidemiologic data. *Environmental Health Perspective.* 115(4):609−615.

Baker, P.G.L., Brunke, E.G., Slemr, F. & Crouch, A.M. 2002. Atmospheric mercury measurements at Cape Point, South Africa. *Atmospheric Environment*. 36(14):2459-2465.

Belelie, M.D., Piketh, S.J., Burger, R.P., Venter, A.D., Naidoo, M. 2018. Characterisation of ambient Total Gaseous Mercury concentrations over the South African Highveld. *Atmospheric Pollution Research*. https://doi.org/10.1016/j.apr.2018.06.001

Bergh, J.P., Falcon, R.M.S. & Falcon, L.M. 2011. Trace element concentration reduction by beneficiation of Witbank Coalfield no. 4 Seam. *Fuel Processing Technology*. 92(4):812-816.

Blake, N.J., Blake, D.R., Sive, B.C., Chen, T.Y., Sherwood Rowland, F., Collins J. E. Jr., Sachse, G.W. & Anderson, B. E. 1996. Biomass burning emissions and vertical distribution of atmospheric methyl halides and other reduced carbon gases in the South Atlantic region. *Journal of Geophysical Research*. 101(D19):24151-24164.

Bowerman, W.W., Roe, A.S., Gilbertson, M., Best, D.A., Sikarskie, J.G. & Summer, C.L. 2002. Using bald eagles to indicate the health of the Great Lakes environment. Lake Reservoir Manage. 7:183−187.

Brunke, E.G., Spires, R. & Mabille, E., 1995. Basic climatology of Cape Point. Internal Report EMAP196001, September 1995.

Brunke, E.G., Labuschagne, C. & Slemr, F. 2001. Gaseous mercury emissions from a fire in the Cape Peninsula, South Africa, during January 2000. *Geophysical Research Letters*. 28(8):1483-1486.

Brunke, E.G., Labuschagne, C., Slemr, F., Ebinghaus, R. & Kock, H. 2010a. Atmospheric mercury measurements at Cape Point, South Africa. *Clean Air*. 18:17–21.

Brunke, E.G., Labuschagne, C., Ebinghaus, R., Kock, H.H. & Slemr, F. 2010b. Gaseous elemental mercury depletion events observed at Cape Point during 2007–2008, *Atmospheric Chemistry & Physics*. 10:1121–1131.

Brunke, E.G., Ebinghaus, R., Kock, H.H., Labuschagne, C. and Slemr, F. 2012. Emissions of mercury in southern Africa derived from long-term observations at Cape Point, South Africa. *Atmospheric Chemistry & Physics.* 12:7465-7474.

Brunke, E.G., Walters, C., Mkololo, T., Martin, L., Labuschagne, C., Silwana, B., Slemr, F., Weigelt, A., Ebinghaus, R., Somerset, V. 2016. Mercury measurements (2007-2013) made in the atmosphere and in rainwater at Cape Point, South Africa. *Atmospheric Environment*, 125, 24–32. doi:10.1016/j.atmosenv.2015.10.059

Byrne, A. 2017. Trouble in the air: Recent developments under the 1979 Convention on Long-Range Transboundary Air Pollution. RECIEL. 2017;26:210–219.

Chen, L., Liu, M., Xu, Z., Fan, R., Tao, J., Chen, D., Zhang, D., Xie, D., Sun, J. 2013. Variation trends and influencing factors of total gaseous mercury in the Pearl River Delta – A highly industrialised region in South China influenced by seasonal monsoons. *Atmospheric Environment*. 77:757-766. https://doi.org/10.1016/j.atmosenv.2013.05.053

Chiloane, K.E., Beukes, J.P., Van Zyl, P.G., Maritz, P., Vakkari, V., Josipovic, M., Venter, A.D., Jaars, K., Tiitta, P., Kulmala, M., Wiedensohler, A., Liousse, C., Mkhatshwa, G.V., Ramandh, A. and Laakso, L. 2017. Spatial, temporal and source contribution assessments of black carbon over the northern interior of South Africa. *Atmospheric Chemistry and Physics*. 17, 6177–6196, doi:10.5194/acp-17-6177-2017.

Clean Air Network. 1999. The Problem with Mercury. Clean Air Network Fact Sheet. August 1999. (202):289-2429

Coburn, S., Dix, B., Edgerton, E., Holmes, C.D., Kinnison, D., Liang, Q., ter Schure, A., Wang, S. & Volkamer, R. 2015. Mercury oxidation from bromine chemistry in the free troposphere over the southeastern US. *Atmospheric Chemistry and Physics*. 15:28317-28360.

Collett, K.S, Piketh, S.J. & Ross, K.E. 2010. An assessment of the atmospheric nitrogen budget on the South African Highveld. *South African Journal of Science*. 106(5/6), Article 220, 9 pp.

Connell, D.W. 2005. Basic concepts of environmental chemistry. Second Edition. ISBN: 1-56670-676-9. T&F Group. 441p.

Dabrowski, J.M., Ashton, P.J., Murray, K., Leaner, J.J., Mason, R.P. 2008. Anthropogenic mercury emissions in South Africa: Coal combustion in power plants. *Atmospheric Environment*. 42(27):6620-6626.

Dabrowski, J.M. 2010. Emissions of Mercury Associated with Coal-Fired Power Stations in South Africa. Department of Environmental Affairs 2010:1-11.

Dibble, T.S., Zelie, M.J. & Mao, H. 2012. Thermodynamics of reactions of ClHg and BrHg radicals with atmospherically abundant free radicals, *Atmospheric Chemistry & Physics*. 12:10271–10279.

Dickerson, R.R., Rhoads, K.P., Carsey, T.P., Oltmans, S.J., Burrows, J.P. & Crutzen, P.J.J. 1999. Ozone in the Remote Marine Boundary Layer: A Possible Role for Halogens. *Journal of Geophysical Research*. 104(D17:21):385-395.

Drevnick, P.E., Engstrom, D.R., Driscoll, C.T., Balogh, S.J., Kamman, N.C., Long, D.T., Muir, D.G.C., Parsons, M.J., Rolfhus, K.R., Rossmann, R. & Swain, E.B. 2011. Spatial and temporal patterns of mercury accumulation in lacustrine sediments across the Laurentian Great Lakes region. *Environmental Pollution*. 161:252-260.

Driscoll, C.T., Mason, R.P., Chan, H.M., Jacob, D.J. & Pirrone, N. 2013. Mercury as a Global Pollutant: Sources, Pathways, and Effects. *Environmental Science & Technology*. 47:4967−4983

Dommergue, A., Sprovieri, F., Pirrone, N., Ebinghaus, R., Brooks, S., Courteaud, J., Ferrari, C.P. 2010. Overview of mercury measurements in the Antarctic troposphere. *Atmospheric Chemistry & Physics*. 10:3309−3319.

Du Preez, S.P., Beukes, J.P. and Van Zyl, P.G., Cr(VI) generation during flaring of CO-rich off-gas from closed ferrochromium submerged arc furnaces, Metallurgical and Materials Transactions B, 46, 1002–1010, doi:10.1007/s11663-014-0244-3, 2015.

Ebinghaus, R., Jennings, S.G., Schroeder,W.H., Berg, T., Donaghy, T., Guentzel, J., Kenny, C., Kock, H.H., Kvietkus, K., Landing, W., Muhleck, T., Munthe, J., Prestbo, E.M., Schneeberger, D., Slemr, F., Sommar, J., Urba, A., Wallschlager, D. & Xiao, Z. 1999. International field intercomparison measurements of atmospheric mercury species at Mace Head, Ireland. *Atmospheric Environment*. 33:3063–3073.

Ebinghaus, R., Kock, H.H., Temme, C., Einax, J.W., Lowe, A.G., Richter, A., Burrows, J.P. & Schroeder, W.H. 2002. Antarctic springtime depletion of atmospheric mercury. *Environmental Science & Technology*. 36(6):1238−1244.

Engle, M.A., Gustin, M.S., Lindberg, S.E., Gertler, A.W. & Ariya, P.A. 2005. The influence of ozone on atmospheric emissions of gaseous elemental mercury and reactive gaseous mercury from substrates. *Atmospheric Environment*. 39(39):7506-7517.

Ericksen, J.A., Gustin, M.E., Lindberg, S.E., Olund, S.D. & Krabbenhoft, D.P. 2005. Assessing the Potential for Re-emission of Mercury Deposited in Precipitation from Arid Soils Using a Stable Isotope. Environ. Sci. Technol. 39: 8001-8007.

European Commission: Directorate-General for Environment, Hulla & Co Human Dynamics, Jasmina, K.B. 2016. Handbook on the implementation of EU environmental legislation. Section 3 – Air quality legislation. Vol 4. ISBN 978-92-79-62013-3.

Evers, D.C., Lane, O.P., Savoy, L., Goodale, W. 2004. Assessing the Impacts of Methylmercury on Piscivorous Wildlife Using a Wildlife Criterion Value Based on the Common Loon, 1998−2003, Gorham Report BRI 2004-05 submitted to the Maine Department of Environmental Protection; BioDiversity Research Institute: Gorham, ME, 2004.

Evers, D.C., Han, Y.J., Driscoll, C.T., Kamman, N.C., Goodale, W.M., Lambert, K.F., Holsen, T.M., Chen, C.Y., Clair, T.A. & Butler, T.J. 2007. Biological mercury hotspots in the Northeastern United States and Southeastern Canada. *Bioscience* 57(1):1−15.

Evers, D.C., Jackson, A.K., Tear, T.H. & Osborne, C.E. 2012. Hidden risk: Mercury in terrestrial ecosystems of the Northeast; Biodiversity Research Institute: Gorham, ME, 2012.

Fabian, P. and Singh, O.N. 1999. Reactive Halogen Compounds in the Atmosphere. The Handbook of Environmental Chemistry. Vol 4. ISSN 1433-6855

FAO. 2011. Fishery and Aquaculture Statistics; Food and Agriculture Organization of the United Nations: Rome; p 415.

FAO/WHO. 2011. Report of the Joint FAO/WHO Expert Consultation on the Risks and Benefits of Fish Consumption, 25−29 January 2010, Report # 979; Food and Agriculture Organization of the United Nations and World Health Organization: Rome.

Feng, X.B., Shang, L.H., Wang, S.F., Tang, S.L. & Zheng, W. 2004. Temporal variation of total gaseous mercury in the air of Guiyang, China. Journal of Geophysical Research. Atmospheres. 109(D3):2156-2202.

Ferek, R.J., Reid, J.S., Hobbs, P.V., Blake, D.R. & Liousse, C. 1998. Emission factors of hydrocarbons, halocarbons, trace gases and particles from biomass burning in Brazil. *Journal of Geophysical Research*. 103(D24):32,107-32,118.

Fitzgerald, W.F., Mason, R.P., Vandal, G.M., 1991. Atmospheric cycling and air-water exchange of mercury over mid-continental regions. *Water Air Soil Pollution*. 56(1):745-767.

Garnham, B.L., and Langerman, K.E. 2016. Mercury emissions from South Africa's coal-fired power stations. *The Clean Air Journal*. 26(2):14-20.

Grandjean, P., Weihe, P., White, R.F., Debes, F., Araki, S., Yokoyama, K., Murata, K., Sørensen, N., Dahl, R. & Jørgensen, P.J. 1997. Cognitive deficit in 7-year-old children with prenatal exposure to methylmercury. *Neurotoxicol. Teratol*. 19(6):417−428.

Gierens, R.T., Laakso, L., Mogensen, D., Vakkari, V., Beukes, J.P., Van Zyl, P.G., Hakola, H., Guenther, A., Pienaar, J.J. & Boy, M. 2014. Modelling new particle formation events in the South African savannah. *South African Journal of Science*. 110(5-6):1-12.

Gierens, R.T., Henriksson, S., Josipovic, M., Vakkari, V., Van Zyl, P.G., Beukes, J.P., Wood, C.R., O'Connor, E.J., Observing continental boundary-layer structure and evolution over

the South African savannah using a ceilometer, Theoretical and Applied Climatology, published online with volume and page numbers not yet assigned, doi:10.1007/s00704-018-2484-7, 2018.

Goodsite, M., Plane, J. & Skov, H. (2004). A theoretical study of the oxidation of Hg-0 to HgBr2 in the troposphere. *Environmental Science & Technology*. 38(6):1772–1776.

Goodsite, M., Plane, J., and Skov, H. (2012). Correction to A theoretical study of the oxidation of Hg0 to HgBr2 in the troposphere. *Environmental Science & Technology*. 46:5262–5262.

Greaver, T.L., Sullivan, T.J., Herrick, J.D., Barber, M.C., Baron, J.S., Cosby, B.J., Deerhake, M.E., Dennis, R.L., Dubois, J.J.B., Goodale, C.L., Herlihy, A.T., Lawrence, G.B., Liu, L., Lynch, J.A. & Novak. K.J. 2012. Ecological effects of nitrogen and sulfur air pollution in the US: what do we know? The Ecological Society of America. *Front Ecol Environ*. 10(7):365–372.

Gustin, M.S., Lindberg, S.E., Austina, K., Coolbaugh, M., Vette, A. & Zhang, H. 2000. Assessing the contribution of natural sources to regional atmospheric mercury budgets. The Science of the Total Environment. 259:61-71

Gustin, M.S. 2002. Are mercury emissions from geologic sources significant? A status report. *The Science of the Total Environment*. 304:153–167

Gustin, M.S., Biester, H. & Kim, C.S. 2002. Investigation of the light-enhanced emission of mercury from naturally enriched substrates. Atmospheric Environment 36:3241–3254

Gustin, M.S., Ericksen, J. & Fernandez, G.C. 2008. Determination of the Potential for Release of Mercury from Combustion Product Amended Soils: Part 1—Simulations of Beneficial Use, Journal of the Air & Waste Management Association, 58:5, 673-683,

Gworek, B., Dmuchowski, W., Baczewska, A.H., Brągoszewska, P., Bemowska-Kalabun, O. & Wrzosek-Jakubowska, J. 2017. Air Contamination by Mercury, Emissions and Transformations—a Review. *Water Air Soil Pollut.* 228(123):1-31.

Harada, Y. 1968. Congenital (or fetal) Minamata disease. In Minamata disease. Study group of Minamata disease; Japan: Kumamoto University. 1968:93-118.

Holmes, C.D., Jacob, D.J., Mason, R.P. & Jaffe, D.A. 2009. Sources and deposition of reactive gaseous mercury in the marine atmosphere. *Atmospheric Environment*. 43:2278-2285.

Holmes, C.D. 2010. Multiscale models of atmospheric mercury: bromine chemistry, air-sea exchange, and global transport. Doctor of Philosophy in the subject of Earth and Planetary Sciences, Harvard University.

Holmes, C.D., Jacob, D.J., Corbitt, E.S., Mao, J., Yang, X., Talbot, R. & Slemr, F. 2010. "Global atmospheric model for mercury including oxidation by bromine atoms." *Atmospheric Chemistry and Physics*. 10:12037-12057.

Holmes, C. D. (2012). Quick cycling of quicksilver. *Nature Geoscience.* 5:95-96.

Hynes, A., Donohoue, D., Goodsite, M., Hedgecock, I., Pirrone, N., & Mason, R. 2009. Our current understanding of major chemical and physical processes affecting mercury dynamics in the atmosphere and at air-water/terrestrial interfaces, in: Mercury Fate and Transport in the Global Atmosphere, edited by: Pirrone, N. and Mason, R. P., chap. 14, Springer.

Jaars, K., Van Zyl, P.G., Beukes, J.P., Hellén, H., Vakkari, V., Josipovic, M., Venter, A.D., Räsänen, M., Knoetze, L., Cilliers, D.P., Siebert, S.J., Kulmala, M., Rinne, J., Guenther, A., Laakso, L., and Hakola, H., Measurements of biogenic volatile organic compounds at a grazed savannah grassland agriculture landscape in South Africa, Atmospheric Chemistry and Physics, 16, 15665–15688, doi:10.5194/acp-16-15665-2016, 2016.

Jaars, K., Vestenius, M., Van Zyl, P.G., Beukes, J.P., Hellén, H., Vakkari, V., Venter, M., Josipovic, M. and Hakola, H., Receptor modelling and risk assessment of volatile organic compounds measured at a regional background site in South Africa, Atmospheric Environment, 172, 133–148, doi:10.1016/j.atmosenv.2017.10.047, 2018.

Jammalamadaka, S.R. and Lund, U.J. 2006. The effect of wind direction on ozone levels - a case study. *Environmental Ecological Statistics*. 13:287.

Jia, L. and Xu, Y. 2014. Effects of Relative Humidity on Ozone and Secondary Organic Aerosol Formation from the Photo-oxidation of Benzene and Ethylbenzene. *Aerosol Science and Technology*. 48(1):1-12.

Kaden, D.A., Mandin, C., Nielsen, G.D. & Wolkoff P. 2010. Formaldehyde. In: WHO Guidelines for Indoor Air Quality: Selected Pollutants. Geneva: World Health Organization.

Kamman, N.C., Chalmers, A., Clair, T.A., Major, A., Moore, R.B., Norton, S.A. & Shanley, J.B. 2005. Factors influencing mercury in freshwater surface sediments of northeastern North America. *Ecotoxicology.* 14:101−111.

Kim, S.H., Han, Y.J., Holsen, T.M. Yi, S.M. 2009. Characteristics of atmospheric speciated mercury concentrations (TGM, Hg(II) and Hg(p)) in Seoul, Korea. *Atmospheric Environment* 43(20):3267-3274 ·https://doi.org/10.1016/j.atmosenv.2009.02.038

Kim, N.S. & Lee, B.K. 2010. Blood total mercury and fish consumption in the Korean general population in KNHANES III, 2005. *Science of the Total Environment*. 408(20):4841−4847.

Kim, M.K. & Zoh, K.D. 2012. Fate and Transport of Mercury in Environmental Media and Human Exposure. *Journal of Preventive Medicine & Public Health*. 45:335-343.

Kock, H.H., Bieber, E., Ebinghaus, R., Spain, T.G. & Thees, B. 2005. Comparison of long-term trends and seasonal variations of atmospheric mercury concentrations at the two European coastal monitoring stations Mace head, Ireland, and Zingst, Germany. *Atmospheric Environment*. 39:7549–7556.

Kocman, D., Horvat, M. & Wilson, S. 2013. Global Releases of Mercury to Aquatic Environments. Chapter 4 in: Technical Background Report for the Global Mercury Assessment 2013. Arctic Monitoring and Assessment Programme, Oslo, Norway/UNEP Chemicals Branch, Geneva, Switzerland. vi. 263 p.

Kolker, A., Quick, J. C., Senior, C. L. & Belkin, H. E. 2012. Mercury and Halogens in Coal—Their Role in Determining Mercury Emissions From Coal Combustion. U.S. Department of the Interior U.S. Geological Survey. Fact Sheet 2012-3122.

Kolker, A. & Quick, J.C. 2015. Mercury and Halogens in Coal, Chap 2 in: Mercury Control: for Coal-Derived Gas Streams, Granite, E. J., Pennline, H. W. Senior, C. John Wiley & Sons, First Ed. Published 2015.

Korhonen, K., Giannakaki, E., Mielonen, T., Pfüller, A., Laakso, L., Vakkari, V., Baars, H., Engelmann R., Beukes, J. P., Van Zyl, P. G., Ramandh, A., Ntsangwane, L., Josipovic, M., Tiitta, P., Fourie, G., Ngwana, I., Chiloane, K. & Komppula, M. 2014. Atmospheric boundary layer top height in South Africa: measurements with lidar and radiosonde compared to three atmospheric models. *Atmospheric Chemistry & Physics*. 14:4263–4278.

Laban, T.L., Van Zyl, P.G., Beukes, J.P., Vakkari, V., Jaars, K., Borduas-Dedekind, N., Josipovic, M., Thompson, A.M., Kulmala, M. and Laakso, L. 2018. Seasonal influences on

surface ozone variability in continental South Africa and implications for air quality. *Atmospheric Chemistry and Physics*. 18, 15491–15514, doi:10.5194/acp-18-15491-2018.

Lalonde, J. D., Poulain, A. J., & Amyot, M. 2002. The role of mercury redox reactions in snow on snow-to-air mercury transfer. Environmental Science and Technology, 36(2), 174–178.

Lan, X., Talbot, R., Castro, M., Perry, K. & Luke, W. 2012. Seasonal and diurnal variations of atmospheric mercury across the US determined from Amnet monitoring data. *Atmos. Chem. Phys*. 12:10569–10582.

Lan, X., Talbot, R., Laine, P., Lefer, B., Flynn, J. & Torres, A. 2014. Seasonal and Diurnal Variations of Total Gaseous Mercury in Urban Houston, TX, USA. *Atmosphere*. 5:399-419.

Lawler, M.J., Finley, B.D., Keene, W.C., Pszenny, A.A.P. & Read, K.A. 2009. Pollution-enhanced reactive chlorine chemistry in the eastern tropical Atlantic boundary layer, *Geophysical Research Letters*. 36:L08810.

Leaner, J., Dabrowski, J.M., Mason, R.P., Resane, T., Richardson, M., Ginster, M., Gericke, G., Petersen, C.R., Masekoameng, E., Ashton, P.J. & Murray, K. 2008. Mercury emissions from point sources in South Africa. Interim Report of the UNEP Global Partnership on Atmospheric Mercury Transport and Fate Research. N. Pirrone and R. Mason.

Lin, C.J. & Pehkonen, S.O. 1999. The chemistry of atmospheric mercury: A review. *Atmospheric Environment* 33(13):2067-2079.

Lin, C.J., Pongprueksa, P., Vanjani, T., Ho, T.C., Chu, H., Jang, C., Braverman, T., Streets, D.G. & Fu, J.S. 2006. Trans-Pacific chemical transport of mercury: sensitivity analysis on potential Asian emission contribution to mercury deposition in North America using CMAQ-Hg. In: The 5th CMAS Conference, Research Triangle Park, NC, 16–18 October 2006

Lindberg, S.E., Brooks, S., Lin, C.J., Scott, K.J., Landis, M.S., Stevens, R.K., Goodsite, M.E & Richter, A. 2002. The dynamic oxidation of gaseous mercury in the Arctic Troposphere at polar sunrise. *Environmental Science & Technology* 36:1245-1256.

Lindberg, S., Bullock, R., Ebinghaus, R., Engstrom, D., Feng, X., Fitzgerald, W., Pirrone, N., Prestbo, E., and Seigneur, C. 2007. A Synthesis of Progress and Uncertainties in Attributing the Sources of Mercury in Deposition. *Ambio*. 36(1): 19-32.

Liu, B., Keeler, G.J., Dvonch, J.T., Barres, J.A., Lynam, M.M., Marsik, F.J. & Morgan, J.T. 2007. Temporal variability of mercury speciation in urban air. *Atmospheric Environment*. 41:1911–1923.

Liu, B., Keeler, G.J., Dvonch, J.T., Barres, J.A., Lynam, M.M., Marsik, F.J. & Morgan, J.T. 2010. Urban-rural differences in atmospheric mercury speciation. *Atmospheric Environment*. 44:2013–2023.

Liu, N., Qiu, G., Landis, M.S., Feng, X., Shang, L. 2011. Atmospheric mercury species measured in Guiyang, Guizhou province, southwest China. *Atmospheric Research* 100(1):93-102. https://doi.org/10.1016/j.atmosres.2011.01.002

Lobert, J. M., Keene, W. C., Logan, J. A. & Yevich, R. 1999. Global chlorine emissions from biomass burning: Reactive Chlorine Emissions Inventory. *Journal of Geophysical Research*. 104(D7):8373-8389.

Lodenius, M., Tulisalo, E., and Soltanpour-Gargari, A. 2003. Exchange of mercury between atmosphere and vegetation under contaminated conditions, Sci. Total Environ., 304, 169–174.

Lourens, A.S., Beukes, J.P., Van Zyl, P.G., Fourie, G.D., Johanna W., Burger, J.W., Pienaar J.J., Read, C.E., Jordaan, J.H. 2011. Spatial and temporal assessment of gaseous pollutants in the Highveld of South Africa. *South African Journal of Science*. 107(1/2)-(269):1-8.

Lyman, S.N. & Gustin, M.S. 2009. Determinants of atmospheric mercury concentrations in Reno, Nevada, USA. *Sci. Total Environ*. 408:431–438.

Lyman, S.N. and Jaffe, D.A. 2011. Formation and fate of oxidized mercury in the upper troposphere and lower stratosphere, *Nature Geoscience*. 5:114–117.

Mahaffey, K., Clickner, R. & Jeffries, R. 2009. Adult women's blood mercury concentrations vary regionally in USA: Association with patterns of fish consumption (NHANES 1999−2004). *Environ. Health Perspect*. 117:47−53.

Manö, S. & Andreae, M.O. 1994. Emission of Methyl Bromide from Biomass Burning. *Science*. 263(5151): 1255

Marsik, F. J., Keeler, G. J., & Landis, M. S. 2007. The dry deposition of speciated mercury to the Florida Everglades: measurements and modeling. Atmospheric Environment, 41(1), 136–149.

Martínez-Coronado, A., Esbrí, J.M. & Higueras, P. 2016. Time variations of gaseous and reactive mercury in the industrial area of Puertollano (south-central Spain). Temporal cycles with marked variations. *Atmospheric Environment*. 134:198-207.

Masekoameng, K.E., Leaner, J. & Dabrowski, J. 2010. Trends in anthropogenic mercury emissions estimated for South Africa during 2000–2006. *Atmospheric Environment*. 44(25):3007-3014.

Mason, R.P., Choi, A.L., Fitzgerald, W.F., Hammerschmidt, C.R., Lamborg, C.H., Soerensen A.L., & Sunderland, E.M., 2012. Mercury biogeochemical cycling in the ocean and policy implications. Environmental Research. 119:101-117.

Meng, B., Feng, X., Qiu, G., Liang, P., Li, P., Chen, C. & Shang, L. 2011. The process of methylmercury accumulation in rice (Oryza sativa L.). *Environmental Science & Technology*. 45:2711−2717.

McDowell, M.A., Dillon, C.F., Osterloh, J., Bolger, P.M., Pellizzari, E., Fernando, R., de Oca, R.M., Schober, S.E., Sinks, T., Jones, R.L. & Mahaffey, K.R. 2004. Hair mercury levels in US children and women of childbearing age: Reference range data from NHANES 1999−2000. *Environ. Health Perspect*. 112 (11):1165−1171.

meteoblue. (n.d.). Climate Sasolburg. [online] Available at: https://www.meteoblue.com/en/weather/forecast/modelclimate/sasolburg_south-africa_957487 [Accessed 6 Nov. 2017].

Nair, U.S., Wu, Y., Walters, J., Jansen, J. & Edgerton, E.S. 2012. Diurnal and seasonal variation of mercury species at coastal-suburban, urban, and rural sites in the southeastern united states. *Atmos. Environ*. 47:499–508.

Nair, U.S., Wu, Y., Holmes, C.D., Ter Schure, A., Kallos, G. & Walters, J.T. (2013). Cloud-resolving simulations of mercury scavenging and deposition in thunderstorms. *Atmospheric Chemistry & Physics*. 13:10143–10157.

Obrist, D., Tas, E., Peleg, M., Matveev, V., Faïn, X., Asaf, D. & Luria, M., 2011. Bromineinduced oxidation of mercury in the mid-latitude atmosphere. *Nature Geoscience*. 4:22-26.

Pacyna, E.G., Pacyna, J.M., Steenhuisen, F. & Wilson, S. 2006. Global anthropogenic mercury emission inventory for 2000. *Atmospheric Environment*. 40(22):4048-4063.

Parrella, J.P., Jacob, D.J., Liang, Q., Zhang, Y., Mickley, L.J., Miller, B., Evans, M.J., Yang, X., Pyle, J.A., Theys, N., & Van Roozendael, M. 2012. Tropospheric bromine chemistry: implications for present and pre-industrial ozone and mercury. *Atmospheric Chemistry & Physics*. 12:6723–6740.

Pirrone, N., Hedgecock, I.M. & Sprovieri, F. 2008. New Directions: Atmospheric mercury, easy to spot and hard to pin down: Impasse? *Atmospheric Environment*. 2008, 42, 8549−8551.

Pirrone, N. 2010. Presentation: Summary of Part B: Mercury. CNR - Institute of Atmospheric Pollution Research, Rome, Italy. 6th Meeting of the TF HTAP. Mercure Brussels Center Louise, Brussels 14-16 June 2010

Pirrone, N., Cinnirella, S., Feng, X., Finkelman, R.B., Friedli, H.R., Leaner, J., Mason, R., Mukherjee, A.B., Stracher, G.B., Streets, D.G. & Telmer, K. 2010. Global mercury emissions to the atmosphere from anthropogenic and natural sources. *Atmospheric Chemistry & Physics*. 10(13):5951−5964.

Pirrone, N., Cinnirella, S., Dastoor, A., Ebinghaus, R., Gratz, L., Hedgecock, I., Sprovieri, F. & Tranikov, O. 2013. Atmospheric Pathways, Transport and Fate. Chapter 3 in: Technical Background Report for the Global Mercury Assessment 2013. Arctic Monitoring and Assessment Programme, Oslo, Norway/UNEP Chemicals Branch, Geneva, Switzerland. Edition VI, 263 pp.

Prinn, R.G. 2003. Ozone, Hydroxyl Radical, and Oxidative Capacity. Massachusetts Institute of Technology, Cambridge, MA, USA. Treatise on Geochemistry. 4:1-19 pp.

Rafaj, P., Cofala, J., Kuenen, J., Wyrwa, A & Zyśk, J. 2014. Benefits of European Climate Policies for Mercury Air Pollution. *Atmosphere*. 5(1): 45-59.

Rice, D.C., Schoeny, R. & Mahaffey, K. 2003. Methods and rationale for derivation of a reference dose for methylmercury by the US EPA. *Risk Analysis*. 23(1):107−115.

Sakamoto, M., Murata, K., Tsuruta, K., Miyamoto, K. & Akagi, H. 2010. Retrospective study on temporal and regional variations of methylmercury concentrations in preserved umbilical cords collected from inhabitants of the Minamata area, Japan. *Ecotoxicol. Environ. Saf*. 73(6):1144−1149.

Schroeder, W.H. & Munthe, J. 1998. Atmospheric mercury—an overview. *Atmospheric Environment.* 32(5):809-822.

Scorgie, Y., Krause, N. & Petzer, G. 2006. Air Quality Impact Assessment for the Proposed New Coal-Fired Power Station in the Lephalale Area, Limpopo Province. Report No. APP/06/BWK-01 Rev 1.0.

Scott, G.M. & Mdluli, T.N. 2012. The Minamata Treaty / Protocol: Potential Implications for South Africa. Clean Air Journal. 22(2):17-19.

Selin, N.E., Jacob, D.J., Park, R.J., Yantosca, R.M., Strode, S., Jaegl´e, L. & Jaffe, D. 2007. Chemical cycling and deposition of atmospheric mercury: Global constraints from observations. *Journal of Geophysical Research*. 112(D02308):1-14.

Selin, N.E. 2009. Global biogeochemical cycling of mercury: A review. Annual Review of Environment and Resources. 34:43-63.

Sioen, I., Van Camp, J., Verdonck, F.A.M., Van Thuyne, N., Willems, J.L., De Henauw, S. W.J. 2007. How to use secondary data on seafood contamination for probabilistic exposure assessment purposes? Main problems and potential solutions. *Hum. Ecol. Risk Assess*. 13(3):632−657.

Slemr, F., Brunke, E.G., Labuschagne, C., Ebinghaus, R. 2008. Total gaseous mercury concentrations at the Cape Point GAW station and their seasonality. *Geophysical Research Letters*. 35:1-5.

Slemr, F., Brunke, E.G., Ebinghaus, R., Kuss, J. and Edgerton, E.S. 2011. Worldwide trend of atmospheric mercury since 1995. *Atmospheric Chemistry & Physics.* 11:4779-4787.

Slemr, F., Brunke, E.G., Whittlestone, S., Zahorowski, W., Ebinghaus, R., Kock, H.H. & Labuschagne, C. 2013. 222Rn-calibrated mercury fluxes from terrestrial surface of southern Africa. *Atmospheric Chemistry & Physics*. 13:6421–6428.

Song, X., Cheng, I. & Lu, J. 2009. Annual atmospheric mercury species in downtown Toronto, Canada. *Journal of Environmental Monitoring*. 11:660–669.

South Africa. 2005. NOTICE OF INTENTION TO DECLARE THE VAAL TRIANGLE AIR-SHED PRIORITY AREA IN TERMS OF SECTION 18(1) OF THE NATIONAL ENVIRONMENTAL MANAGEMENT: AIR QUALITY ACT 2004, (ACT NO. 39 OF 2004). *Government Gazette*. 28132(484):4, 14 Oct.

South Africa. 2007. NOTICE OF INTENTION TO DECLARE THE HIGHVELD PRIORITY AREA IN TERMS SECTION 18(1) OF THENATIONAL ENVIRONMENTAL MANAGEMENT AIR QUALITY ACT, 2004 (ACT NO. 39 OF 2004). *Government Gazette*. 29864(396):32, 4 May.

South Africa. 2010. NOTICE OF INTENTION TO DECLARE THE WATERBERG PRIORITY AREA IN TERMS OF SECTION 18(1) OF THE NATIONAL ENVIRONMENTAL MANAGEMENT: AIR QUALITY ACT, 2004 (ACT NO. 39 OF 2004). *Government Gazette*. 33600(939):4, 8 Oct.

Sprovieri, F., Pirrone, N., Ebinghaus, R., Kock, H. & Dommergue, A. 2010. A review of worldwide atmospheric mercury measurements. Atmospheric Chemistry & Physics. 10:8245–8265.

Stamenkovic, J., Lyman, S. & Gustin, M.S. 2007. Seasonal and diel variation of atmospheric mercury concentrations in the Reno (Nevada, USA) Airshed. *Atmospheric Environment*. 41:6662–6672.

Stephens, C.R., Shepson, P.B., Steffen, A., Bottenheim, J.W., Liao, J., Huey, L.G., Apel, E., Weinheimer, A., Hall, S.R., Cantrell, C., Sive, B.C., Knapp, D.J., Montzka, D.D. & Hornbrook, R.S. 2012. The relative importance of chlorine and bromine radicals in the oxidation of atmospheric mercury at Barrow, Alaska. *Journal of Geophysical Research*. 117(D00R11):1-16.

Streets, D.G., Devane, M.K., Lu, Z., Bond, T.C., Sunderland, E.M. & Jacob, D.J. 2011. All-time releases of mercury to the atmosphere from human activities. *Environ. Sci. Technol*. 45(24):10485−10491.

Subir, M. Ariya, P.A. & Dastoor, A.P. 2012. A review of the sources of uncertainties in atmospheric modeling II. Mercury surface and heterogeneous chemistry – A missing link. *Atmospheric Environment*. 46:1–10.

Temme, C., Blanchard, P., Steffen, A., Banic, C., Beauchamp, S., Poissant, L., Tordon, R. & Wiens, B. 2007. Trend, seasonal and multivariate analysis study of total gaseous mercury data from the Canadian atmospheric mercury measurement network (CAMNet). *Atmospheric Environment*. 41:5423–5441.

Timonen, H., Ambrose, J.L & Jaffe, D.A. 2013. Oxidation of elemental Hg in anthropogenic and marine airmasses. *Atmospheric Chemistry and Physics Discussions*. 13:2827–2836.

Tokos J., Hall B., Calhoun J. & Prestbo E.M. 1998. Homogeneous gasphase reaction of Hg0 with H2O2, O3, CH3I, and (CH3)2S: implications for atmospheric Hg cycling. *Atmospheric Environment*. 32(5):823-827.

Tossell, J.A. 2003. Calculation of the Energetics for Oxidation of Gas-Phase Elemental Hg by Br and BrO. *Journal of Physical Chemistry*. 107(39):7804-7808.

Trüe, A. 2010. Environmental mercury monitoring in the South African Highveld region. Department of Chemistry Faculty of Science, Tswane University of Technology. Magister Technologiae: Chemistry: p. 99.

Trüe, A., Forbes, P.B.C., Panichev, N., Okonkwo, J. & Forbes, P.B.C. 2012. Determination of the mercury content of lichens and comparison to atmospheric mercury levels in the South African Highveld region. *Clean Air*. 21(1):19-25.

UNEP Chemicals Branch. 2008. The Global Mercury Assessment: Sources, Emissions and Transport. United Nations Environment Programme, UNEP-Chemicals, Geneva.

UNEP Chemicals Branch. 2013. Global Mercury Assessment 2013: Sources, Emissions, Releases and Environmental Transport. United Nations Environment Programme, UNEP Chemicals Branch, Geneva, Switzerland

US EPA. 1992. Mercury compounds. Technology Transfer Network Air Toxics Web Site http://www.epa.gov/ttn/atw/hlthef/mercury.html#ref8.

Venter, A.D., Vakkari, V., Beukes, J.P., van Zyl, P.G., Laakso, H., Mabaso, D., Tiitta, P., Josipovic, M., Kulmala, M., Pienaar, J.J., & Laakso, L. 2012. An air quality assessment in the industrialised western Bushveld Igneous Complex, South Africa. *South African Journal of Science*. 108:84–93.

Venter, A.D., Beukes, J.P., van Zyl, P.G., Brunke, E.G., Labuschagne, C., Slemr, F., Ebinghaus, R. & Kock, H. 2015. Statistical exploration of gaseous elemental mercury (GEM) measured at Cape Point from 2007 to 2011. *Atmospheric Chemistry and Physics Discussions*. 15(3):4025-4053.

Venter, A.D., Van Zyl, P.G., Beukes, J.P., Josipovic, M., Hendriks, J., Vakkari, V. and Laakso, L., Atmospheric trace metals measured at a regional background site (Welgegund) in South Africa, Atmospheric Chemistry and Physics, 17, 4251–4263, doi:10.5194/acp-17-4251-2017, 2017.

Von Glasow, R., von Kuhlmann, R., Lawrence, M. G., Platt, U. &Crutzen, P. J. 2004. Impact of reactive bromine chemistry in the troposphere. *Atmospheric Chemistry and Physics*. 4:2481–2497.

Wagner, N.J. & Hlatshwayo, B. 2005. The occurrence of potentially hazardous trace elements in five Highveld coals, South Africa. *International Journal of Coal Geology*. 63(3-4)228-246.

Wiener, J.G. & Spry, D.J. (1996). Toxicological significance of mercury in freshwater fish. In Environmental Contaminants in Wildlife: Interpreting Tissue Concentrations; Beyer, W.N., Heinz, G.H., Redmon-Norwood, A.W., Eds.; Lewis Publishers: Boca Raton, FL, 1996.

Yang, X., Cox, R., Warwick, N., Pyle, J., Carver, G., O'Connor, F. & Savage, N. 2005. Tropospheric bromine chemistry and its impacts on ozone: A model study. *Journal of Geophysical Research*. 110(D23311):1-18.

Yang, X., Pyle, J.A., Cox, R.A., Theys, N., & Van Roozendael, M. 2010. Snow-sourced bromine and its implications for polar tropospheric ozone. *Atmospheric Chemistry & Physics*. 10:7763–7773.

Yates, D.E., Mayack, D.T., Munney, K., Evers, D.C., Major, A., Kaur, T., Taylor, R.J. 2005. Mercury levels in mink (mustela vison) and river otter (lontra canadensis) from northeastern North America. *Ecotoxicology*. 14:263−274.

Yorifuji, T., Tsuda, T., Inoue, S., Takao, S. & Harada, M. 2011. Long-term exposure to methylmercury and psychiatric symptoms in residents of Minamata, Japan. *Environ. Int*. 37(5):907−913.

Zhang, H. & Lindberg, S.E. 2001. Sunlight and iron (III)-induced photochemical production of dissolved gaseous mercury in freshwater. *Environmental Science & Technology*. 35(5):928-935.

Appendix A:

The 5th, 25th, 75th and 95th percentiles, as well as mean and median values for the three measurement sites consideredwere indicated Marapong.

	TGM (ng.m^{-3})		
Site	**Eco-Park**	**Elandsfontein**	**Marapong**
5th percentile	2.57	0.96	0.37
25th percentile	2.88	1.23	0.80
75th percentile	3.58	3.05	1.86
95th percentile	9.23	6.67	4.28
Mean	3.95	2.49	1.61
Median	3.00	1.63	1.22